A Critical Analysis of the Acoustic Emission Technique for NDE of Pressure Vessels

by

Pak W. Shum

Thesis submitted to the Faculty of the
Virginia Polytechnic Institute and State University
in partial fulfillment of the requirements for the degree of
Master of Science
in
Engineering Mechanics

APPROVED:

John C. Duke, Jr., Chairman

J.W. Grant

R. W. Landgraf

ABSTRACT

As a nondestructive examination, the acoustic emission technique is used to detect the presence of discontinuities inside of pressurized components. However, doubts still exist concerning the loading procedure to accomplish the acoustic emission testing, especially, in a pressure vessel where a uniform pressure can produce a nonuniform stress distribution due to the presence of the singularities such as the nozzles and supports. The combined loading of vapor and hydrostatic pressure can also generate a nonuniform stress distribution throughout the pressure vessel. According to the Kaiser effect, a structure with a nonuniform stress distribution should have a different acoustic emission testing result when compared to a structure with a uniform stress distribution. In this present study, the necessity to perform a stress analysis prior to the acoustic emission testing is examined. Furthermore, for the purpose of the stress analysis, two approaches are discussed, the membrane stress analysis and the finite element approach.

By means of the membrane stress analysis, it is shown that the combined loading of the hydrostatic and vapor pressure does not produce a significant variation of stress throughout the spherical vessel. Actually, a computer program based on the membrane stress analysis is written to determine the stress distribution due to the combined loading. The limitation of the membrane stress analysis to handle problem with the presence of bending stress is also indicated.

The finite element approach is used to perform the stress analysis of the singularities where the bending stress is important. The finite element computer program ABAQUS is used to perform the finite element stress analysis, and the mechanical computer-aided engineering program PATRAN is also used to construct the finite element model and to interpret the stress analysis results. The convenience and the success of these computer programs to handle this kind of problem are confirmed. The application of different types of finite elements to perform the stress analysis is also discussed. Results from the experiments performed by Gill, Catching and Paine [9] to measure the stress distribution of a pad reinforced nozzle is used as a benchmark to determine the performance of these finite elements. As a consequence, concrete recommendations concerning the selections of the finite elements and the stress analysis procedure are given.

Finally, the influence of the stress distribution throughout the spherical pressure vessel on the acoustic emission is discussed, and the actual interpretation of the acoustic emission testing results based on the level of activity of acoustic emission without considering the nonuniform stress distribution throughout the structure is questioned.

ACKNOWLEDGEMENTS

The author wishes to express his appreciation to his graduate advisor Prof. John C. Duke, Jr. for his patience, his constructive criticisms and his effort to assure the accomplishment of this research project. As a consequence, the author has experienced a valuable education opportunity. Appreciation is also extended to Prof. R. W. Landgraf and Prof. Grant for offering their assistance in the most required moment during the realization of this research project. Many thanks go to Dr. Ronnie Miller for suggesting the initial idea for this project. The author also wishes to thanks Mike Horne, Ali Rezai, Chao Yi-Chwan, and Paige Smith for their support. Special thanks go to Kin Liao and Steven Lee for their valuable suggestion and encouragement. My thanks to Joe Wiencko, my many friends from the Hong Kong Club for their help in daily life. Finally, the author wishes to express his special thanks to his parents for their sacrifices and everything they have ever done so that the dreams of the author may come true.

TABLE OF CONTENTS

LIST OF FIGURES

LIST OF TABLES

1.) INTRODUCTION:

In the petroleum industry, the transformation of petroleum into chemical products usually involves high pressure and temperature; as a consequence, the physical components within the processing system can be considered as a pressurized component. Since the pressurized component normally operates in a corrosive environment, very often cracks or flaws occur inside the pressurized component. According to fracture mechanics, in most of the cases, it is possible to determine the critical crack size related to the state of stresses within the component and the geometry of the crack. As a matter of fact, cracks arriving at a critical size inside a chemical processing system can be considered as one of the major causes of failure; therefore, reliable nondestructive examination (NDE) must be applied to prevent catastrophic disaster. Currently, several NDE methods have been used in the petroleum industry to detect the discontinuity inside the structure. Radiographic inspection, eddy current inspection, liquid penetrant inspection, magnetic particle inspection, ultrasonic inspection and acoustic emission inspection, are the most commonly used methods. Although each method of NDE has advantages and disadvantages, radiographic inspection is the method used most to search for internal imperfections due to the fact that a permanent record can be obtained and the most comprehensive results interpretation criteria has been established by the ASME code [ASME, 17]. In some cases, actually, the most convenient NDE technique for a particular situation is neglected just because of difficulty in results interpretation. For this reason, studies should be done to provide information for better understanding of the NDE results.

As a NDE method, the acoustic emission technique offers an economical way to evaluate the integrity of the whole structure without disassembly, and possibly without significant disruption of production. Therefore, a lot of expectation has been built up around this method. However, the task of interpreting the acoustic emission test data has never been easy. Especially, when the result of the acoustic emission testing is directly related to the loading situation of the structure. This interesting relationship, actually, motivates the present study in which the acoustic emission approach is discussed based on the stress analysis of a spherical pressure vessel.

2) ACOUSTIC EMISSION:

2.1) HISTORICAL BACKGROUND:

It was well known before the twentieth century that metals emitted "sounds" while undergoing deformation or chemical transformation. However, the first scientific study of the acoustic emission was done by Josef Kaiser in Munich, Germany in the 1950's [ASNT, 18] . Two important phenomena related to acoustic emission were discovered by Kaiser. In the first place, all materials emitted acoustic emission; in the second place, acoustic emission would be observed only if the specimens were loaded to exceed the previous loading level. The second statement which received the name of "Kaiser effect" demonstrated the intrinsic relationship between the acoustic emission and the mechanism of materials deformation. Based on the study of the Kaiser effect, a lot of interesting insights about the acoustic emission arose. Two of them are: the Dunegan corollary and the Felicity effect.

The Dunegan corollary can be considered as an application of the Kaiser effect in pressure vessel testing strategy. According to the Dunegan corollary, if the vessel has the required fitness for the service, cyclic loading of the vessel to the proof pressure will not produce any relevant acoustic emission. However, if there is any harmful discontinuities present inside the pressure vessel, the growing of the discontinuity which increases the stress concentration around it, will produce a significant amount of acoustic emission. In conclusion, in order to determine the "fitness for-purpose" of a pressure vessel, cyclic loadings between the proof pressure and the minimum pressure which can be zero should be applied.

The Felicity effect observed in composite material is apparently the contradiction of the Kaiser effect. Instead of emitting acoustic emission at a load level higher than the previous loading situation, the composite material begins to emit at a lower level. The reason is, in composite material the viscous behavior of the matrix increases the stress at the fiber during successive reloading to the same loading level. As a consequence, the integrity of a composite material can be successfully predicted by the acoustic emission technique. Since the phenomena characterized by the Felicity effect are time dependent, the Felicity effect demonstrates the importance of "time at load" as well as load level to the acoustic emission behavior.

2.2) FUNDAMENTALS OF ACOUSTIC EMISSION:

According to the ASTM subcommittee E07.04 acoustic emission can be defined as: "The transient elastic waves resulting from local internal microdisplacement in a material. By extension the term also describes the technical discipline and measurement technique relating to the phenomenon." [ASNT, 18] . In other words, materials or structures undergoing a process, such as plastic deformation, macro or microcrack growth or dislocation, emits elastic waves that propagate from the source throughout the structure and to the surface. As a consequence, a waveform surface displacement can be detected. Furthermore by analyzing the characteristic of this surface displacement useful information can be obtained concerning the nature and the location of the origin of the elastic wave.

Basically, an acoustic emission testing system is composed of sensors, amplifiers with filters, measurement circuitry, data buffers and perhaps a microcomputer. Since the acoustic emission sometimes produce a surface displacement less than 10^{-12} m, piezoelectric sensors with high sensitivity have been widely used for detection. The ASM Metal Handbook Volume 17 provide a more detailed discussion of acoustic emission system and different type of sensors. [ASM, 16]

In general terms, there are two types of acoustic emission signals: the burst type and the continuous type.

The continuous type has the appearance of the Gaussian Random noise. The amplitude of the continuous type is a function of acoustic emission activity. It is believed that the continuous type emission is produced by dislocation movement[ASM, 16].

The burst type is characterized by a discrete waveform with damping. Typically, burst type emission can reach a higher amplitude than the continuous type. As a matter of fact, this kind of emission is the most important for the acoustic emission testing due to the fact that the burst type emission is often related to processes such as plastic deformation, microcrack and macrocrack growth[ASM, 16].

Several methods are used to interpret the output signals of an acoustic emission test [ASNT, 17]:

The Emission Count or Ringdown Count is the simplest approach to perform the

analysis of acoustic emission signals. By counting the number of times that the peaks of a discrete signal exceeds a preselected threshold, the severity of the acoustic emission activity can be quantified. However, the emission ringdown count only represents a qualitative approximation of the acoustic emission signal.

The acoustic emission energy is another means of quantifying acoustic emission signals. When the acoustic emission phenomenon occurs energy is released from the source. Furthermore, the surface displacement caused by the acoustic emission is translated into electrical energy by the sensor; therefore, the electrical energy can be calculated using the following equation:

$$U = \frac{1}{R}\int_0^{\alpha} V^2(t)\, dt$$

As an advantage the energy measurement is directly related to the instability inside the structure; actually, some researchers believe there is a direct correspondence between the energy released by the source and the energy collected during the acoustic emission monitoring. However, due to the limitation of the electronic equipment, sometimes the energy measurement only represents the averaged energy of the event [Kline, 15].

The acoustic emission signal amplitude also provide useful information about the integrity of the system. By studying the characteristic of the amplitude distribution of the acoustic emission signals some deformation mechanism can be recognized; consequently, prediction concerning the integrity of the structure can be done. Furthermore, the amplitude of the acoustic emission signal represents the intensity of the damage associated with the source. However, the amplitude of a acoustic emission signal is affected by the separation between the source and the sensor, and the calibration of the acoustic emission system becomes crucial with this measurement approach [Kline, 15].

With the development of the digital techniques most acoustic emission signal collection is performed by computer systems, e.g. Spartan [Spartan, 27]. Usually, computer software is used within the system to represent the quantification of the acoustic emission signals against the parameters of testing such as loading, duration, number of cycles, etc.

In order to detect a discontinuity inside the structure, most of the NDE methods require the identification of a suspect area a priori, or the complete structure should be scanned for this purpose. In contrast, the acoustic emission technique can localize the discontinuity within a considerable area by means of a strategical location of sensors. For example, the acoustic

emission testing of a butane storage sphere of 51 ft. diameter was performed with 12 sensors [ASNT, 18]. Basically, the localization of the discontinuity was performed by measuring the difference in time of arrival of an acoustic emission signal to the different sensors [ASNT, 18]. By assuming a known wave velocity and distance between the sensors, the acoustic emission source location can be fully determined. Actually, the triangulation method is preferred in the acoustic emission testing of a pressure vessel. This method consists of measuring the difference between acoustic emission signal arrival times to different pairs of sensors inside a triangular formation. After that the source can be located by means of Apollonian triangle [ASNT, 18] or the intersection of two hyperbole [Scott, 25]. Computers have provided help in the location of discontinuity by computing the distance of the discontinuity very rapidly. [Spartan, 27].

2.3) ADVANTAGES AND DISADVANTAGES OF THE ACOUSTIC EMISSION TECHNIQUE

In practice, the infallible NDE method does not exit, therefore the recognition of the limit of the NDE method is very important for its application. In order to evaluate the limitation of the acoustic emission technique, a list of advantages and disadvantages of the method has been prepared. A more complete discussion of the advantage and disadvantage of the acoustic emission technique can be found in the book of Nondestuctive Testing Handbook [18].

Advantages of the acoustic emission technique:

1) In comparison to the other NDE methods, the acoustic emission technique requires less time for evaluating the condition of the entire structure.

2) The acoustic emission technique can establish the dynamic relationship between the damage and the loading imposed on the structure during the monitoring procedure.

3) The application of the acoustic emission on line monitoring in the petroleum industry avoids unnecessary shutdowns. Thus, the maintenance cost of the petroleum and chemical plant can be reduced enormously.

4) Since the transducer can be located at a remote position from the discontinuity, the acoustic emission technique provides a practical approach to measure discontinuities in inaccessible areas.

5) The application of the acoustic emission technique during hydrostatic testing can prevent catastrophic accident by early detection of discontinuities, this application is especially useful in the requalification of in service pressurized component.

6) The acoustic emission method does not require induction of external energy to the structure under examination. Therefore, possible damage of the structure and the possible error of interpretation caused by the artificial excitation source is minimum. Although, acoustic emission is generally performed as part of a procedure that includes changing the mechanical state of the structure, e.g. hydrostatic proof testing, cool down method, etc. However, unnecessary damage to the structure can be avoided by following the recommendations suggested in the ASME Code [ASME, 22].

Disadvantages of the Acoustic Emission Technique:

1) Most of the standards of discontinuity evaluation are based on a static approach; i.e. the severity of the damage is based on the size and orientation of the discontinuity. Conversely, the acoustic emission technique measures the interaction between the loading and the deformation process. In other words, the acoustic emission technique can only detect a discontinuity that changes the local state of stress within a material suddenly. Thus, a discontinuity that remains stable cannot be detected in spite of its size and orientation.

2) The acoustic emission technique is more practical for locating a discontinuity than determining quantitatively the size of the discontinuity.

3) Background noise produced by the operation of the system such as the relative movement of the joints can cause significant acoustic emission making it difficult to detect the presence of an actual discontinuity.

4) Since the propagation of stress waves from an acoustic emission inside a finite medium are divergent, the characteristic of the acoustic emission signal collected at the surface of the structure may differ enormously from the acoustic emission signal produce by the discontinuity. Therefore, the details of the acoustic emission signal is highly dependent on the geometry of the structure.

2.4) CURRENT APPLICATION OF THE ACOUSTIC EMISSION TECHNIQUE IN THE PETROLEUM INDUSTRY

Inside the petroleum and chemical industries, acoustic emission testing has successfully been performed to detect discontinuities inside pressurized components. Mainly, three groups of metal alloys have been used to build these pressurized components: medium carbon steel, low alloy steel, and austenistic stainless steel; furthermore, all of these metals may be considered ductile. Due to the fact that yielding of ductile material is one of the major sources of acoustic emission, the acoustic emission technique has become popular for assessing the condition of the pressurized component. Moreover, the pressurized component is frequently subjected to creep and stress rupture that produce a significant amount of acoustic emission. Additionally, hydrogen embrittlement and thermal shock induced cracks can also be detected by the acoustic emission technique. Also, the carbon steel is clad with stainless steel to prevent severe corrosion; delamination between the base and the cladding material, however, constitutes the major disadvantage of this construction method. Acoustic emission, having the ability to monitor continuously the pressurized component, can detect this defect in the very beginning.

2.4.1) APPLICATION OF THE ACOUSTIC EMISSION TECHNIQUE ON THE PRESSURE VESSEL

The pressure vessel constitutes one of the most important component of the petroleum and chemical industry. Three principal applications of the acoustic emission technique on the pressure vessel are [ASNT, 18]:

1) The hydrostatic testing of a new pressure vessel:

According to the ASME code [ASME, 22], a new pressure vessel constructed under the specification of the ASME code must be submitted to a hydrostatic test with a testing pressure of 1.5 times the design pressure. By using the acoustic emission technique as a complementary technique, a lot of discontinuities overlooked by the other NDE techniques can be detected [ASNT, 18], especially, when the vessel is spot tested (only 85% of the welded joints are radiographically inspected).[ASME,22]

2) Qualification of in Service Pressure Vessel:

A pressure vessel normally suffers deterioration during the service period, therefore, the NDE testing is applied to determine the condition of the pressure vessel. Due to the fact that only dynamic discontinuities produce acoustic emission, the integrity or the degree of deterioration of the vessel can be measured by means of the acoustic emission technique. Acoustic emission is also ideal because it does not necessarily require that the vessel be removed from service.

3) On Line Monitoring of a Pressure Vessel:

The early detection of crack growth and the development of existing cracks, can provide useful information to predict the remaining life of the pressure vessel under consideration. As a consequence, the shutdown of the facility for repair or replacement can be planned more efficiently lessening the impact on production. However, the continuous monitoring of the pressure requires a passive and highly sensitive technique such as acoustic emission. Furthermore, in case where a shutdown is required, the on line acoustic emission monitoring of the vessel can provide useful information for determining the critical areas that should be examined in more detail with other NDE techniques such as radiographic, ultrasonic or eddy current testing; thus, the shutdown period can be reduced significantly.

2.4.2) APPLICATION OF THE ACOUSTIC EMISSION TECHNIQUE FOR THE RECERTIFICATION OF GAS TRAILER TUBING [ASNT, 18]

Another successful application of the acoustic emission technique is the recertification of gas trailer tubing. According to regulations of the U.S. Department of Transportation, the gas trailer tubing should be inspected periodically every five years. Instead of hydrostatic testing which requires dismantling of the trailer and cleaning of the surface after the testing, the gas tubes are loaded with gas and the acoustic emission testing is performed. After that the area suspected to have discontinuities are inspected with ultrasonic techniques to determine the integrity of the gas tube. This procedure has reduced the cost of operation and provides more maintenance information than the hydrostatic testing.

2.4.3) APPLICATION OF THE ACOUSTIC EMISSION TECHNIQUE TO THE FIBER REINFORCED VESSEL [ASNT, 18]

A high rate of failure occurs in the fiber reinforced vessel (almost 2 failures per year). Therefore, this kind of vessel must be inspected frequently to avoid major catastrophe. Due to the internal structural complexity of the composite material, the acoustic emission technique seems to be the most appropriate technique to locate the possible defective areas. After that the suspicious areas can be examined with other NDE techniques. Otherwise, an expensive complete scanning of the fiber reinforced vessel has to be done with other NDE techniques. Actually, the major success of the acoustic emission technique has been achieved on such fiber reinforced vessels. In ASME section V [ASME, 17], there is a complete standardization of the acoustic emission procedure including the loading of the vessel.

Finally, there are a lot of other applications of the acoustic emission technique in the petroleum and chemical industry [ASNT, 18] such as leak detection of buried pipe line and machinery condition monitoring. In conclusion, there is a wide range of application of the acoustic emission technique in the petroleum and chemistry industry. However, pressure vessel monitoring has been selected as the topic for this present study because of the importance of this component to the petroleum industry. In addition, the stress analysis of the singularities such as the nozzle due to the loading condition is still under investigation currently [Primm, 23].

2.5) CONDITIONS FOR AN APPROPRIATE INTERPRETATION OF THE ACOUSTIC EMISSION TESTING RESULTS

Physically acoustic emission is a wave propagation phenomenon, therefore, phenomena such as attenuation affect the sensitivity of the testing system. For practical purpose, attenuation in real structures can only be estimated according to previous experience [ASNT, 18]. Also, background noise causes serious problems in the interpretation of the acoustic emission signal. A lot of effort has been focussed in the study of the noise discrimination of the acoustic emission testing system [Williams, 30]. Usually the method of frequency discrimination is used to overcome this problem. Since the frequency of the noise is normally lower than the frequency of the acoustic emission signals emitted by an imperfection, the noise can be filtered by recognizing its frequency. Also, in structural monitoring, guard sensors have been used to isolated the source of the noise. In facts, a noise assessment of the structure under testing is always recommended before performing any acoustic emission testing.

Until now most of the factors mentioned were related to the physics of the acoustic emission; i.e, the wave propagation in solid. However, as it has been discussed before, the structure must be loaded in certain ways directly or indirectly, in almost all the applications of the acoustic emission technique. Actually, the Kaiser effect emphasizes the importance of the loading situation in relation to the acoustic emission. Specifically, for a spherical vessel that constitutes the case of study in the present thesis, the Kaiser effect can be achieved by raising the pressure above the operating pressure. Actually, the acoustic emission testing with pressure loading is one of the most common practice in the petroleum industry [Peacock, 21]. However, a pressure vessel tested by the acoustic emission technique may undergo a nonuniform loading situation, for example, a vessel partially filled with liquid, and with vapor pressure at the top section. Also, most pressure vessels contain details such as nozzles and supports. Therefore, a uniform stress distribution over the whole structure is unlikely to occur. Since the stress distribution is highly related to the stress intensity factor which determines the behavior of a crack growth [Angelsen, Conely & Williams, 3], cracks located in different areas of a pressure vessel may have different behavior. Thus, having a stress distribution of a structure undergoing an acoustic emission testing becomes extremely important to achieve a correct interpretation of the acoustic emission testing results. Actually, an acoustic emission testing procedure, "Monpac"

(Monsanto and Physical Acoustic Corporation) includes criteria to classify the severity of acoustic emission signals based on the energy increase and the cumulative energy. As a result, areas of high risk inside the structure can be identified. In fact, the energy released by a material during the deformation process can be written as a function of the stress and strain. A pressure vessel; therefore, with different stress distributions in different areas of the structure may have different energy levels. Although the loading is uniform over the whole structure, erroneous interpretation of the acoustic emission testing results may occur because the loading situation has been oversimplified.

3) APPROACH TO PERFORM THE STRESS ANALYSIS:

3.1) METHODOLOGY

As mentioned in chapter two, in order to interpret correctly the results of the acoustic emission testing, it is necessary to have a complete description of the stress distribution throughout the specimen under test. In the present study, a spherical thin wall pressure vessel was used for the purpose of stress analysis. A pressure vessel, used as a storage device or reactor, constitutes the major component of any pressurized system in the petroleum industry. The required thickness for a spherical pressure vessel to support relatively high pressures is usually smaller in comparison to the other kinds of pressure vessels such as cylindrical or square vessels. Moreover, the smooth curvature of the spherical vessel avoids the presence of the discontinuous stress in the jointing between the head and the body. A more detailed discussion about the discontinuous state of stress is done by Harvey [12]. For all these reasons, the spherical vessel is usually preferred in situations where a high design pressure is present; however, the spherical vessel has the disadvantage of being difficult to construct.

It is worth mentioning that most of the pressure vessels used in the petroleum industry are designed based on the ASME code, to be specific the ASME Code, Section VIII, Division 1 [ASME, 22]. Since this code is more design oriented, determination of the maximum stress inside the component is the main purpose. Conversely, the present study explores methods that can be use to determine the distribution of stress throughout the whole component for the acoustic emission testing purpose. Actually, two approaches have been used for this purpose: the simplified membrane theory and the finite element method which will be discussed in the following chapters.

3.1.1) STRESS ANALYSIS OF AN AXI-SYMMETRICALLY LOADED PRESSURE VESSEL BASED ON THE MEMBRANE THEORY

A spherical pressure vessel is most likely to be loaded by a vapor and hydrostatic pressure during its entire service life; this kind of loading is usually symmetric with respect to the vertical axis. Depending upon the state of deformation of the material, which are metals very often, the stress analysis can be based on elasticity or plasticity theories. However, in practice, the major part of the material should be undergoing elastic deformation. Therefore, the stress analysis based on elasticity theory is the most convenient. In this case, similar to most engineering structures such as beams and plates, the most general three dimensional elasticity analysis is usually avoided by the application of engineering assumptions that simplify the governing equation of the problem.

For a spherical thin wall pressure vessel, the structure is generally considered as a shell. The classical theories of shell are very similar to the classical plate theory in the sense that they both use the Love - Kirchhoff assumptions, i.e the normal to the middle surface remains normal after deformation and this normal is not subjected to any deformation after all. However, the big difference between a plate and a shell is the curvature of the shell. Physically the tension tangential to the principal curvature of a shell has a component in the vertical direction because of the curvature; as a consequence, the shell is more efficient than the plate for structures such as a doom or a roof. Since the geometry of a shell is more complicate than a plate, more parameters are required to defined it. As a consequence, the governing equations of a shell are also more complicated and as a matter of convenience, are normally formulated using curvilinear coordinates. Due to the complexity of the governing equations, different assumptions have been used currently to simplify the governing equations obtained by the classical theory. A popular assumption is the basis of "shallow" shell theory, and the applicability of this theory depends strongly on the ratio between the radius of curvature and the wavelength of the harmonic deformation of the shell [Donnell, 7]. Another simplified classical shell theory is the membrane theory in which the bending stress is neglected [Timoshenko & Kruger, 28] and the behavior of the structure is similar to a balloon filled with air. This theory has major acceptance for analysis of thin wall vessels under uniformly distributed internal pressure, which is the case in the present study. For a small element of a spherical vessel shown in Fig. 3.1, the equilibrium

equation can be shown as [Burgreen, 4]:

$$\frac{N_\theta}{R} + \frac{N_\emptyset}{R} = f_n \qquad \text{(eq. 3.1)}$$

$$N_\theta = r_c\left[f_n - \frac{P}{2\pi R^2 \sin^2 \emptyset}\right] \qquad \text{(eq. 3.2)}$$

where the

N_θ : Circumferential stress per unit of thickness

$N_\emptyset$: Meridianal stress per unit of thickness

R : Radius of the spherical vessel

P : Net vertical force as shown in Fig. 3.2

f_n : distributed normal force per unit of area

$\emptyset$: Meridianal angle (see Fig. 3.1)

The solution for a spherical pressure vessel with vapor pressure at the top section(Fig. 3.3) was obtained by using the principle of superposition; i.e. the problem was separated into two case:

Case I : a spherical pressure vessel with hydrostatic pressure.

Case II : a spherical pressure vessel with uniform internal pressure.

Finally, the solution of the spherical pressure vessel with vapor pressure at the top section corresponds to the sum of the solutions of case I and case II.

As a matter of fact, the following solution for a spherical pressure vessel was developed according to the previous discussion.

Case I, a spherical vessel with hydrostatic pressure:

For a pressure vessel as shown in Fig. 3.3, the pressure or the distributed normal force per unit of area in the vessel at any angle $\emptyset$ was written as:

$$f_n = \gamma[R(1 - \cos\emptyset) - Z_0] = \gamma[R(\cos\emptyset_1 - \cos\emptyset)] \qquad \text{(eq. 3.3)}$$

See fig. 3.3 for the definition of the symbols R, $\emptyset$, $\emptyset_1$ and Z_0.

γ : specific density of the liquid contained inside the spherical vessel.

Furthermore, the analysis was separated into two subcase: $\emptyset < \emptyset_0$ (see Fig. 3.3)

$$\emptyset > \emptyset_0$$

In other words, the problem has been solved for the sections above and below the support.

Subcase 1: $\emptyset < \emptyset_0$ (for section above the support)

The net vertical force P :

$$P = \int_A f_n dA * \cos\emptyset \qquad \text{(eq. 3.4)}$$

where $dA = 2\pi R \sin\emptyset R d\emptyset$

Substituting equation 3.3 into equation 3.4:

$$P = \int_{\emptyset_1}^{\emptyset_2} \gamma\left[R(\cos\emptyset_1 - \cos\emptyset)\right] 2\pi R * \sin\emptyset * R * d\emptyset * \cos\emptyset$$

Solving the integral explicitly, the following expression for the net vertical force was obtained:

(For the solution of the integral see appendix I)

$$P = 2\pi R^3 \gamma \left\{ \frac{\cos\emptyset_1}{4}\left[\cos 2\emptyset_1 - \cos 2\emptyset_2\right] + \frac{1}{3}\left[\cos^3\emptyset_2 - \cos^3\emptyset_1\right] \right\} \qquad \text{(eq. 3.5)}$$

Finally, by substituting equation 3.5 into equations 3.1 and 3.2, expressions for the meridianal force and the circumferential force per unit of thickness as a function of the geometric parameters and properties of the fluid were obtained.

Subcase 2: $\emptyset > \emptyset_0$ (for the section below the support)

For the section below the support, the net vertical force was determined by adding the pressure resultant and the weight of the liquid; i.e., P = P + W. The weight of the liquid W was determine in the following way:

$$W = \text{Volume of the liquid} \times \gamma_{liq}$$

Volume of the liquid $= \frac{4\pi R^3}{3} - \pi Z_0^2\left(R - \frac{Z_0}{3}\right)$

Finally, by substituting the P determined from above into the equations 3.1 and 3.2, the meridianal and the circumferential force per unit of thickness for the section below the support was determined.

The meridianal stress $(\sigma_{\emptyset})$ and the circumferential stress (σ_{θ}) was determined as following:

$$\sigma_{\emptyset} = \frac{N_{\emptyset}}{t}$$

$$\sigma_{\theta} = \frac{N_{\theta}}{t}$$

t : thickness of the pressure vessel

Case 2: a spherical vessel with uniform internal pressure:

For a spherical vessel with uniform internal pressure the equations 3.1 and 3.2 became the equations of thin wall vessel equations:

$$\sigma_{\emptyset} = \frac{PR}{2t}$$

$$\sigma_{\theta} = \frac{PR}{2t}$$

Finally, using the principle of superposition the solution for a thin wall spherical vessel with vapor pressure was fully determined. Furthermore, a computer program (see appendix II) was written in Fortran in order to obtain the stress distribution over the whole vessel based on the equations developed before. The computer program was applied to a spherical pressure vessel with the following characteristics:

$Z_0 = 10$ in.

$R = 40$ in.

$\gamma = 0.03609$ lb/in^3

$PV = 200$ lb/in^3

$SD = 27$ in.

$t = 0.75$ in.

where the

Z_0: The liquid level measured from the top of the vessel.

R: Radius of the spherical vessel.

γ: Specific density of the liquid contained inside the spherical vessel.

PV: Vapor pressure at the top of the spherical vessel.

SD: Saddle distance measured from the centerline of the spherical vessel.(Fig. 3.3)

t: Thickness of the spherical pressure vessel.

The membrane analysis results obtained from the program were presented graphically in Fig. 4.1.1 & 4.1.2.

3.1.2) STRESS ANALYSIS OF THE SINGULARITY: NOZZLE AND SUPPORT

The stress distribution around a singularity such as a nozzle has been an interesting research topic during recent decades [ASME, 13]. Mainly two approaches have been used to describe this stress distribution; firstly, the analysis based on shell theory, i.e. the equilibrium equations written in curvilinear coordinates are prescribed between the nozzle and the shell body of the vessel. Furthermore, the kinematic equation with the corresponding engineering assumptions, the compatibility equations and the constitutive relations are combined together to establish a mathematical model such that the problem can be solved properly for different loading situations [Gill, 9]. Very often the purpose of this analysis is to obtain the maximum stress concentration factor for design purposes. Moreover, a limit analysis is usually performed to determine the limit loading. Within the limit analysis, the elastic analysis is performed to provide the lower bound, and the plastic analysis is performed to establish the upper bound. Finally, the limit load is the one that satisfies both the lower and the upper bound. However, the solution of the shell theory is not easy to obtain mathematically. Therefore, the other approach tries to approximate the stress distribution around the singularity by means of an approximation method such as the finite element method. Furthermore, the development of the new generation of computers that reduces enormously the computational time for this approach has increased the popularity of the finite element method. In addition, the finite element method can model the entire structure including the singularities; as a result, the interaction between singularities and the influence of a singularity over the entire structure can be studied. In contrast, the shell theory solution studies the singularity alone, i.e. the nozzle is isolated from the whole structure for the purpose of modeling. For all these reasons, the present study uses the finite element method to study the singularities of the pressure vessel.

3.1.2.1) DESCRIPTION OF THE FINITE ELEMENT METHOD

The finite element method has been frequently used to obtain approximate solutions for different kinds of engineering problems. Originally, this method was developed for the purpose of structural analysis; however, the application of this method quickly spreads into other fields of engineering. A brief historical comment about the finite element method can be found in the book of Reddy [24]. Also Zienkiewicz [31] in his book gives a summarizing of the different disciplines that have been involved in the creation of this method.

As a numerical method, the finite element method has the following characteristics:

1) Once the mathematical model of the problem is formulated, the whole domain of the problem is subdivided into discrete elements.

2) Within the discrete element, an algebraic function is used to approximate the solution of the problem.

3) The discrete elements also called finite elements are assembled such that the system of equations with a unique solution or eigenvalue problem can be obtained. Since the unknowns of this system of equations represent the degrees of freedom necessary to describe the behavior of the model, the solution of this system of equations implies the total definition of the model.

In order to applied the finite element method, it is necessary to formulate the mathematical model of the problem in the variational form. There are a lot of approaches to obtain the variational formulation such as the Ritz, Galerkin, least squares and collocation method. A more detail discussion concerning the variational formulation can be found in the book of Reddy [24]. However, for certain kind of problems such as structural analysis, the displacement approach is used very often and a detailed discussion about this topic can be found in the book of Zienkiewicz [31].

As an advantage, the general procedures of the finite element method can be applied to most of the engineering problems that require mathematical simulation. Furthermore, the mathematical aspects of the problem usually are simplified whenever the finite element method is used. However, choosing the adequate element (size and type) becomes critical for the accuracy of this method in different situations. Also depending on the complexity of the model,

sometimes the entire domain has to be subdivided into a considerable number of finite elements. As a consequence, a high computational cost can be associated with the application of the finite element method. In conclusion, the selection of the finite element can determine the efficiency of the finite element approach in a particular situation.

Basically, two types of elements have been chosen to perform the finite element analysis described here. They are the shell element and the three dimensional element.

Shell element: Some authors consider the shell element as a two dimensional (2-D) approximation of a degenerated three dimensional (3-D) element [Kant & Datye, 14]; i.e, by using appropriated shell theory in conjunction with the finite element method, a 2-D element can be developed to simulated the 3-D behavior of the shell model. Usually two basic assumptions are used; firstly, the quasi-normal direction of the shell remains straight and unchanged in length during the deformation process; secondly, the normal stress component perpendicular to the inplane components is assumed to be negligible. Moreover, there are two kind of shell elements that comply with the mentioned assumptions. Namely, they are the thin shell element and the thick shell element. For the thin shell element, the Kirchhoff assumption is applied; in other words, a normal section remains normal after the deformation process, this assumption is the equivalent of the Euler-Bernoulli assumption in the classical beam theory. As a matter of fact, the shear deformation in a plane with normal perpendicular to the normal direction is assumed to be zero. In contrast, the thick shell element uses the shear flexible theory; i.e. the normal direction does not necessarily remain normal after the deformation process. Consequently, shear deformation in a plane with normal perpendicular to the normal direction can be determined.

3-D solid element: The 3-D solid element is developed according to the three dimensional elasticity theory; i.e., three independent polynomials are used to interpolate the three independent displacements of each node. As a matter of fact, the nine components of strain and stress will be present in the finite element analysis. Incidentally, inside the family of the 3-D solid element there is a subgroup of elements named axi-symmetric solid element. As its name indicates, the axi-symmetric solid elements are developed for situations where the axi-symmetric condition exists, i.e. both the geometry and the loading conditions are symmetric with respect to an axis of symmetry. In this case, only two independent degree of freedoms are required to be specified within the analysis model. Usually, they are the displacements in the radial and the axial direction. However, this kind of element is different from the plane stress or

plane strain element because of the nonzero normal stress and strain components perpendicular to the plane of the symmetry, the circumferential stress and strain will be present. Obviously this kind of element requires less computational time than the general 3-D solid element.

Since the finite element approach uses the Gaussian Quadrature technique[Carnahan, Luther & Wilkers, 5] to perform the integration inside the computation of the stiffness matrix, the number of integration points is important in order to achieve the desired accuracy. In fact, there is a simple rule to determine the number of integration points required for certain degree of polynomials. However, in some situations it is preferred to reduce on purpose the number of integration points so that more realistic solutions according to the physics of the problem can be obtained. Actually, this kind of technique receives for name of the "reduced integration technique" [Zienkiewicz, 31]. In the finite element analysis of the shell structure, especially the thin wall structure, the shear stiffness matrix will most likely "shadow" the bending stiffness matrix. Actually this phenomenon is called "shear locking". As a consequence, the finite element analysis becomes numerically ill conditioned and erroneous results will be obtained. For this reason, the reduced integration is applied during the computation of the shear stiffness matrix. In the case of the 3-D solid element, the scheme of reduced integration is also recommended [ABAQUS theory manual, 1]. Since the problem of shear locking is related to the shell thickness, the numerically ill conditioned problem persists in the 3-D analysis. In addition, the reduced integration scheme requires less computational time than the full integration scheme. Therefore the finite element procedure becomes more efficient. For all these reasons, the present study tries to apply the reduced integration scheme whenever it is acceptable.

3.1.2.2) FINITE ELEMENT APPLICATION PROGRAM

There are finite element computer application programs available commercially. Actually, one of them named ABAQUS produced by Hibbitt, Karlson & Sorensen, Inc. has been used in the present study. Although the procedure of the finite element method is general, the detailed formulation may vary depending on the nature of the problem, i.e. the governing equations and the variables that are involved for each problem may be different from case to case. In this context, ABAQUS can handle a variety of problems; for example, static analysis, dynamic analysis, intermittent contact analysis, etc. Also ABAQUS can handle linear and nonlinear analyses. Moreover, a library of elements for different purposes is given in this program. A complete description of the ABAQUS finite element code can be found in the theory manual [1].

In the present study, the linear static analysis has been performed and different types of elements have been used to determine the applicability of each one. As a matter of fact a more detailed discussion concerning the selection of elements will be given in the following sections.

Like most finite element codes, ABAQUS requires the user to input the mesh of the model, the material properties, the boundary and the loading conditions so that the proper analysis can be performed. However, when the geometry of the model is complicated, for example in the case of a pressure vessel with a non-radial nozzle; likewise, when the topology of the finite element becomes very complicated such as a three dimensional 20 nodes element, the direct input to the finite element code becomes very tedious. Moreover, the interpretation of the finite element results sometimes requires complicated graphical presentation. For all this reason, a "Mechanical Computer-Aided Engineering" (MCAE) program named PATRAN [20] has been used to overcome these difficulties. More than a program of geometric construction, PATRAN is a complete system of MCAE that includes all the major features of the mechanical design process. To be more specific, PATRAN goes from the geometric modeling to the finite element analysis plus the image processing of the results. Furthermore, another important feature of PATRAN is the capacity to interface with almost every major finite element analysis code on the market and with the different computer aided design (CAD) programs. In other words, PATRAN can be used as a whole system by itself or in combination with other finite element application programs as part of a MCAE system. In the present study, PATRAN has been used

to build the geometric and analysis models. The resulting file is then processed by the finite element code. Finally, the finite element results are interpreted by using the PATRAN program.

In the case of the support, the geometry of the support is similar to the non-radial nozzle. Also, the same shell theory applies as in the case of the nozzle. Actually, the support is constructed in such a manner that the joint between the vessel and the support becomes tangential; as a consequence, the membrane theory assumption can be applied in this case. However, it is desired to look at the influence of the support inside the whole structure. Using the same criterion as has been discussed for the nozzle, the same approach will be used for stress analysis of the support, i.e., the finite element approach will be used with the mentioned computer codes.

3.1.2.3) APPLICATION OF THE FINITE ELEMENT METHOD ON A SPHERICAL VESSEL

Due to the geometric complexity of the spherical vessel, it was desired to have an approximate stress distribution of the whole structure so that a region with singularity could be identified. Thus, a first attempt to analyze the whole spherical vessel using lower order elements was performed. Also, the capacity of the computer codes (PATRAN & ABAQUS) for solving this kind of problem was explored. The model called Vessel1 (see Fig.3.4) has the following geometric characteristics:

Table 3.1: Geometric Characteristic of Vessel1

Component	Diameter(in.)	Thickness(in.)	Position
Vessel	120.0	1.0	[2]NA
[1]Nozzle1	12.0	0.492 (Sch 60)	Non radial
[1]Nozzle2	12.0	0.492 (Sch 60)	Radial
Nozzle3	2.0	0.3 (Sch 160)	Top
Nozzle4	2.0	0.3 (Sch 160)	Bottom
Supports	6.0	NA	NA

[1] - Both Nozzle1 and Nozzle2 had a reinforcement of diameter = 24.0 in. × 1.0 in. of thickness

[2] - Not applicable.

For the purpose of the finite element analysis , the element S4R5 [ABAQUS user manual, 2] from the ABAQUS element library has been used. Basically, the S4R5 is a thin shell linear element with four nodes per element. Furthermore, each node has five degree of freedom: three displacement and two rotational degree of freedom. All the quad elements, four nodes shell elements, in ABAQUS are shear flexible elements. Nevertheless, for thin shell application the Kirchhoff assumption is imposed approximately by means of the penalty method [ABAQUS,

theory manual, 1]. A design pressure of 300 lb/in^2 was applied to the centroid of each element. Also, the nodes corresponding to the support region were totally restricted from displacement, in order to look at the approximate stress distribution of the whole vessel and the location of the singularities. A graphical presentation of the von Mises stress distribution over the vessel at the bottom surface is obtained by means of PATRAN (Fig.4.1 & 4.2).

3.1.2.4) FINITE ELEMENT ANALYSIS OF AN EXPERIMENTAL MODEL

In order to determine the reliability of the finite element method and the applicability of different elements, the finite element analysis of an experimental model was performed. The experiment model consisted of a spherical vessel with three nozzle and the experiment was performed by S.S. Gill, R. Kitching and R.T. Paine [10]. The object of the experiment was to measure the stress distribution around a pad reinforced nozzle of a spherical vessel.

In fact, there are several kinds of reinforcement methods such as the integral type reinforcement; however, the pad reinforced method (Fig. 3.5) is the most popular one in the petroleum or chemical industry because of the simple construction and low cost of the reinforcement. Furthermore, any nozzle larger than three inches in diameter shall be reinforced, according to the ASME, Pressure Vessel and Boiler Code [ASME, 22].

3.1.2.4.1) DESCRIPTION OF THE EXPERIMENTAL MODEL

As was mentioned before, an experimental model of a pad reinforced nozzle has been chosen for the present study. Moreover, the experimental model had the following characteristic [Gill, 10]:

Table 3.2: Geometric Characteristic of the Experimental Model

Component	Diameter(in.)	Thickness(in.)	Position
Vessel	72.0	0.5	[5]NA
[1]Nozzle1	16.0	0.5	Top (Radial)
[2]Nozzle2	8.0	0.375	Radial
[3]Nozzle3	24.0	0.75	Bottom (Radial)
[4]Supports	4.0 ×5.0	0.5	NA

[1] - Nozzle1 had a reinforcement of diameter = 32.0 in. × 0.375 in. of thickness

[2] - Nozzle2 had a reinforcement of diameter = 16.25 in. × 0.5 in. thickness

[3] - Nozzle3 had a reinforcement of diameter = 42.0 in. × 0.5 in. thickness

[4] - The supports were brackets attached to the vessel.

[5] - Not applicable.

Steel having a Young's Modulus of 28.8 × 10^6 lbf/in^2 and a Poisson's Ratio of 0.275 has been used to construct the experimental model.

The experiment was performed by Gill, Kitching & Paine [10] as the following. Firstly, electrical resistance strain gauges were attached to the specimen with epoxy adhesive; to be specific, the strain gauges were located at the outside and the inside surface of the specimen in

symmetric positions. Furthermore, the strain gauges were distributed with regular separations in the
meridianal and the circumferential direction. Secondly, the specimen was loaded with water and the testing pressure of 618 lbf/in^2 was obtained by means of a air pump. Finally, the experimental results were collected by means of a digital data acquisition system.

3.1.2.4.2) ASSUMPTIONS AND THE FINITE ELEMENTS USED IN THE ANALYSIS OF THE EXPERIMENTAL MODEL

Before the discussion of the analysis procedure, it is important to mention some assumptions used during the process.

Although the reinforcement pad was not an integral part of the vessel (Fig.3.5), the possible gap between the shell and the reinforcement pad was neglected. In other words, the finite element model was built without allowing relative movements between the shell and the pad. Since the mentioned gap could be opened or closed according to the loading situation, a nonlinear analysis would have to be performed to simulate the model. However, it was almost impossible to determine the separation between this gap, therefore, the assumption of no gap between the pad reinforcement and the shell was necessary to allow for the finite element analysis. (T. Oikawa & T. Oka [29] discussed the validity of this simplified model based on the statistical approach.) Since the geometric configuration of all the nozzles were similar in the same way as the trends of the stress distribution around the nozzle, the comparison between the experimental results and the finite element results have been focused at the nozzle with diameter = 16.0 inch. Furthermore, it was observed in the experimental results that the major variation of stress occurred at the outside surface of the reinforced pad and at the outside surface of the shell surrounding the reinforced pad. Therefore, graphic results of point-to-point comparison have been done at this region to assure the reliability of the finite element model.

Several elements have been used to perform the stress analysis of the experimental model and they are summarized in the following table:

Table 3.3: Finite Element Used in the Stress Analysis of the Experimental Model

Element*	Classification	Topology	Characteristic
S4R5	Shell element	4 node	Linear interpolation between nodes. Shear flexible element with reduced integration. Kirchhoff assumption approximation imposed by the penalty function.
S8R5	Shell element	8 node	Quadratic interpolation between nodes. Shear flexible element with reduced integration. Kirchhoff assumption approximation imposed by the penalty function.
S8R	Shell element	8 node	Quadratic interpolation between nodes. Shear flexible with reduced integration. Recommended for thick shell application.
C3D8	3-D element	8 node	Linear interpolation between nodes. Reduced integration is used.

* ABAQUS description

Table 3.3 (continued): Finite Elements Used in the Stress Analysis of the Experimental Model

Element	Classification	Topology	Characteristic
CAX8R	3-D axi-symmetric element	8 node	Quadratic interpolation between nodes. Reduced integration is used.
C3D20R	3-D solid element	20 node	Quadratic interpolation between nodes. Reduced integration is used.

3.1.2.4.3) PROCEDURE OF ANALYSIS

The first element used to perform the stress analysis was the S4R5, the objective was to look at the approximate stress distribution in the whole structure. Furthermore, the structure was discretized so that the region near the singularity would have a more refined mesh (Fig. 3.6). The zero displacement boundary condition was imposed at the nodes of the support. After the finite element model had been processed by ABAQUS, the distribution of circumferential stress and meridianal stress throughout the structure was displayed by the PATRAN program and the nozzles and supports were identified as the singular regions. In addition, the circumferential stress and the meridianal stress were plotted against the meridianal distance for the nozzle of diameter = 16.0 in. (Fig. 4.3.1 & Fig. 4.3.2) so that the finite element results could be compared to the results from the experimental model. Actually, a more refined mesh was used near the nozzle to observe if there would be any convergence in the finite element results. (Fig. 4.3.3 & Fig.4.3.4)

The second element used to perform the stress analysis was the S8R5. Since the singular region has already been identified with the previous element, more attention was focused on the stress distribution around the nozzle of diameter = 16.0 in. The zero displacement boundary condition was also applied at the nodes of the support. Similar graphics to that Fig. 4.3.1 were developed for the element S8R5. (Fig. 4.3.5 & Fig. 4.3.6).

The third element used to perform the stress analysis was the C3D8. This element was used to obtain a better result near the welded region at the end of the reinforcement pad due to fact that the shearing stress was expected to be important in the region of the weld where the change of thickness occurred. Furthermore, the concept of multi-point constraints based on the Kirchhoff assumption was introduced here to allow a transition of the 3-D elements to 2-D elements. As a matter of fact, a 3-D mesh in the area around the nozzle and a 2-D mesh in a region far from the nozzle (Fig. 3.7) has been used in this analysis. Finally, the stresses around the nozzle of diameter = 16.0 in. was compared with the results from the experimental model (Fig. 4.3.7 & 4.3.8).

The fourth element used to perform the stress analysis was the CAX8R. At this point attention was focused at the stress distribution around the nozzle with the pad reinforcement.

An axi-symmetric model was built using this kind of element (Fig. 3.8). The boundary condition imposed in this model reflected the condition of symmetry (Fig. 3.9). Since the axi-symmetric model required less computational time than the other model, a highly refined mesh was used. It was expected that this model would provide the best results for comparison with the experimental model (Fig. 4.3.9 & 4.3.10).

The fifth element used to perform the stress analysis was the C3D20R. Although the axi-symmetric model might be accurate and efficient, it was limited to a certain type of geometry and loading condition. Therefore, a more general 3-D model was built by using the general 20 nodes 3 dimensional elements (Fig. 3.10). Results were collected and compared with the experimental results (Fig. 4.3.11 & 4.3.12). In facts, only one fourth of the entire section was necessary to simulate the entire model by imposing the correspondent symmetric conditions at the boundaries. Moreover, the concept of multi-point constraints [PATRAN, 20] was applied to build another model with a combination of the C3D20R and the S8R5 elements(Fig. 3.11). The idea was to simplify the model as much as possible and reduce the computational time. Again, the results were collected and compared with the experimental results (Fig. 4.3.13 & 4.3.14).

Finally, a model similar to the mentioned 3-D model was built by using the thick shell element (Fig. 3.12) S8R to verify whether the simplified two dimensional model would give reasonable results (Fig. 4.3.15 & 4.3.16).

Once the applicability of the element was studied, the most adequate element was used to perform the analysis with a pressure loading of 10% higher. As it was mentioned before, the ASME code required that a new vessel should be tested for a pressure of 15% higher than the operating pressure. However, in practice, only a pressure loading of 10% higher was used in the acoustic emission testing to avoid the misfire of the safety valve. The results from this model were obtained and represented in figures 4.4.1 and 4.4.2.

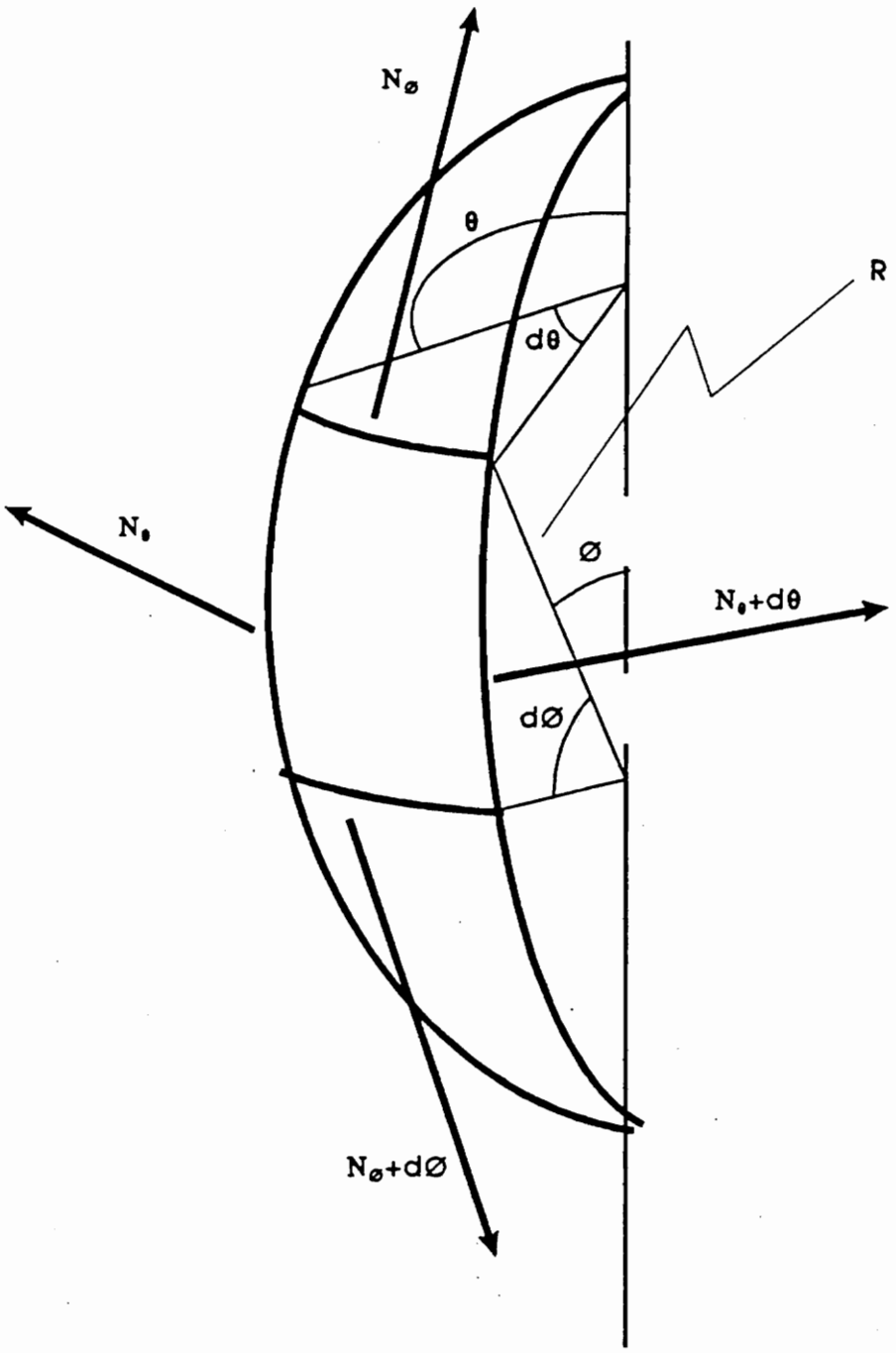

FIG. 3.1
A DIFFERENTIAL ELEMENT
OF A SPHERICAL VESSEL

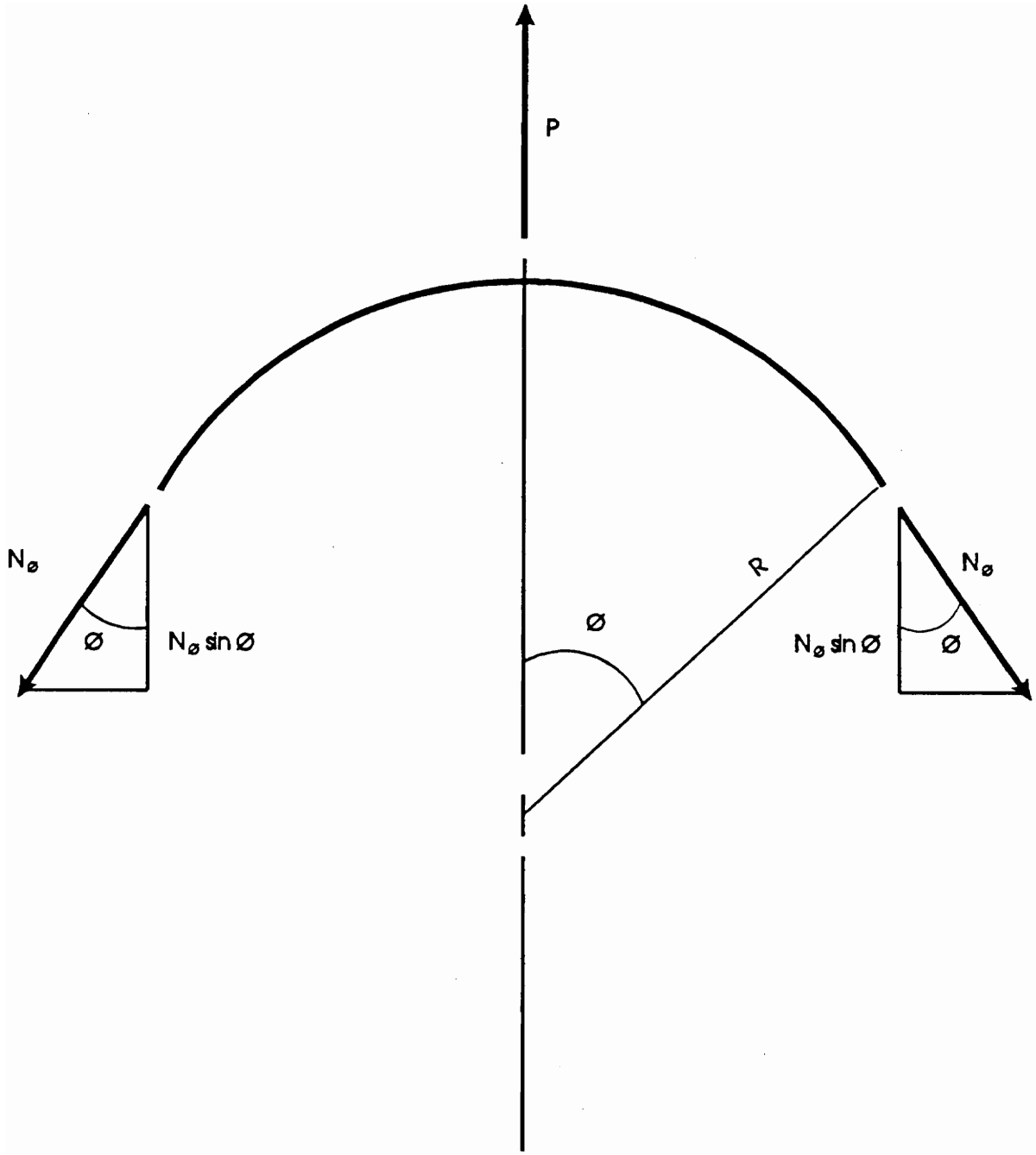

FIG. 3.2
DIAGRAM OF EQUILIBRIUM
AT THE VERTICAL DIRECTION OF A SHELL

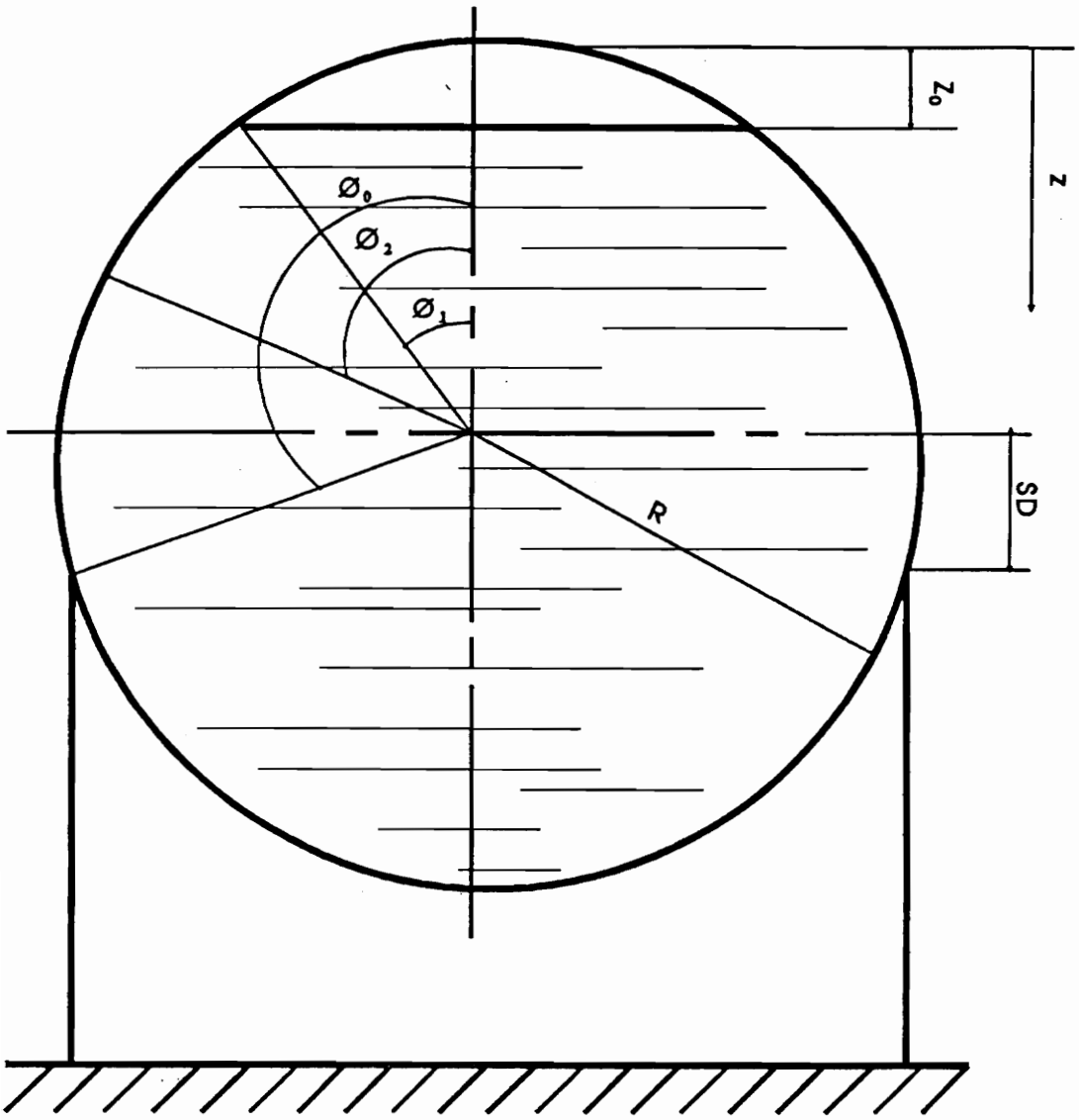

FIG. 3.3
SPHERICAL PRESSURE VESSEL LOADED WITH HYDROSTATIC AND VAPOR PRESSURE

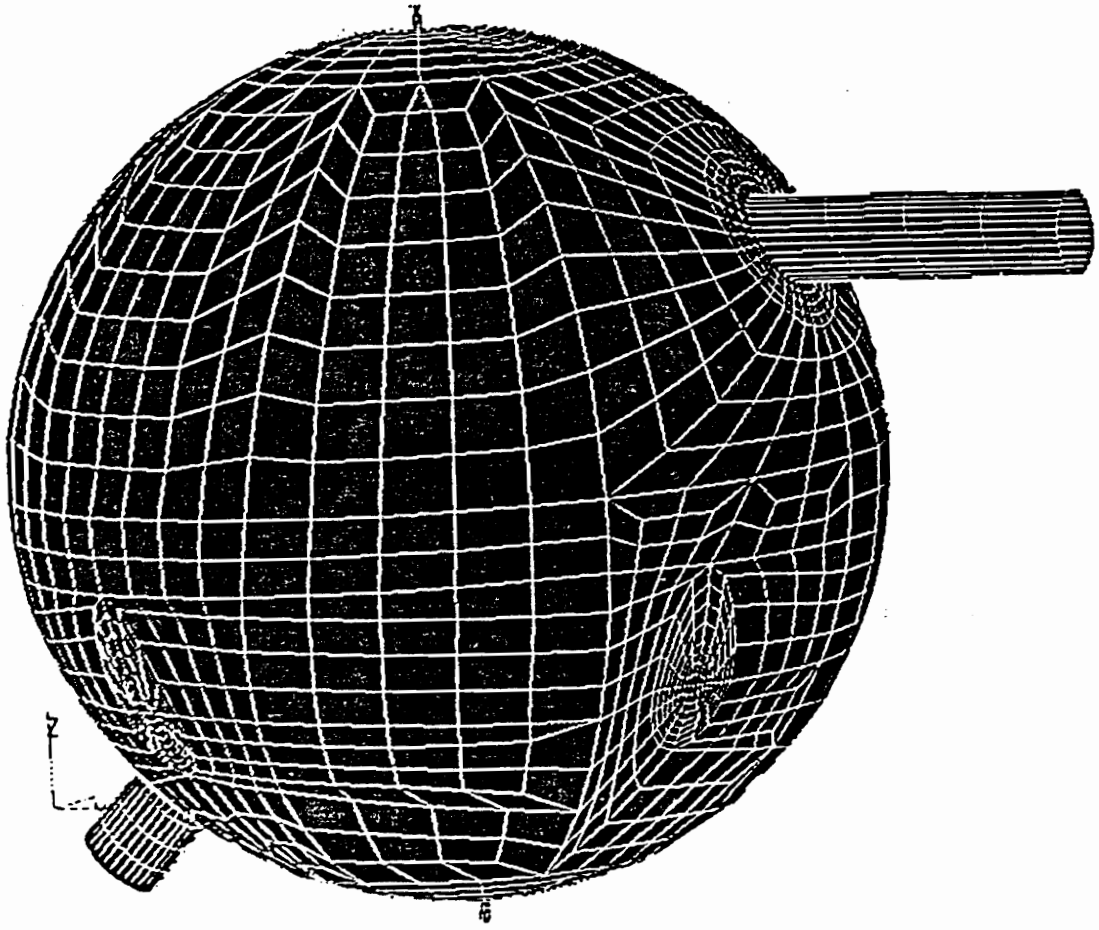

FIG. 3.4 FINITE ELEMENT MODEL OF VESSEL1
(MESHED WITH LINEAR SHELL ELEMENT S4R5)

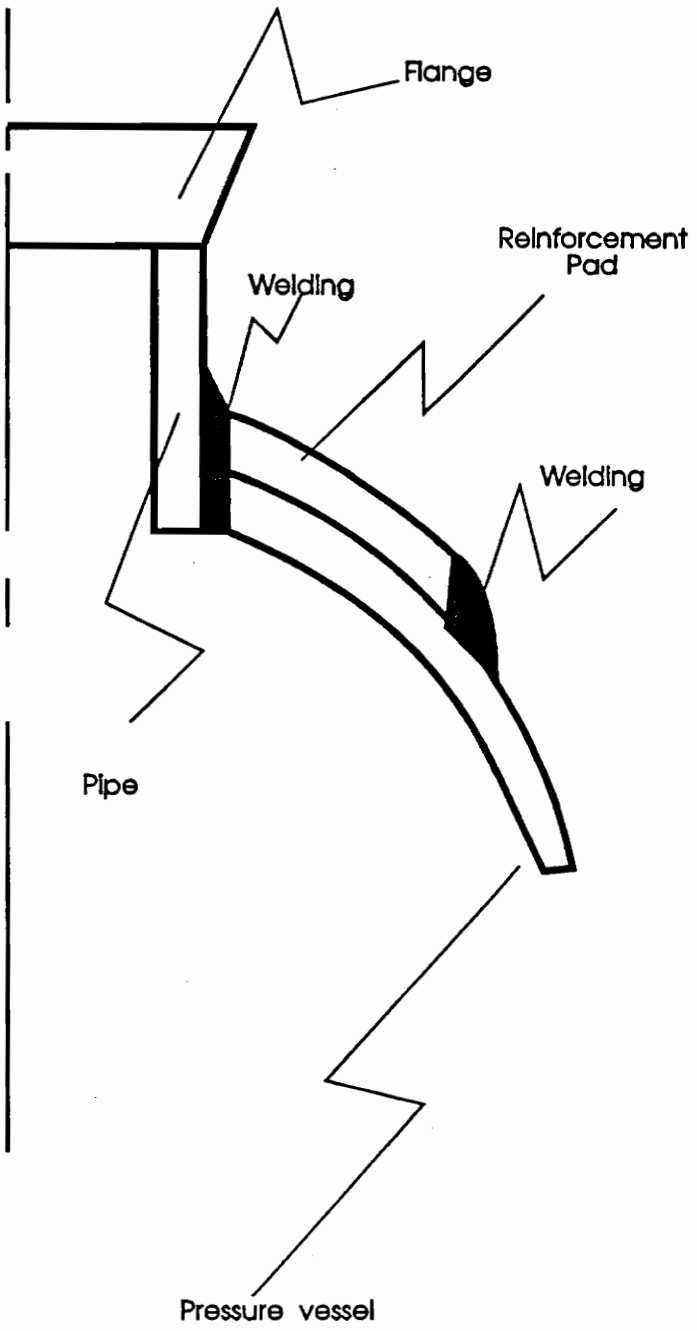

FIG. 3.5
REINFORCEMENT OF A NOZZLE

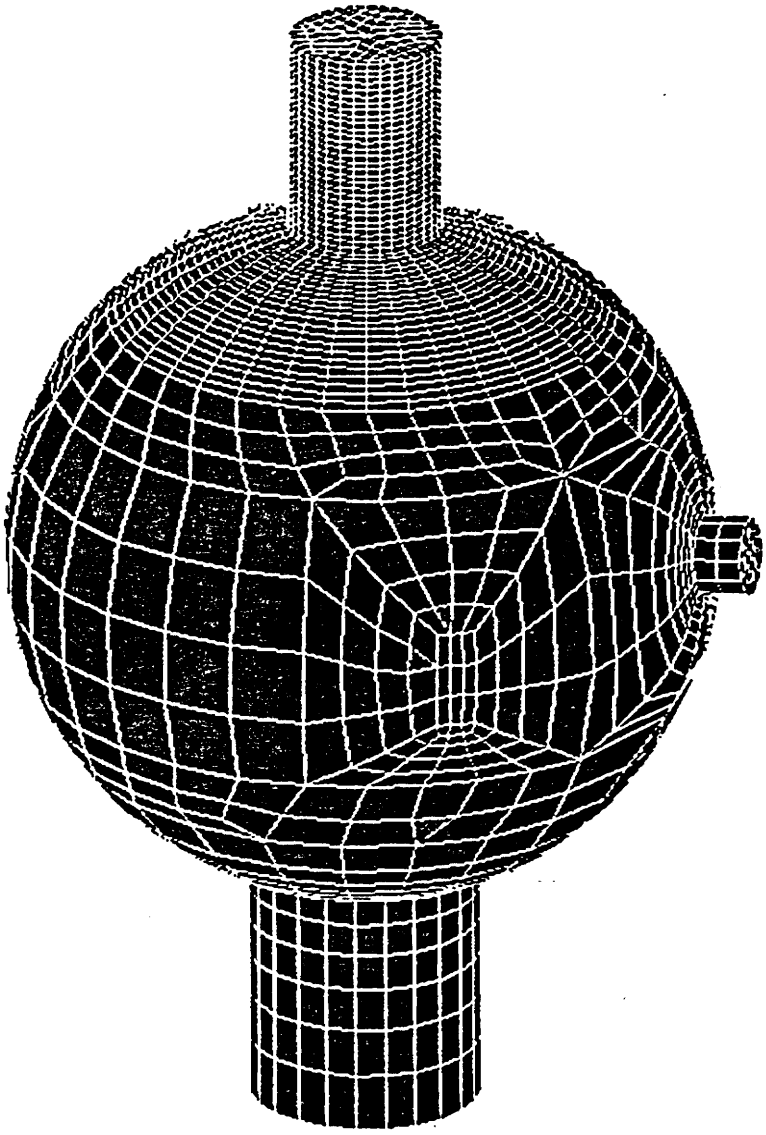

FIG. 3.6 FINITE ELEMENT MODEL
OF THE EXPERIMENTAL VESSEL
(MESHED WITH LINEAR SHELL ELEMENT S4R5)

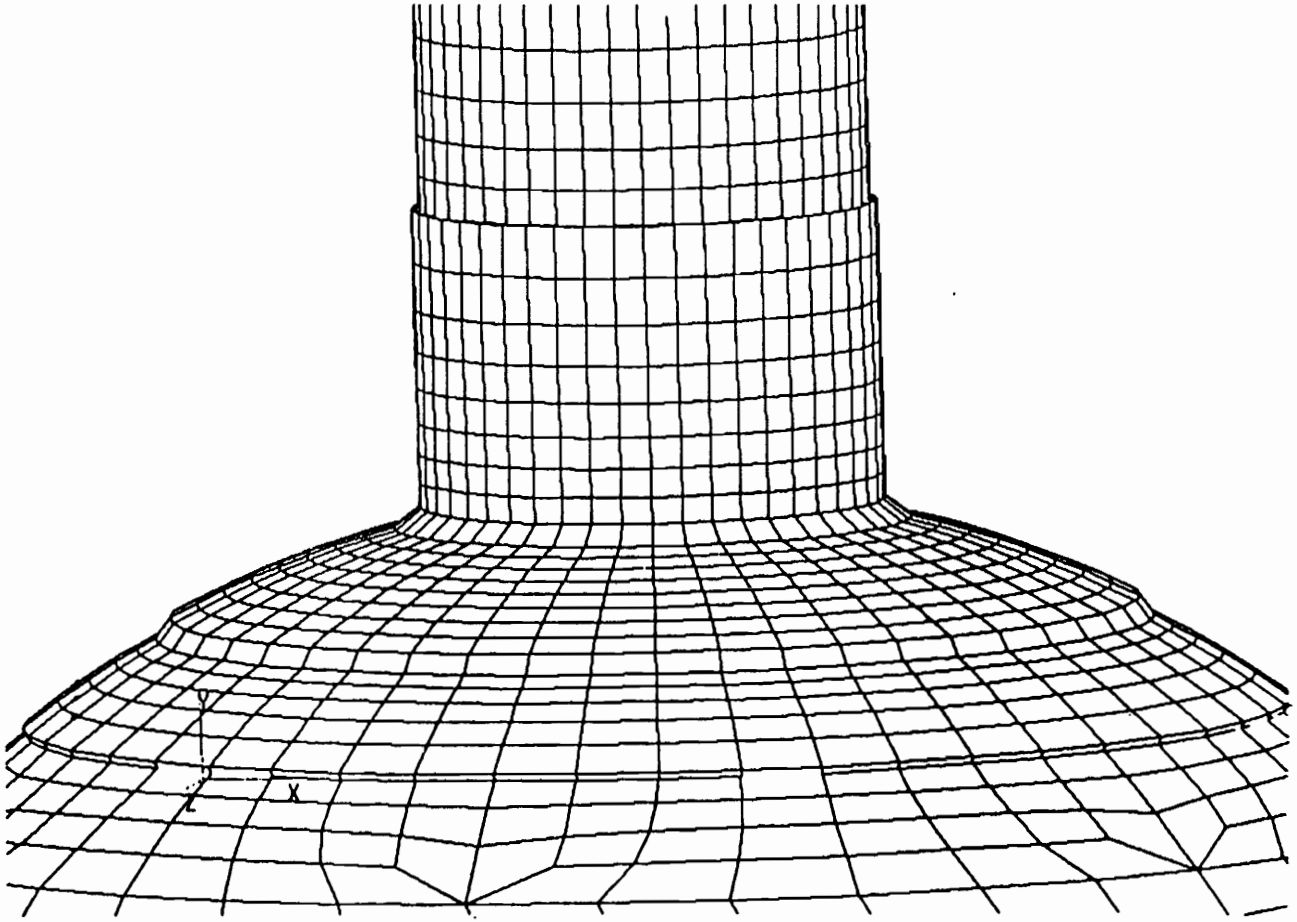

FIG. 3.7 FINITE ELEMENT MODEL
OF THE 16 IN. DIAMETER NOZZLE
(MESHED WITH LINEAR 3-D AND 2-D ELEMENT)

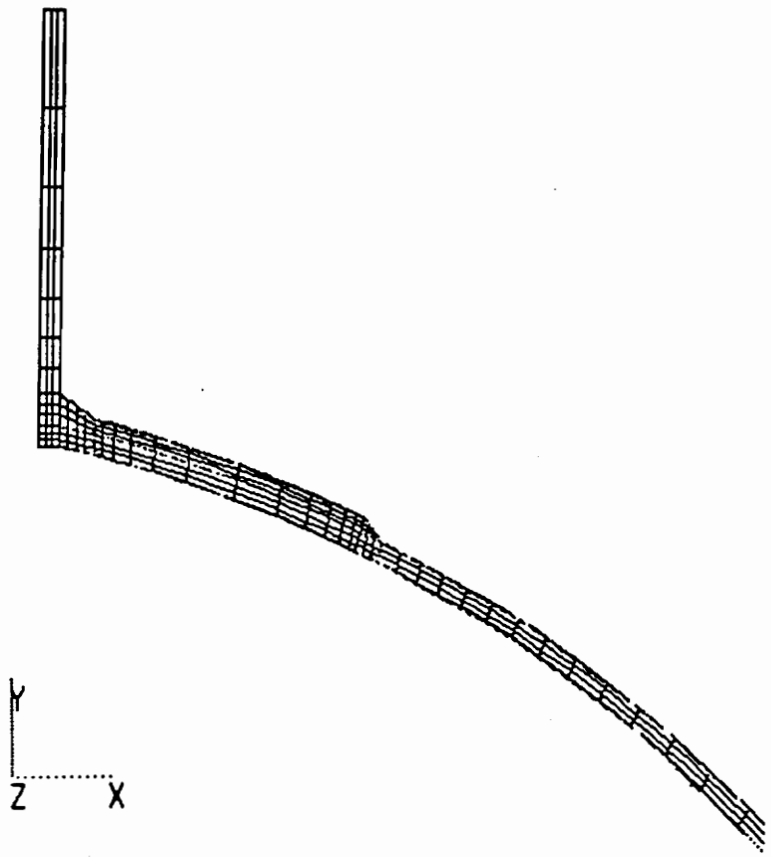

FIG. 3.8 FINITE ELEMENT MODEL
OF THE 16 IN. DIAMETER NOZZLE
(MESHED WITH AXI-SYMMERTRIC ELEMENT)

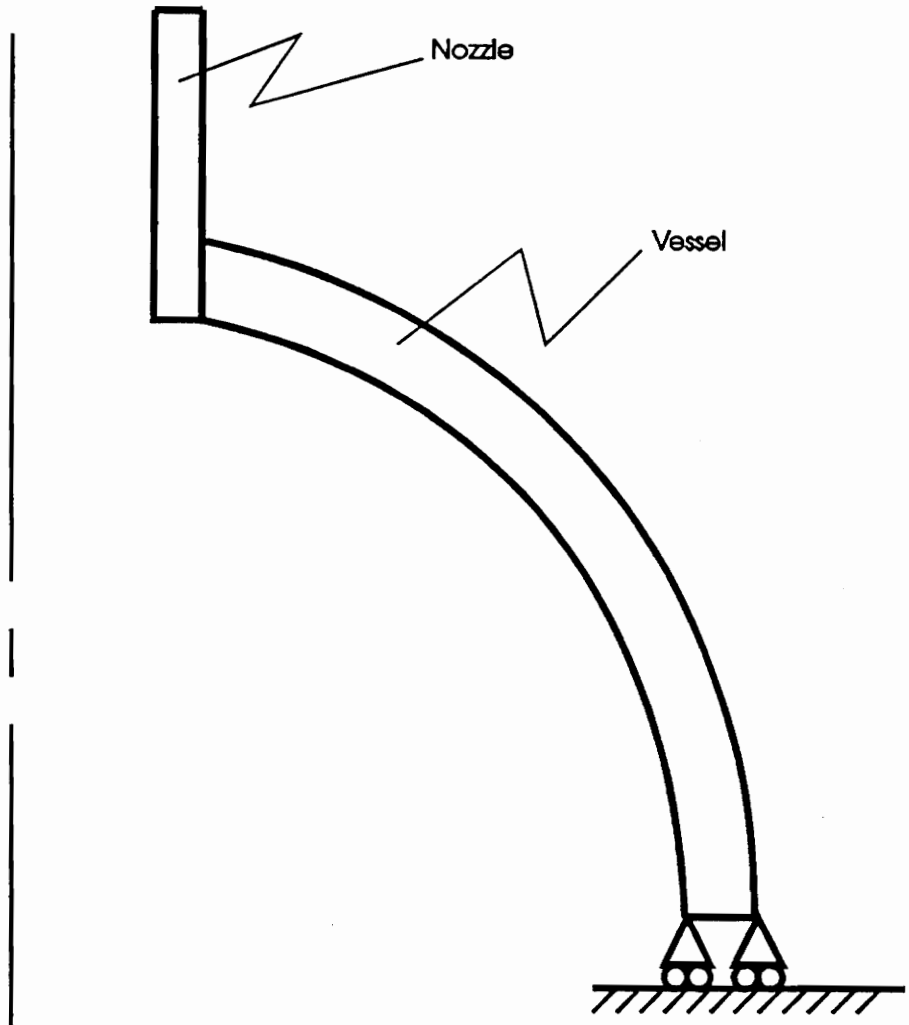

FIG. 3.9
BOUNDARY CONDITION OF THE
AXIS-SYMMETRIC MODEL

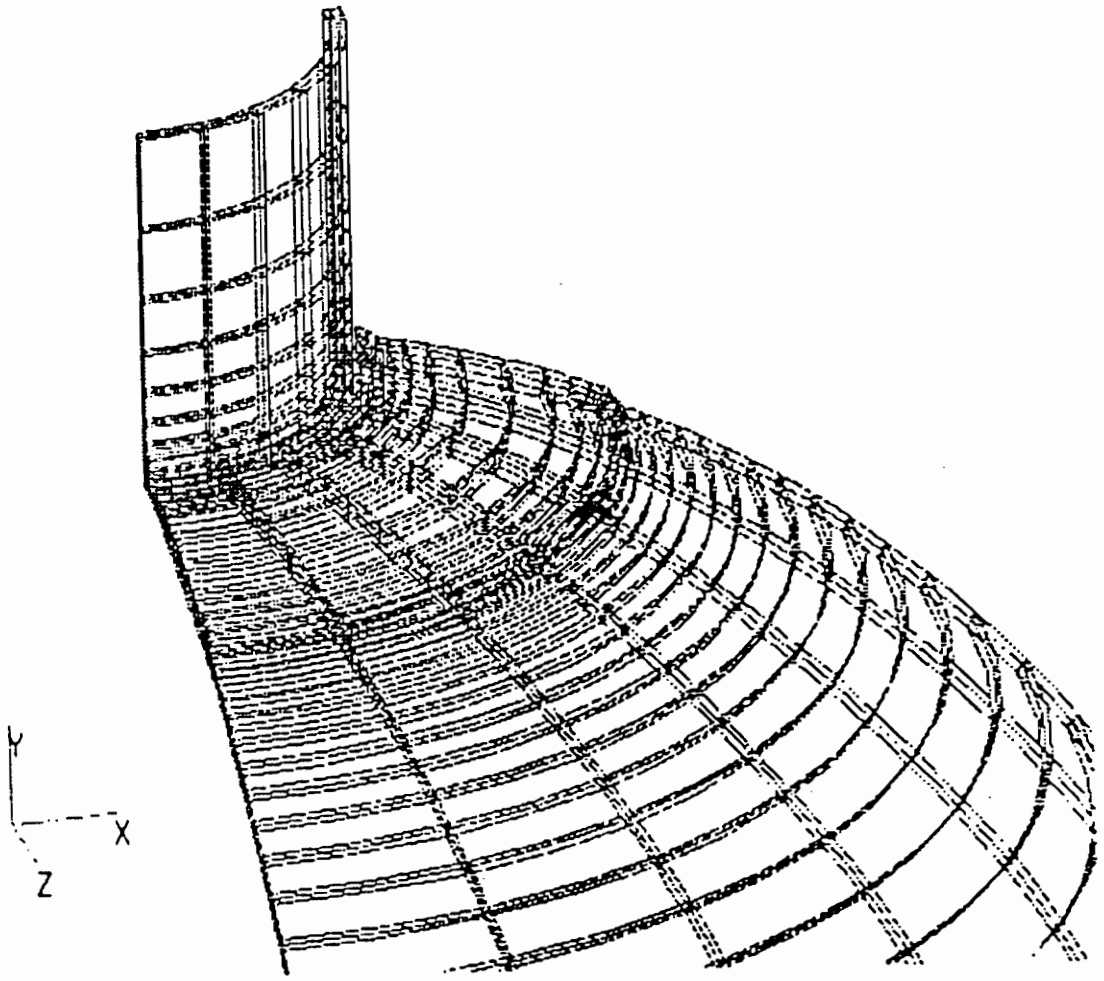

FIG. 3.10 FINITE ELEMENT MODEL
OF THE 16 IN. DIAMETER NOZZLE
(MESHED WITH 3-D QUADRATIC ELEMENT C3D20R)

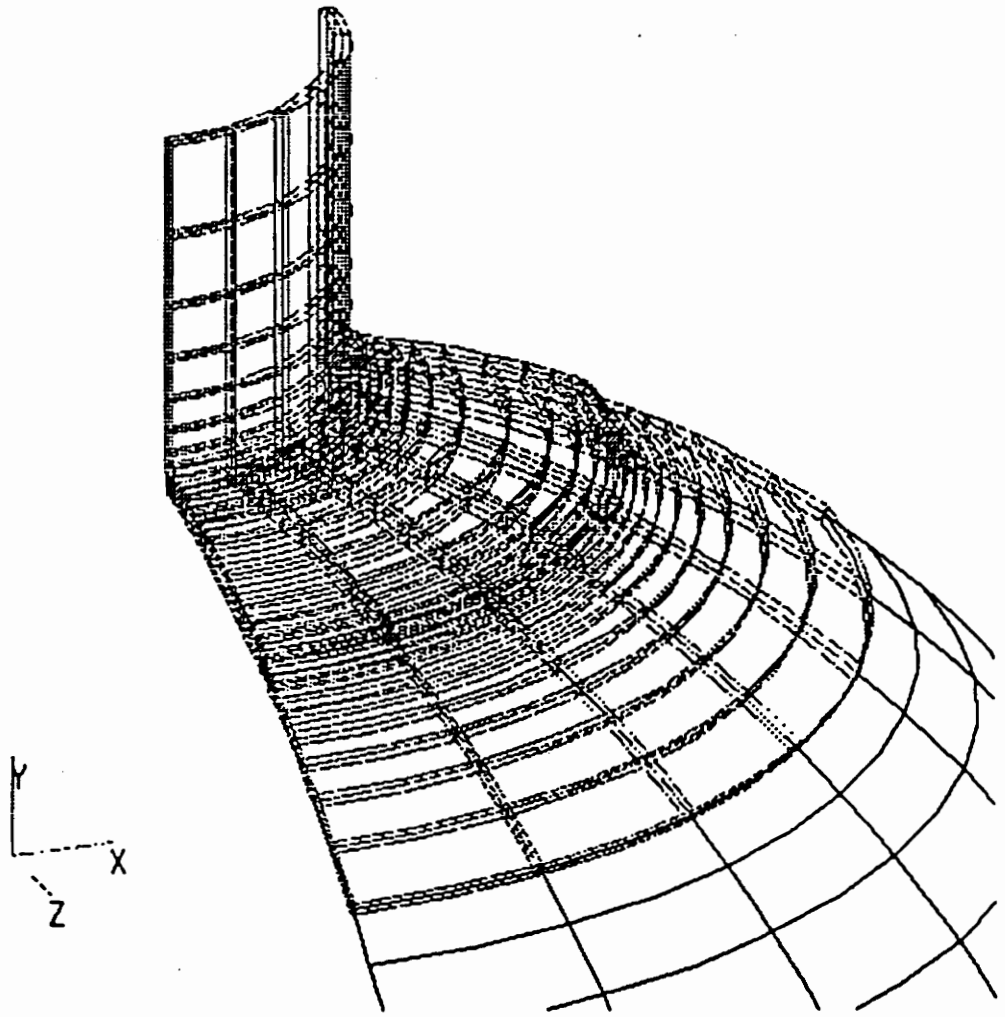

FIG. 3.11 FINITE ELEMENT MODEL
OF THE 16 IN. DIAMETER NOZZLE
(MESHED WITH 3-D AND 2-D QUADRATIC ELEMENT)

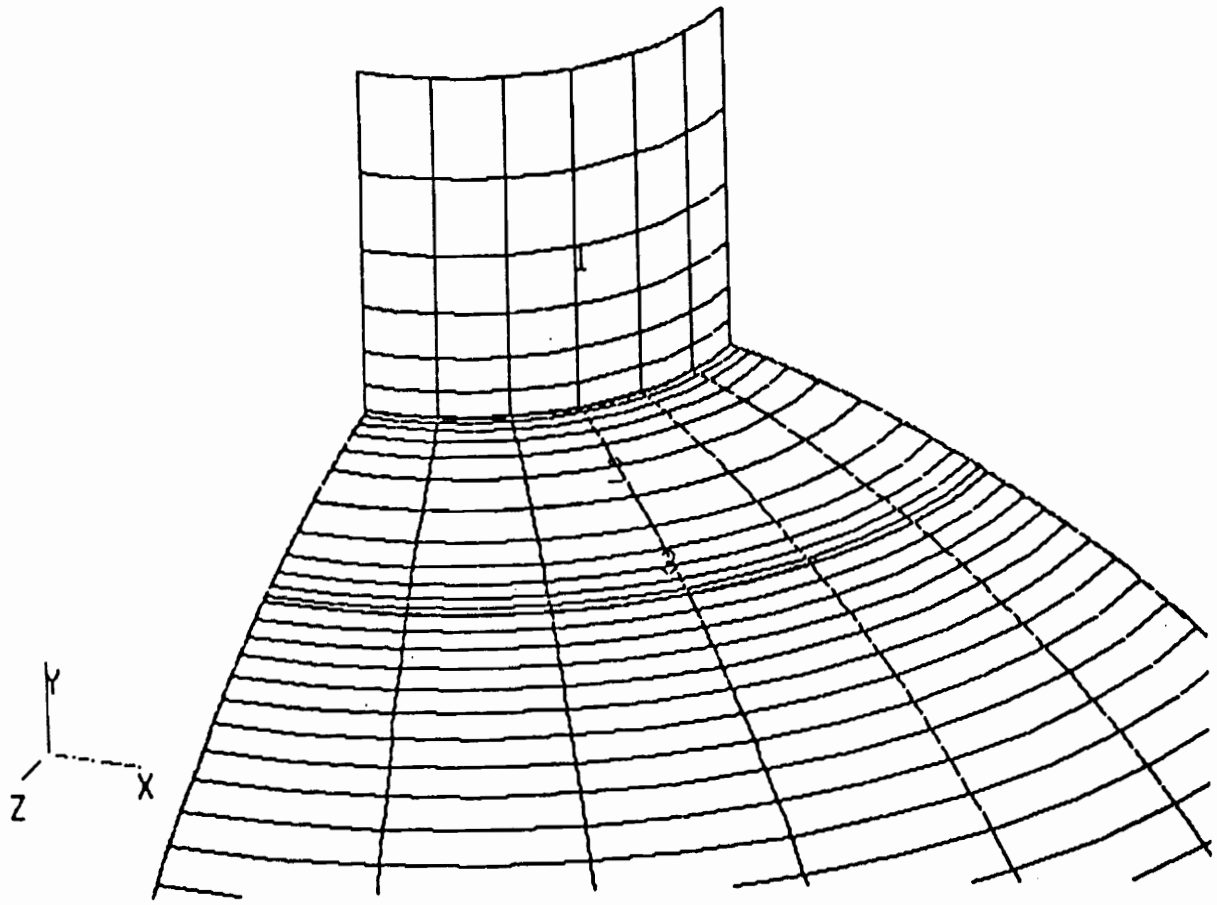

FIG. 3.12 FINITE ELEMENT MODEL
OF THE 16 IN. DIAMETER NOZZLE
(MESHED WITH QUADRTIC SHELL ELEMENT S8R)

4) DISCUSSION OF THE RESULTS:

4.1) SPHERICAL PRESSURE VESSEL WITH HYDROSTATIC PRESSURE:

In Figures 4.1.1 and 4.1.2 the stress analysis results of a spherical vessel based on the membrane solution were presented. These graphs represent the meridianal stress and the circumferential stress on the spherical vessel respectively. Since the membrane solution assumes a zero stress variation over the thickness of the vessel, the results becomes very simple to display. Actually, in Figures 4.1.1 and 4.1.2, the stresses are plotted against the distance Z measured from the top of the vessel (Fig. 3.3). As can be observed the stress varies slightly as the distance Z increased. A maximum variation of 20 % was observed at the area adjacent to the support. However, it is difficult to draw conclusions concerning the area around the support, because the membrane solution neglects the presence of the bending stress. In other areas of the spherical pressure vessel, the hydrostatic pressure does not affect significantly the stress distribution; actually, the slope of the stress curve versus distance Z is almost zero in these regions. Therefore, a membrane analysis including the vapor pressure and the hydrostatic pressure should be used for a very big vessel. Since the variation of stress distribution due to the hydrostatic pressure is almost insignificant, cracks or imperfections located within the vessel will not have a different behavior because of the liquid level. Consequently, the hydrostatic pressure should not affect significantly the acoustic emission of the structure.

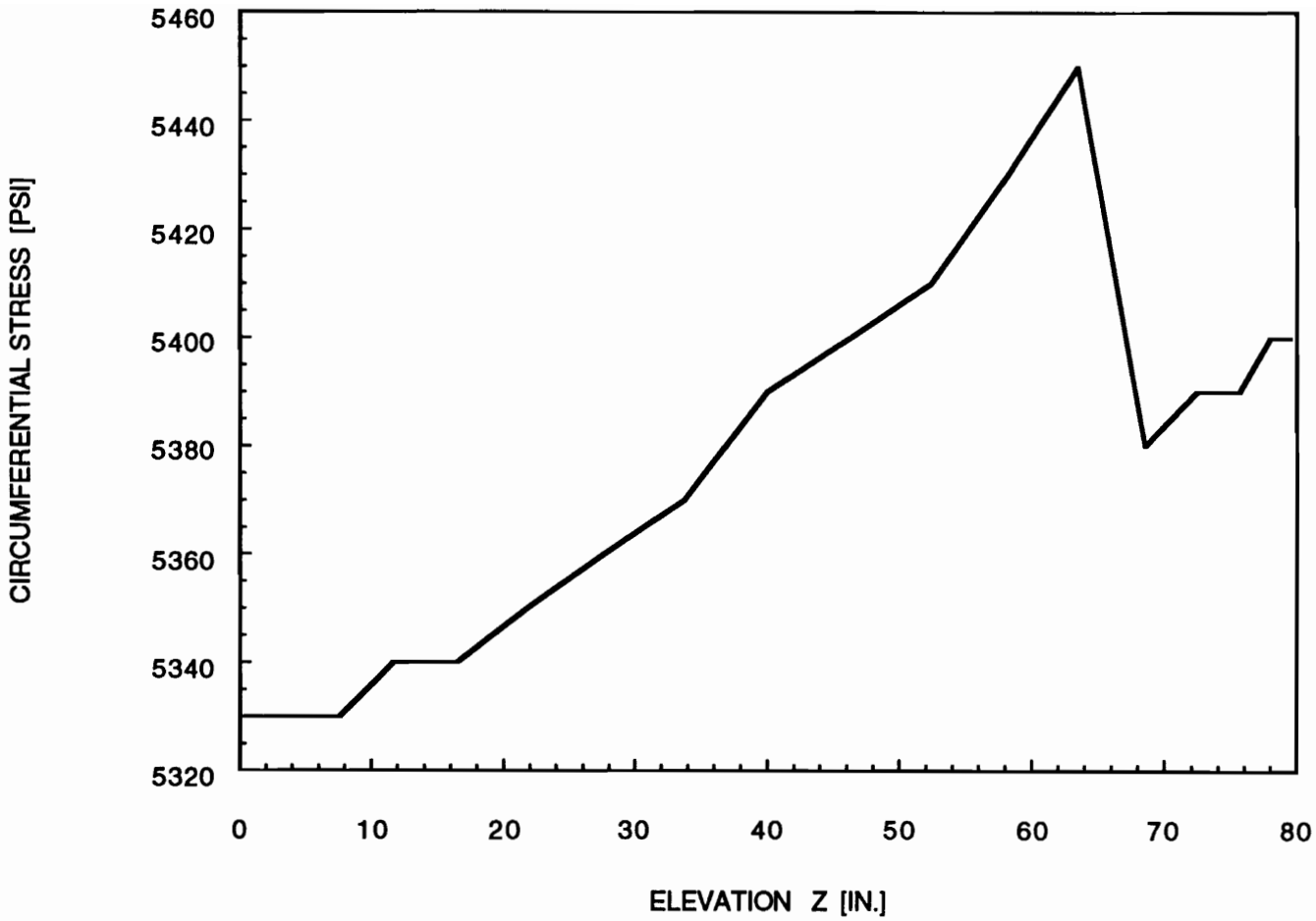

FIG. 4.1.1
CIRCUMFERENTIAL STRESS VS DISTANCE Z

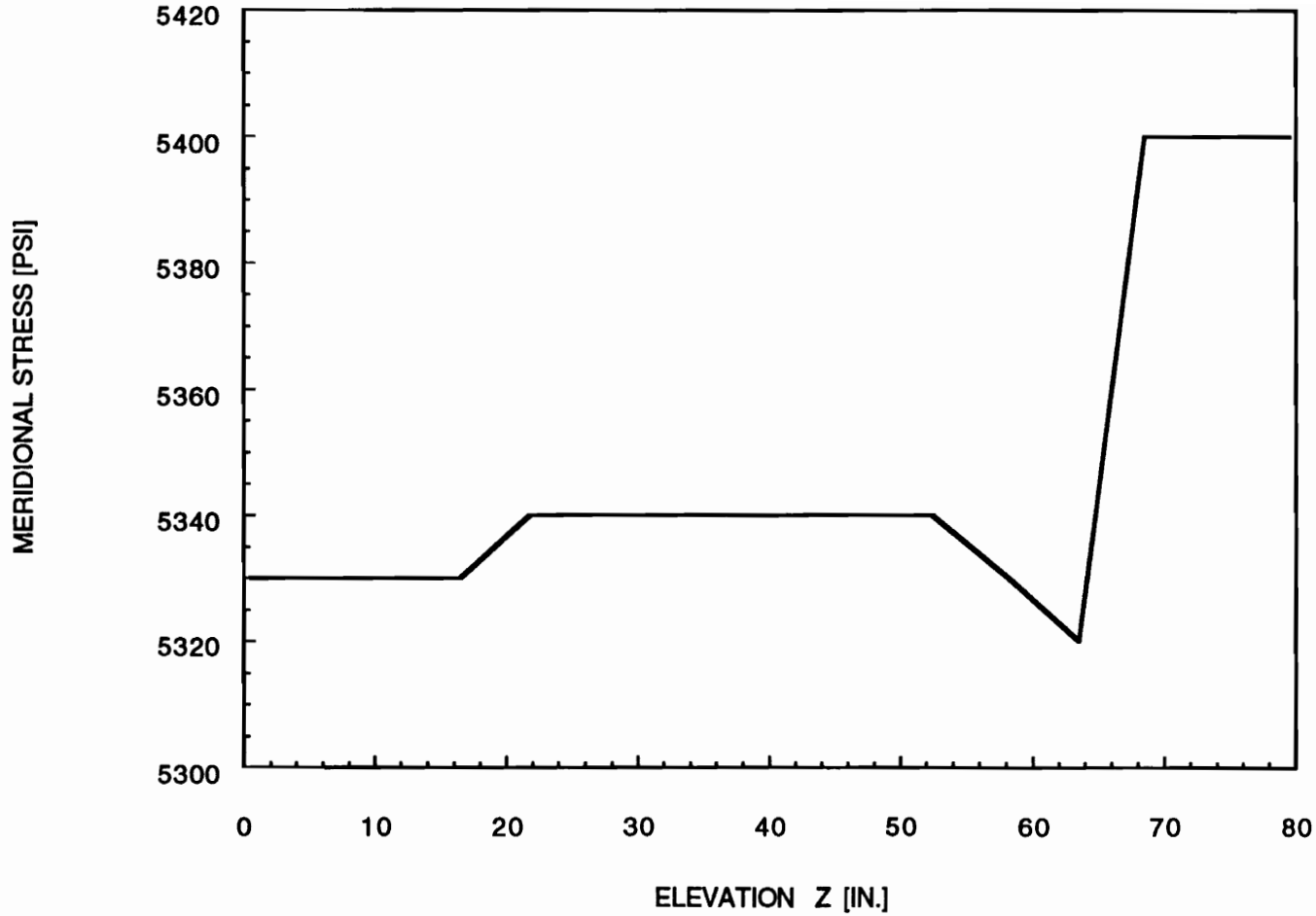

FIG. 4.1.2
MERIDIANAL STRESS VS DISTANCE Z

4.2) STRESS DISTRIBUTION OVER A SPHERICAL VESSEL WITH NOZZLES AND SUPPORTS:

According to the membrane stress analysis, the pressure vessel support represents an area of singularity. However, the membrane stress analysis cannot handle properly this singularity because the bending stress is neglected. Therefore, the finite element approach was used to handle this kind of problem. As it was mentioned in chapter 3.1.2, the stress analysis of the model Vessel1 was performed by ABAQUS and the results were processed by PATRAN. Since the object of this analysis was to explore the capacity of the program and to have a general description of the singularity of the pressure vessel. The most simple shell element S4R5 (Table 3.3) has been used.

Concerning the capacity of ABAQUS and PATRAN, several observations can be made. Since the linear elastic analysis is the simplest case within the finite element analysis, ABAQUS does not have any trouble handling this kind of problem. However, the input to and output from ABAQUS becomes very tedious because of the geometric complexity. By using PATRAN, the input to ABAQUS becomes much more simple. Since PATRAN possesses a lot of geometric construction features, for instance the function "project" that determines the projection of a plane onto a three dimensional body, the complicated geometric calculation of the intersection between a cylinder and a sphere has been avoided. Moreover, PATRAN allows the rotation of the object under construction to provide a complete visualization from different angles. During the construction of the model Vessel1, geometric errors such as the nozzle location, have been avoided thanks to this important aspect of PATRAN. Another major difficulty in the finite element approach is the interpretation of results. In the case of the model Vessel1, approximately 3000 elements have been used to construct the finite element model; as a consequence, a large output file is obtained. The computer program PATRAN is particularly useful in this kind of situation where the visualization of data is concerned. Different colors are used to represent different magnitude of stress (Fig. 4.2.1 and 4.2.2). As a consequence, a stress distribution mapping can be obtained and the singularities within the structure can be identified immediately.

Due to the fact that structures with different geometries are involved in the construction of the model Vessel1. The von Mises stress has been used as a parameter to identify the singularities of the pressure vessel (Fig. 4.2.1 and 4.2.2). It can be observed that the regions near the nozzle and the support are areas of singularities by the colors of these areas which are different to the rest of the structure. As a consequence, imperfection found in this area should behave differently with respect to an imperfection within the rest of the vessel; although the same load of pressure has been applied to the vessel.

In chapter 2, according to the Kaiser effect, there is a intrinsic relation between the load level and the acoustic emission that can be obtained from a specimen under testing; therefore, the nonuniform stress distribution inside the structure must have some consequence on the acoustic emission. According to the "MONPAC" (Monsanto Physical Acoustic Corporation) procedure, the amount of acoustic emission energy obtained from a specific area is compared to a set of experimental data to determine whether there is a hazardous imperfection within this area. However, this set of experimental data has to be obtained under a certain condition of loading. Therefore, the question immediately arises from the results of Vessel1 whether the interpretation of the acoustic emission testing results in the areas of singularity is credible. In other words, the loading condition under which the acoustic emission testing is performed, may or may not satisfy the requirement of the "MONPAC" (Monsanto Physical Acoustic Corporation) procedure. Nevertheless, before getting into a more detail discussion about the influence of the stress distribution on the interpretation of the acoustic emission testing results, it is worthwhile to discuss the accuracy of the finite element approach which constitutes the principle instrument of analysis for this present study.

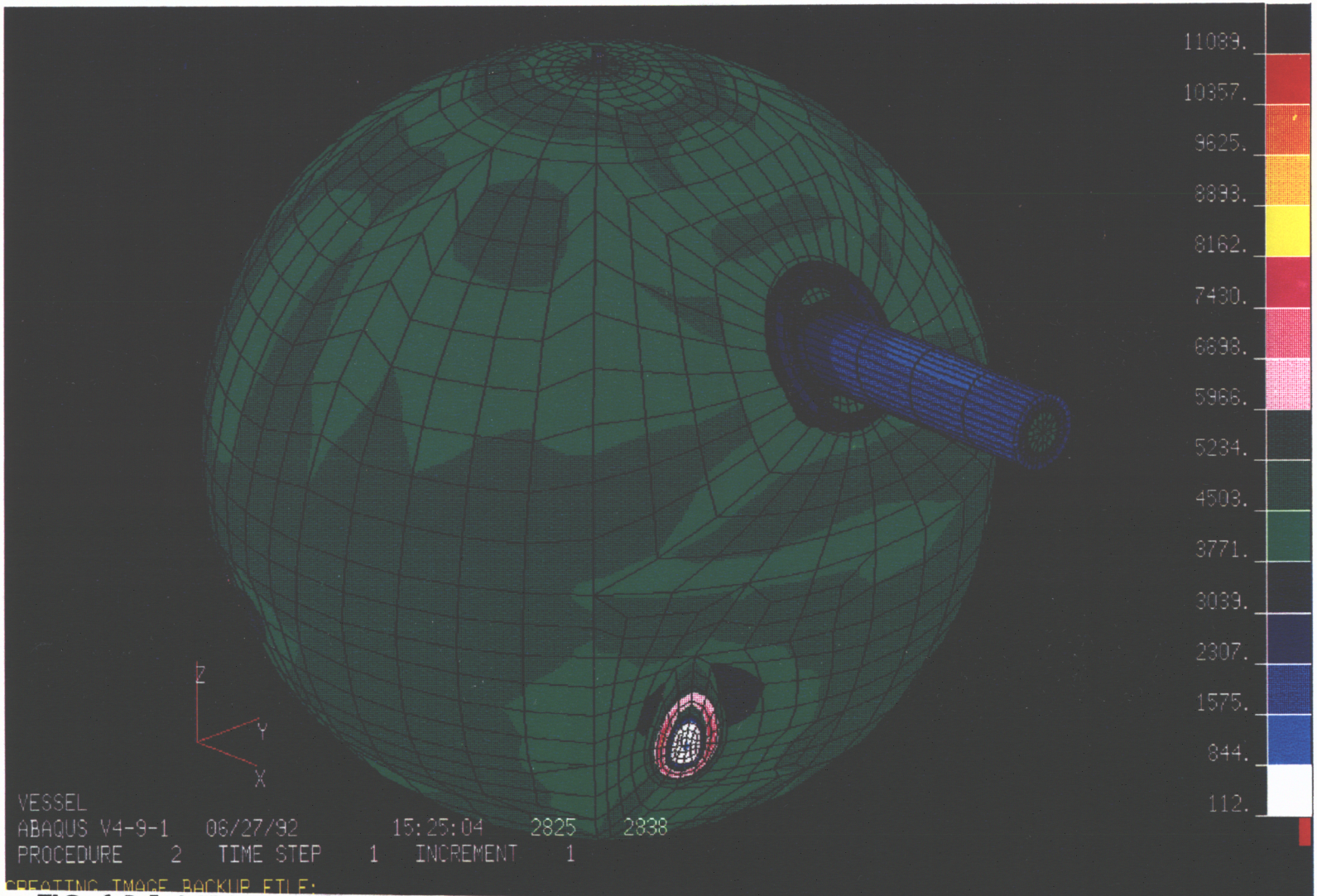

FIG.4.2.1 VON MISES STRESS DISTRIBUTION THROUGHOUT THE MODEL VESSEL1 (VIEW 1)

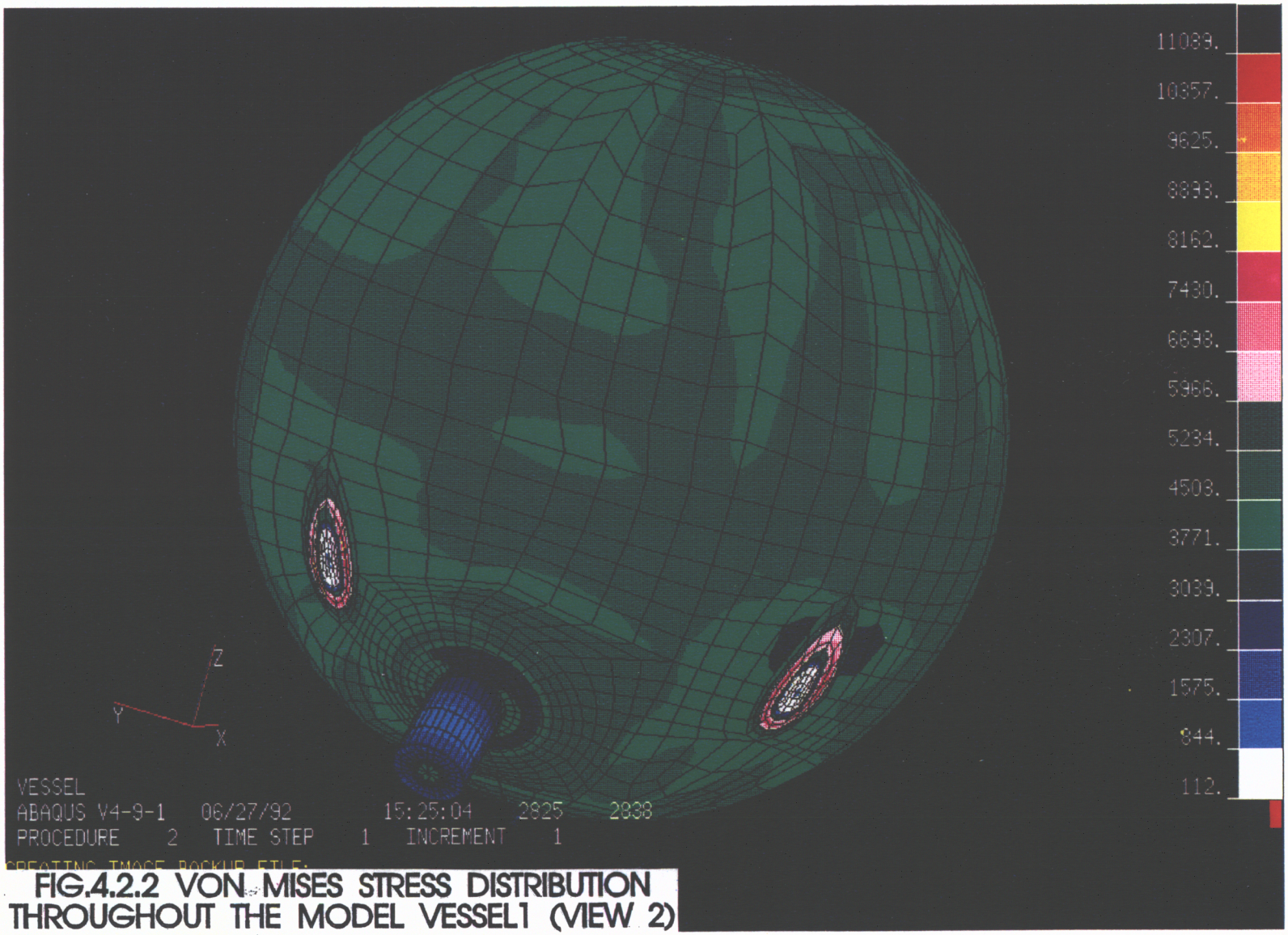

FIG.4.2.2 VON MISES STRESS DISTRIBUTION THROUGHOUT THE MODEL VESSEL1 (VIEW 2)

4.3) ACCURACY OF THE STRESS ANALYSIS RESULTS RELATED TO THE CHOSEN ELEMENTS

Several elements have been used to performed the stress analysis of an experimental model (Table 3.3) and the results are as following:

The linear shell element S4R5: As it can be observed from the figures 4.3.1 and 4.3.2, the results obtained by the finite element approach agrees with the experimental results near the intersection of the nozzle and the vessel. However, the finite elements results can only provide an average value from that point to the end of the reinforcement pad. Also the circumferential stress results are more accurate than the meridianal stress results in the region of intersection. This is because the meridianal deformation suffers the major deviation from the membrane deformation due to the presence of the intersection. Also, the change of thickness occurs at the end of the reinforcement can not be handled appropriately by the linear shell element because the shear stress is important whenever a transition of thickness occurs by means of welding. Since the linear element S4R5 has the approximated Kirchhoff assumption imposed, it fails to follow the trends of the stress distribution near the end of the reinforcement. In order to make sure that the problems mentioned before are not due to the mesh refinement, a h-version refinement [Reddy, 24] has been used. The results from this model with a refined mesh (Fig. 4.3.3 & 4.3.4) do not show any increase in accuracy between the finite element results and the experimental results.

The quadratic shell element S8R5: Since the linear shell element does not provide a satisfactory result in comparison with the experimental results, the quadratic shell element S8R5 has been used. Although the finite element model does not require an interpolation function higher than the linear polynomial function; the quadratic element should provide a better result because the quadratic element allows a more flexible deformation along the parametrized direction of the element. In fact, the quadratic element is a shear flexible element. Despite all the advantages of the quadratic element, the results have not improved significantly in the region between the intersection and the ending point of the reinforcement. The reason for lack of improvement is the lack of flexibility in the thickness direction of the shell element that causes the deviation of the results.

The linear three dimensional element C3D8: The three dimensional linear element

provides a better result for the meridianal stress at the region where the reinforcement pad ended. However, in other area the finite element results obtained by using this element deviated strongly from the experimental result, because this element is too rigid and ill conditioning occurs [Zienkiewicz, 31]; although the change of thickness can be prescribed appropriately by this element.

The axi-symmetric element CAX8R: The axi-symmetric element is indeed a three dimensional quadratic element that takes advantage of the axi-symmetric condition (in the vertical direction), since there is a gap between the reinforcement pad and the shell surface, the flexibility in the thickness direction becomes crucial for a successful modeling of a pad reinforced nozzle. The axi-symmetric element CAX8R having the required flexibility in the thickness direction becomes the most ideal element for this analysis. Actually, the element CAX8R provides the best result (Fig. 4.3.9 & 4.3.10) among all those used in the present study. Moreover, the axi-symmetric model requires almost 80 % less elements and nodes; consequently, less computational time is required. However, this element can be used only for a radial nozzle where the axi-symmetric condition exists. In the case of a non-radial nozzle, a more general element has to be used to build the finite element model.

The three dimensional quadratic element C3D20R: This element is the most general 3-D element that has been used in this study. As is expected, the results obtained by using this element represent a good approximation to the experimental results (Fig. 4.3.11 & 4.3.12). Furthermore, the results are very similar to the results obtained by using the CAX8R . The fact that the C3D20R element model provides an acceptable approximation to the experimental result is important because the C3D20R element can handle the situation of a non-radial nozzle. Since the only experimental result available is for the radial nozzle, the success of the C3D20R element in modeling the radial nozzle provides support for the use of this element in the non-radial nozzle. Also, a finite element model with a transition from 3-D to 2-D element has been used and the results are similar to the model with 3-D elements (Fig. 4.3.12 & Fig. 4.3.13). Also, it is important to observe that both the experimental results and the finite element results converge to the membrane solution at a distance less than the length of the reinforcement pad. Therefore, the length of the reinforcement pad can be used as a general criterion to determine the size of the 3-D element region (Fig 3.11).

For the case of the C3D20R and the CAX8R elements, the finite elements results are still an averaged approximation to the experimental results in the region near the end of the

reinforcement. The reason is, the finite element model assumes no gaps between the reinforcement pad and the shell surface, which is not true. A nonlinear analysis would be more appropriate for representing the real physical system. However, the "trends" of the stress variation around the singularity should be enough to discuss the approach of the acoustic emission testing. In fact, this present study does not pretend to determine the exact stress distribution around the singularity but to obtain an approximated stress distribution that reveals the possible influence of this mechanics aspect on the acoustic emission testing. The acoustic emission technique, furthermore, based on the wave propagation phenomenon, cannot achieve an exact measurement of the discontinuity due to the distortion explained in chapter 2. Therefore, a more exact stress analysis solution may become impractical because too much computational effort is required and the the acoustic emission technique cannot achieve the corresponded accuracy.

As it has been mentioned in chapter 3, there are other methods to reinforce a nozzle, for example the integral reinforcement. Since the integral reinforcement is constructed of a one piece forged material. The difficulty induced by the relative movement between a reinforcement pad and the shell does not exist; as a consequence, the model with the element C3D20R or CAX8R is perfectly applicable Certainly, the finite element results should be better than the case of a pad reinforcement.

So far, only the finite element results of the nozzle have been discussed. The support that constitutes another important component of a pressure vessel has not been discussed. However, the geometry of a support is very similar to a nozzle. Geometrically, both components are the result of a spherical and a cylindrical intersection. Since no hole on the spherical vessel will be opened in the area of intersection between the support and the vessel, reinforcement is not required very often. From the study of the nozzle stress analysis by the finite element approach, it can be observed that the two dimensional shell element can handle appropriately the intersection area. Also, there is no relative movement between the reinforcement pad and the shell surface. Therefore, it is assumed that the 2-D finite element model with shell element can be used to model this part of the pressure vessel. Furthermore, in case of a reinforcement pad being used, the model with element C3D20R or CAX8R should be used to perform the stress analysis.

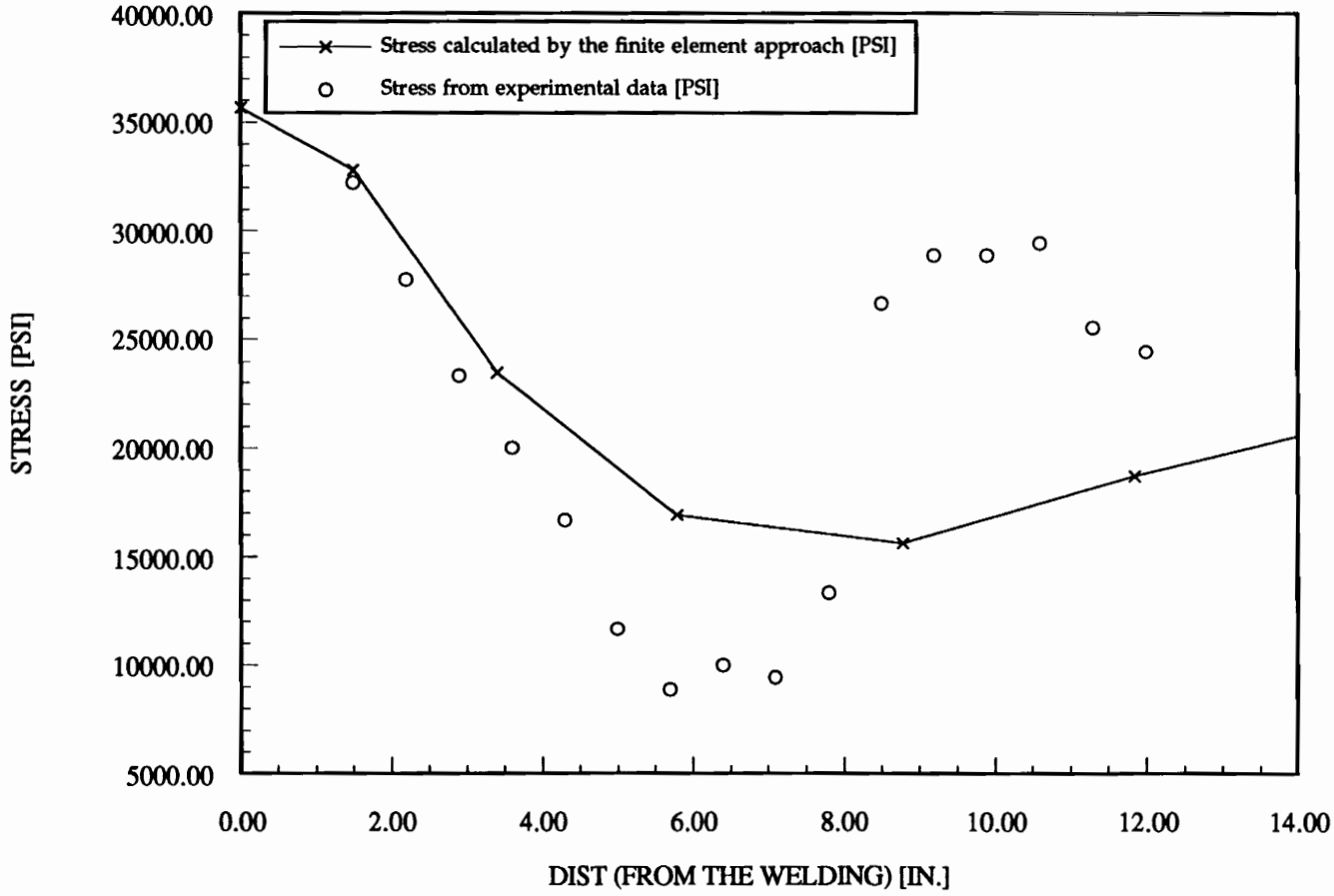

FIG. 4.3.1
CIRCUMFERENTIAL STRESS AT THE TOP SURFACE OF THE REINFORCEMENT PAD (LINEAR ELEMENT S4R5)

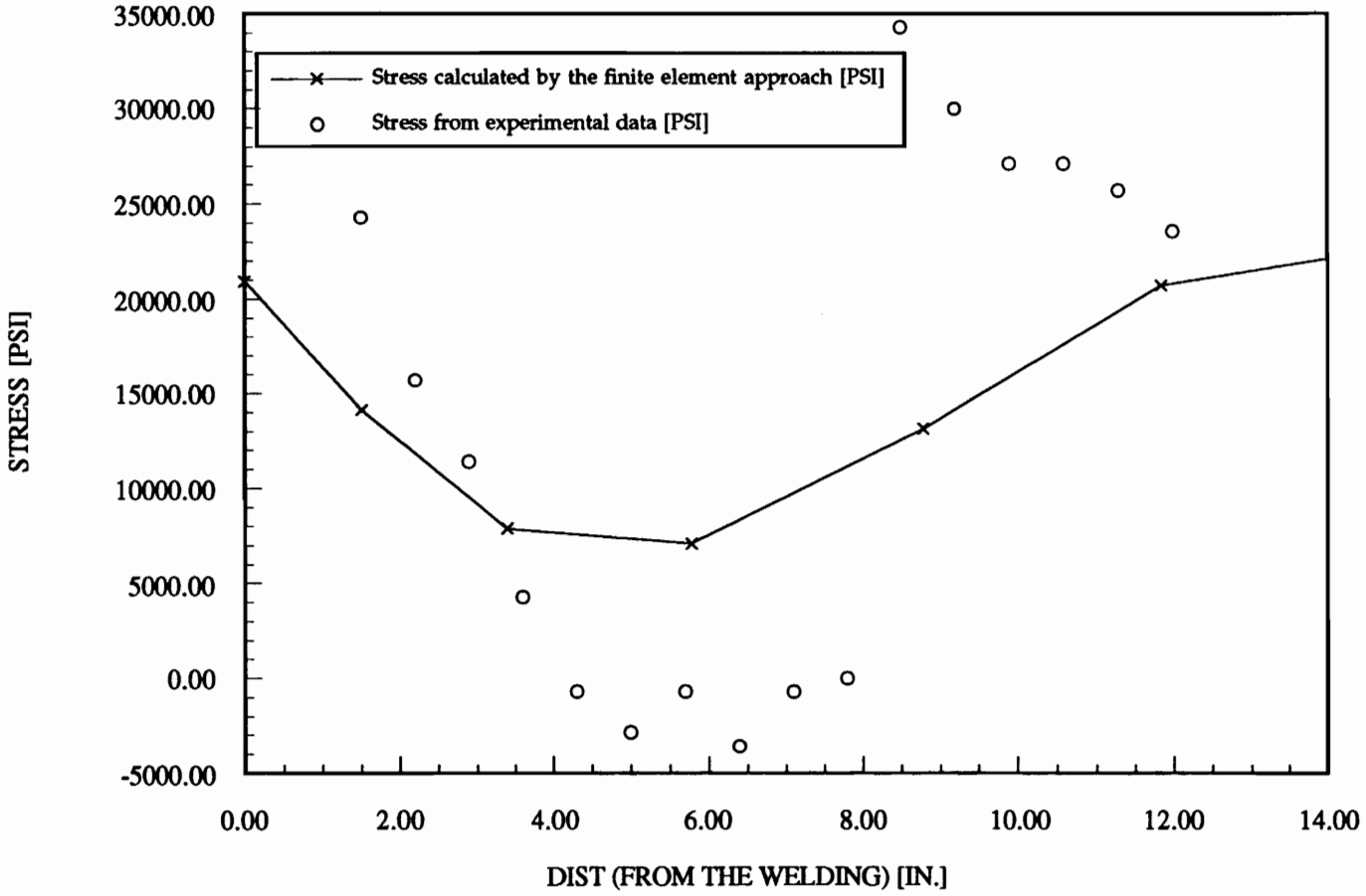

FIG. 4.3.2
MERIDIANAL STRESS AT THE TOP SURFACE OF THE REINFORCEMENT PAD (LINEAR ELEMENT S4R5)

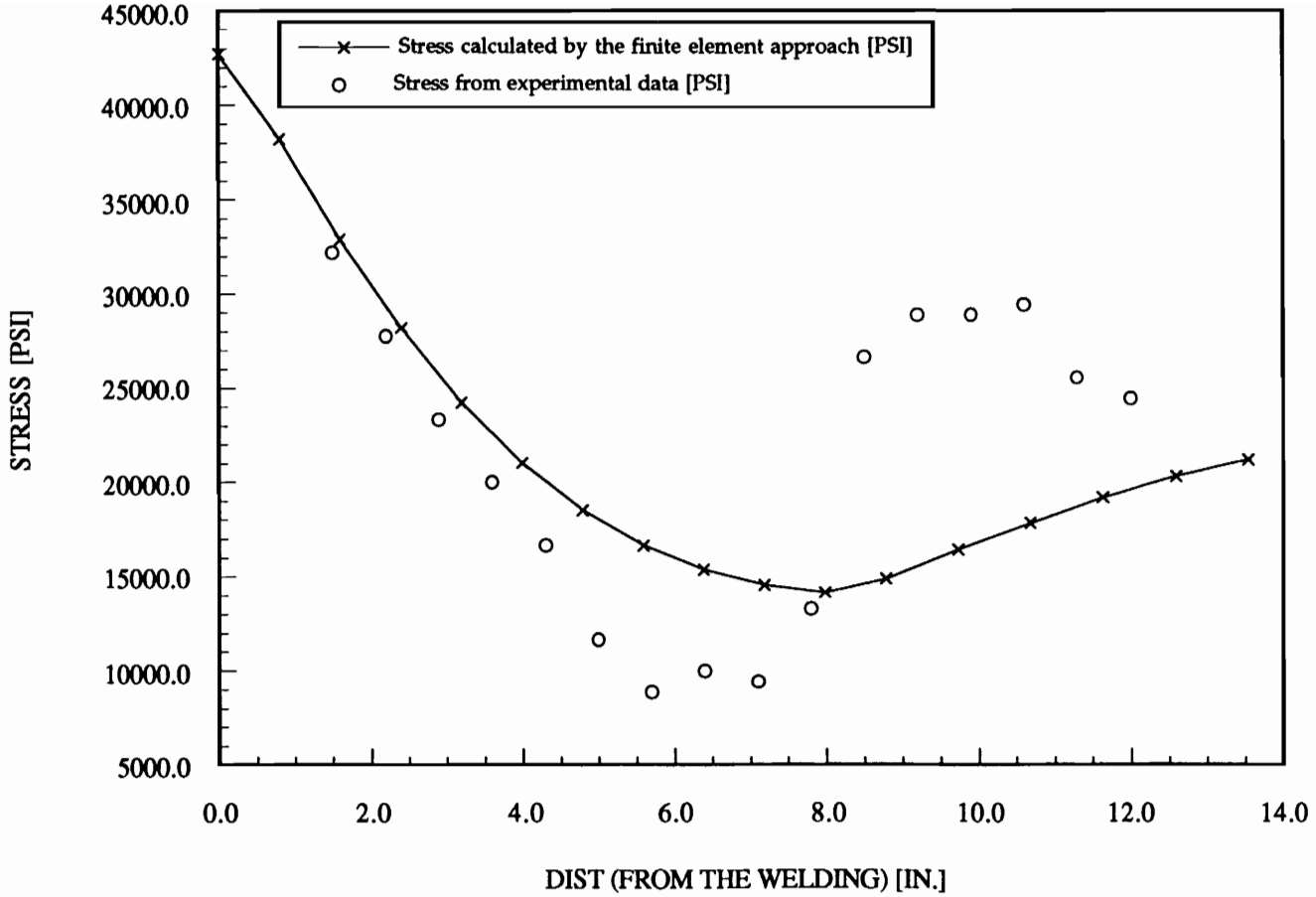

FIG. 4.3.3
CIRCUMFERENTIAL STRESS AT THE TOP SURFACE OF THE REINFORCEMENT PAD (LINEAR ELEMENT S4R5, REFINED MESH)

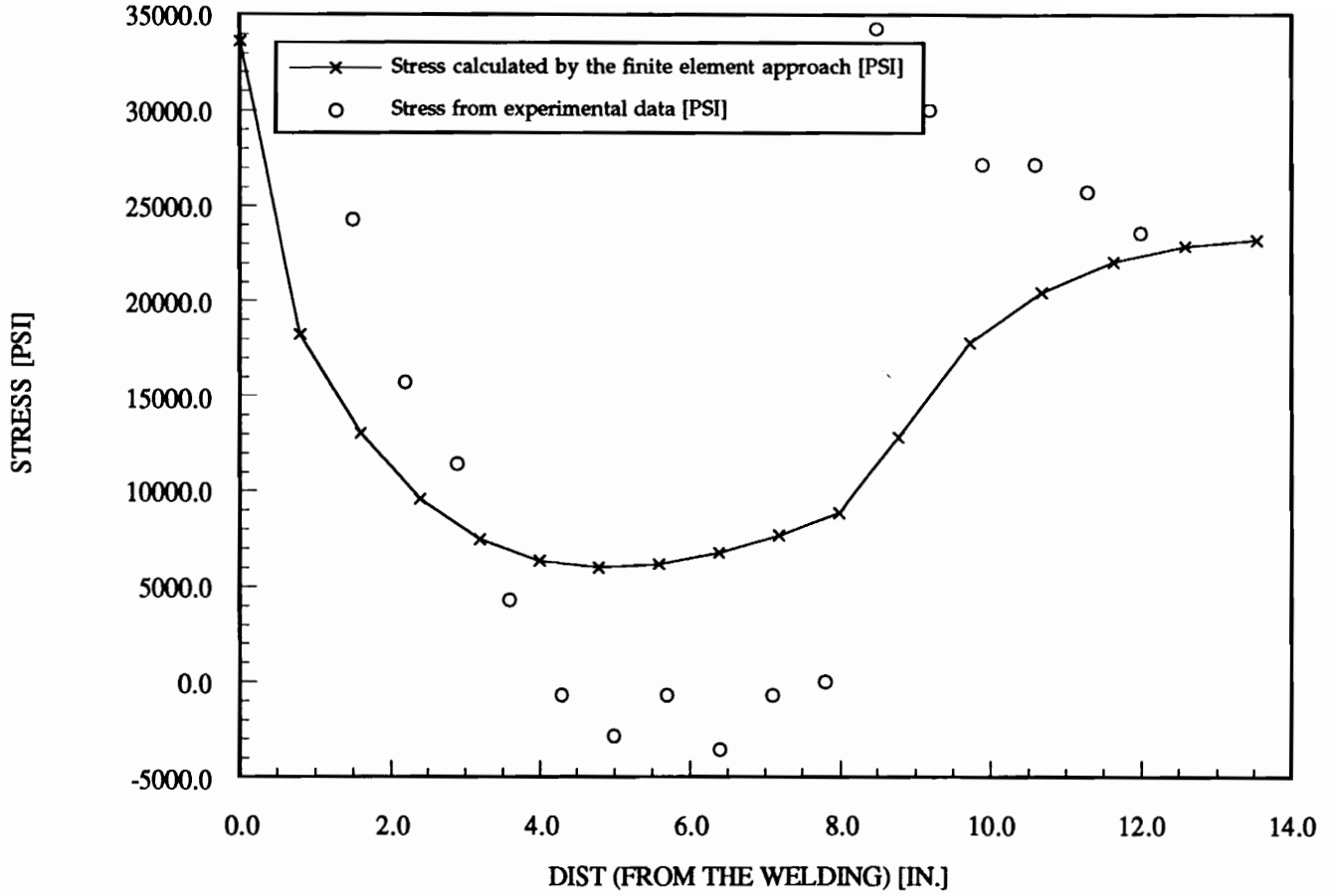

FIG. 4.3.4
MERIDIANAL STRESS AT THE TOP SURFACE OF THE REINFORCEMENT PAD (LINEAR ELEMENT S4R5, REFINED MESH)

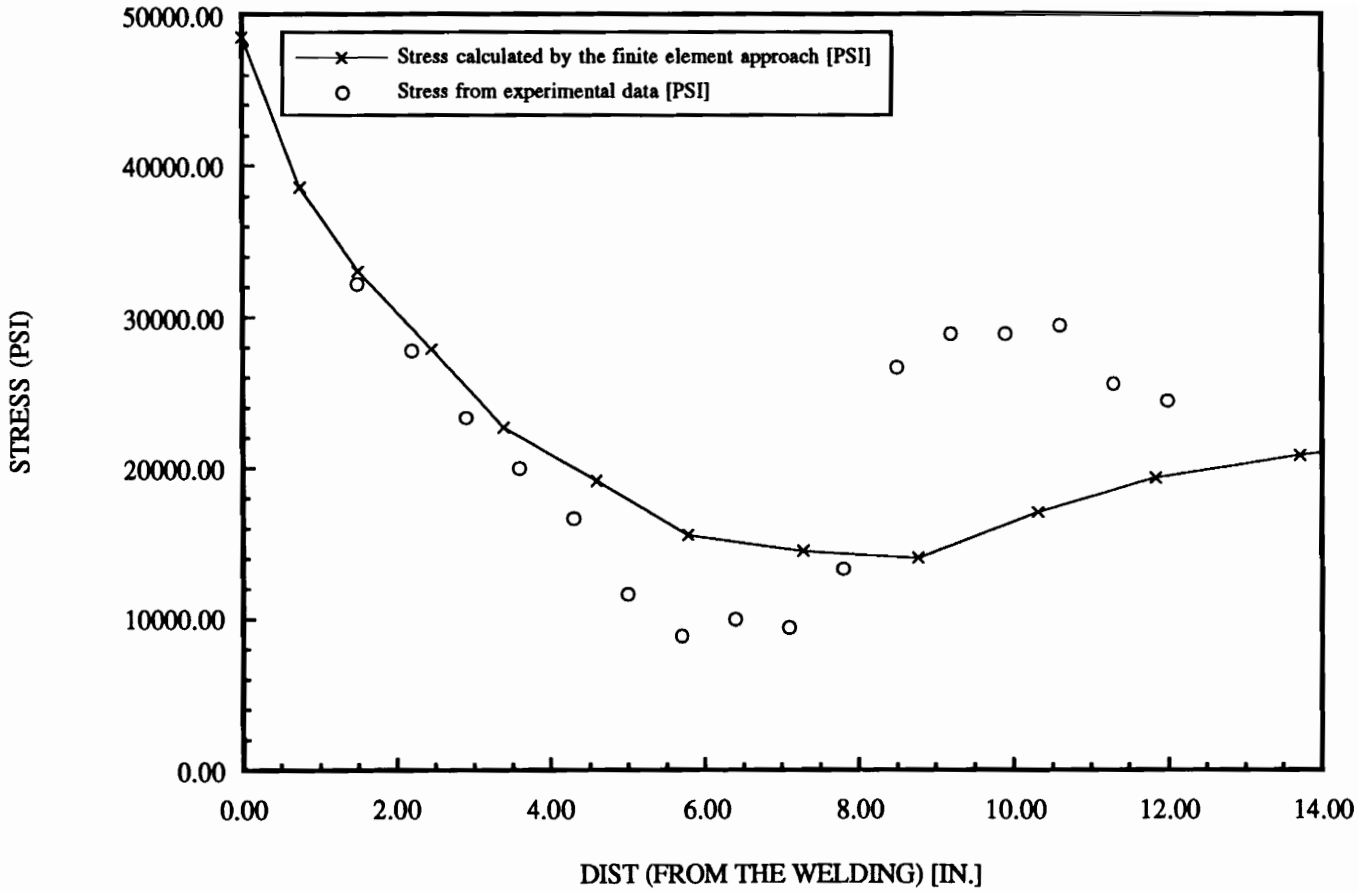

FIG. 4.3.5

CIRCUMFERENTIAL STRESS AT THE TOP SURFACE OF THE REINFORCEMENT PAD (QUADRATIC ELEMENT S8R5)

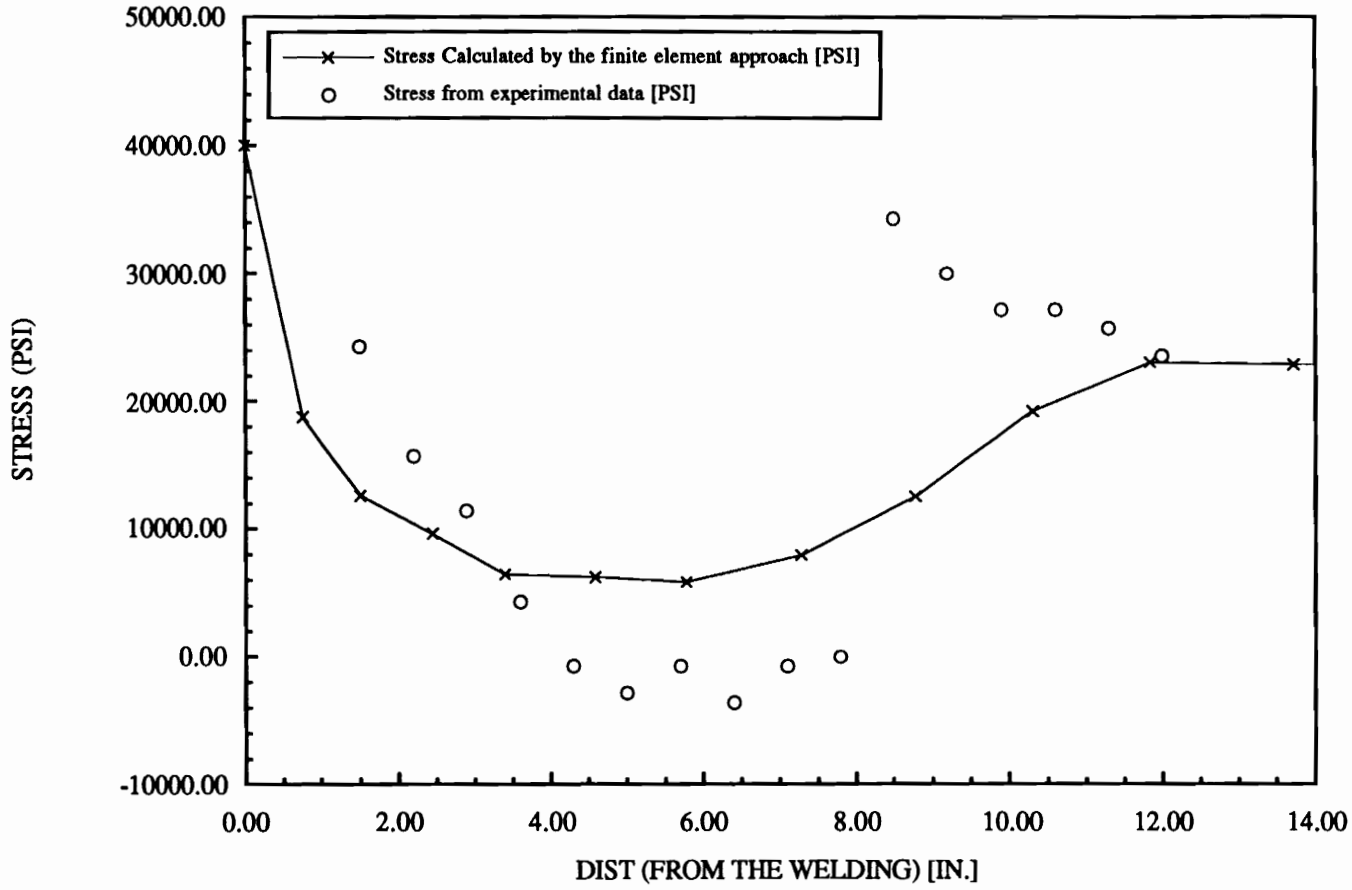

FIG. 4.3.6
MERIDIANAL STRESS AT THE TOP SURFACE OF THE REINFORCEMENT PAD (QUADRATIC ELEMENT S8R5)

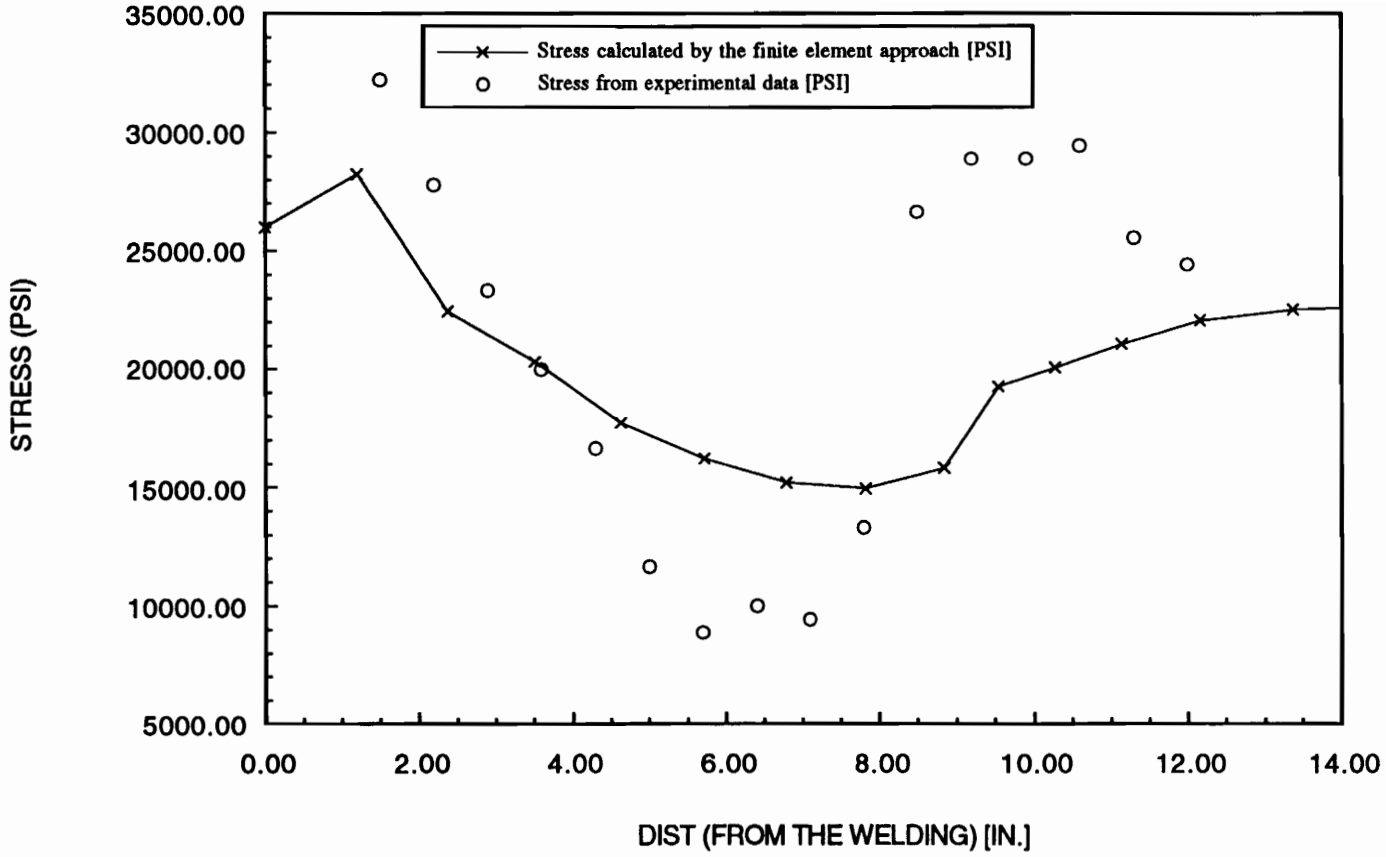

FIG. 4.3.7
CIRCUMFERENTIAL STRESS AT THE TOP SURFACE OF THE REINFORCEMENT PAD (3-D LINEAR ELEMENT C3D8)

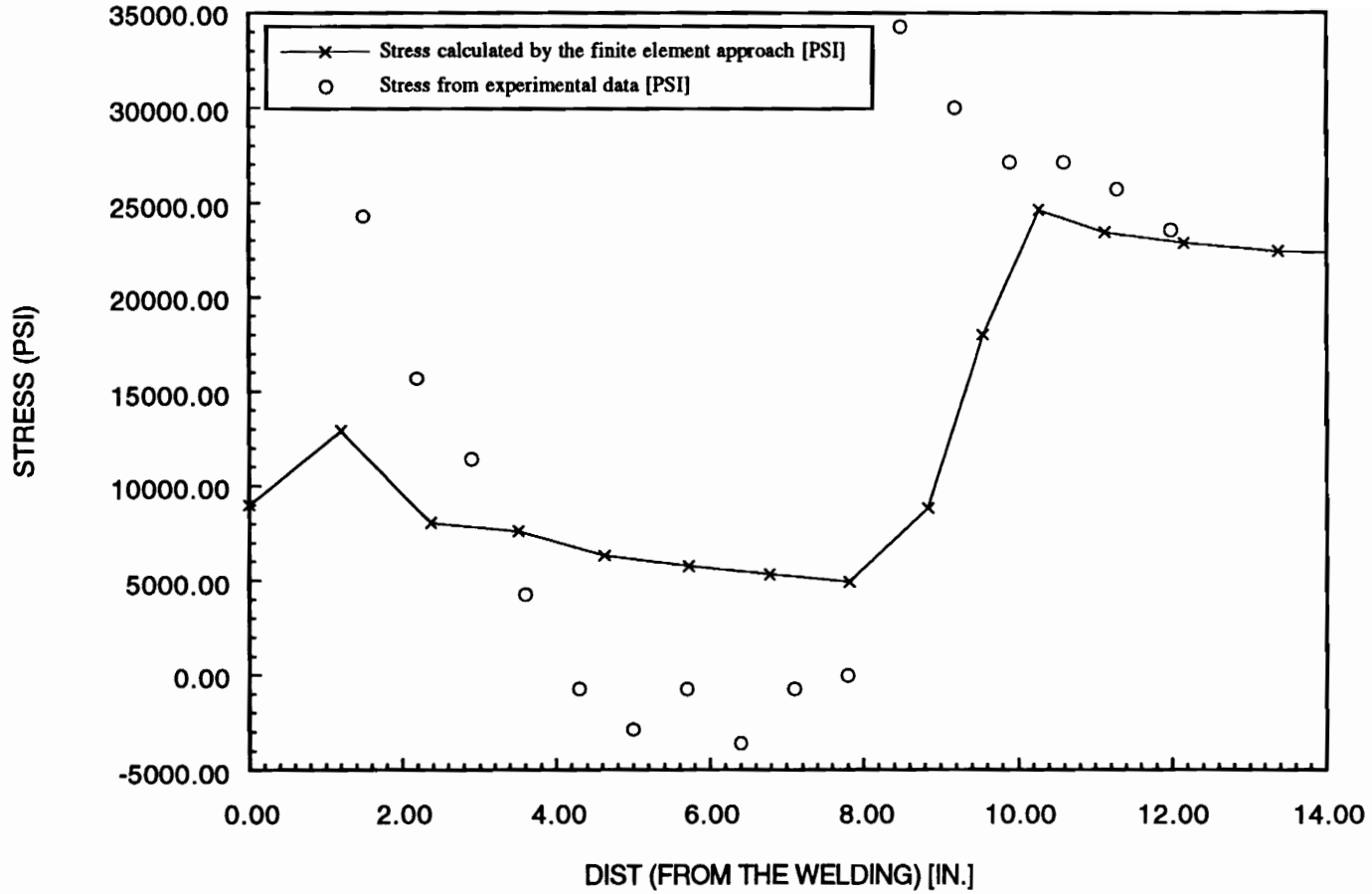

FIG. 4.3.8
MERIDIANAL STRESS AT THE TOP SURFACE OF THE REINFORCEMENT PAD (3-D LINEAR ELEMENT C3D8)

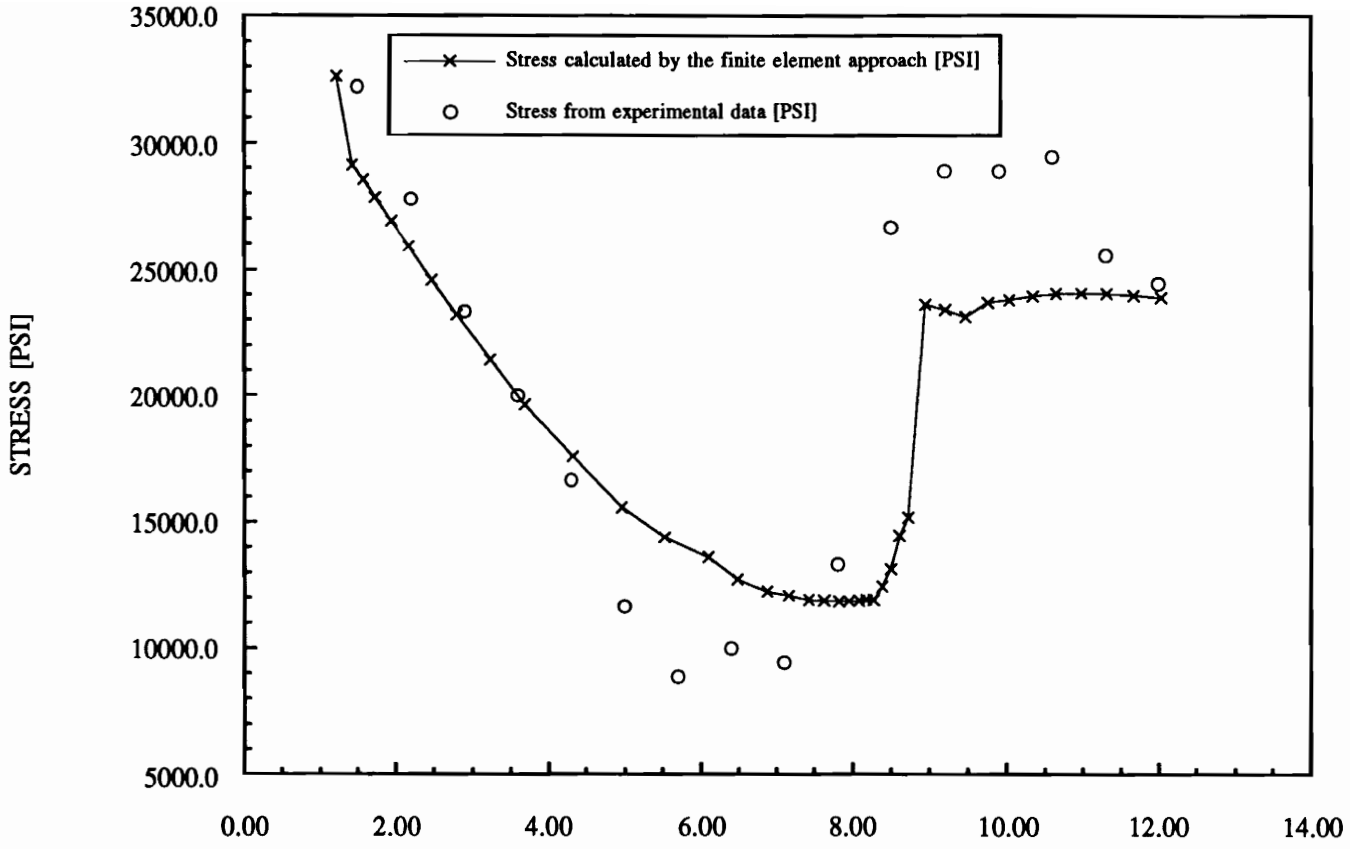

FIG. 4.3.9
CIRCUMFERENTIAL STRESS AT THE TOP SURFACE OF THE REINFORCEMENT PAD (AXI-SYMMETRIC ELEMENT CAX8R)

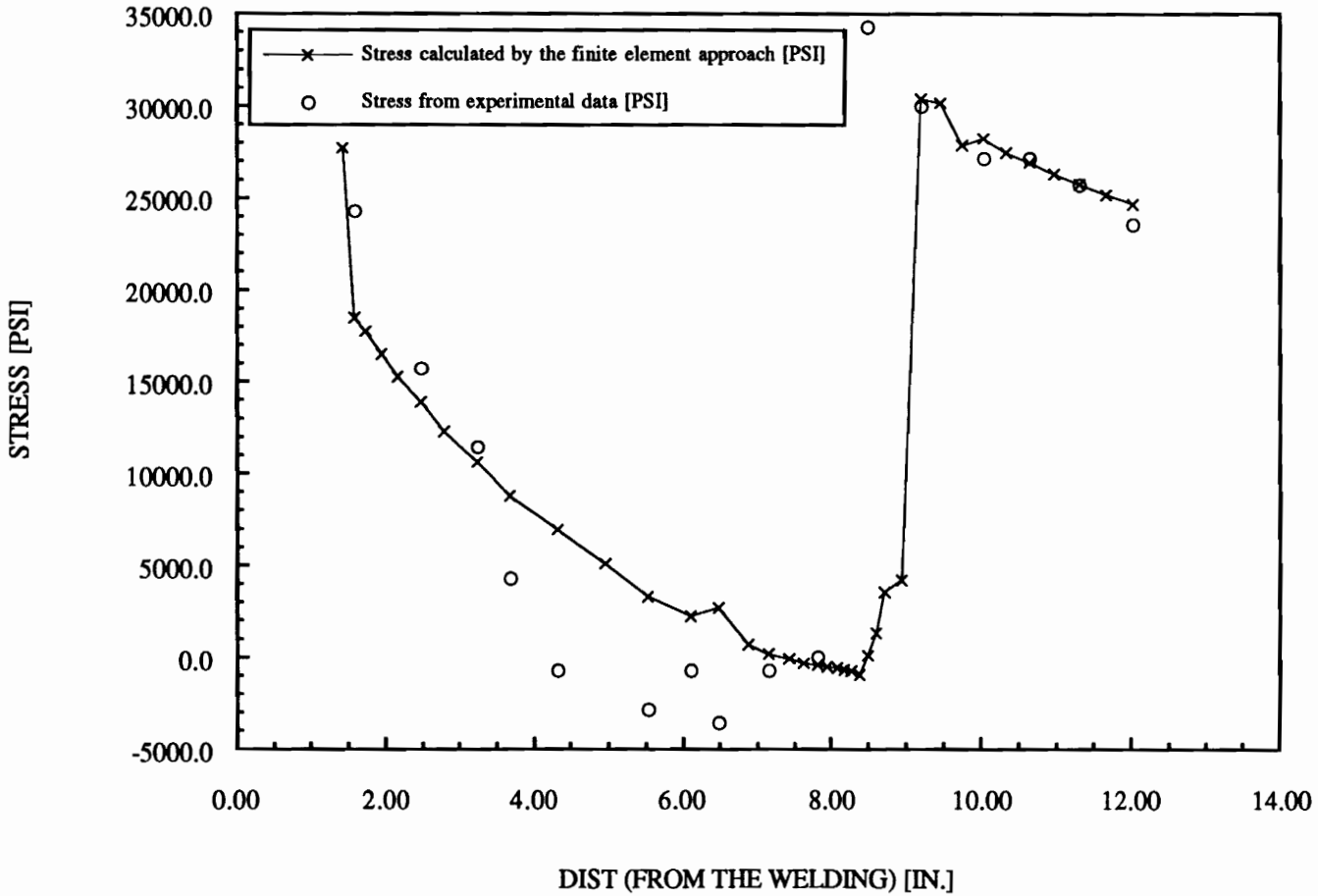

FIG. 4.3.10
MERIDIANAL STRESS AT THE TOP SURFACE OF THE REINFORCEMENT PAD (AXI-SYMMETRIC ELEMENT CAX8R)

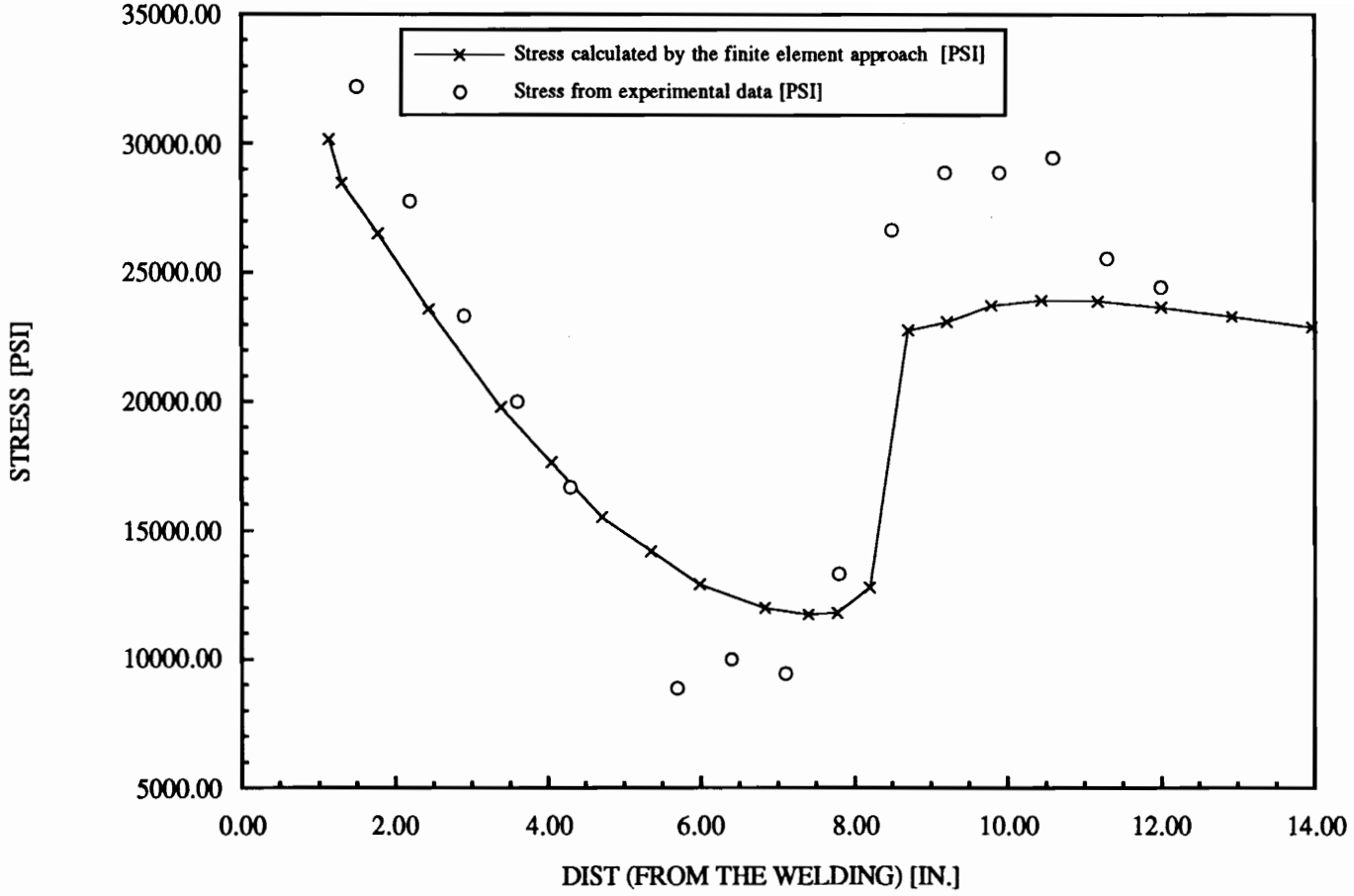

FIG. 4.3.11
CIRCUMFERENTIAL STRESS AT THE TOP SURFACE OF THE REINFORCEMENT PAD (3-D QUADRATIC ELEMENT C3D20R)

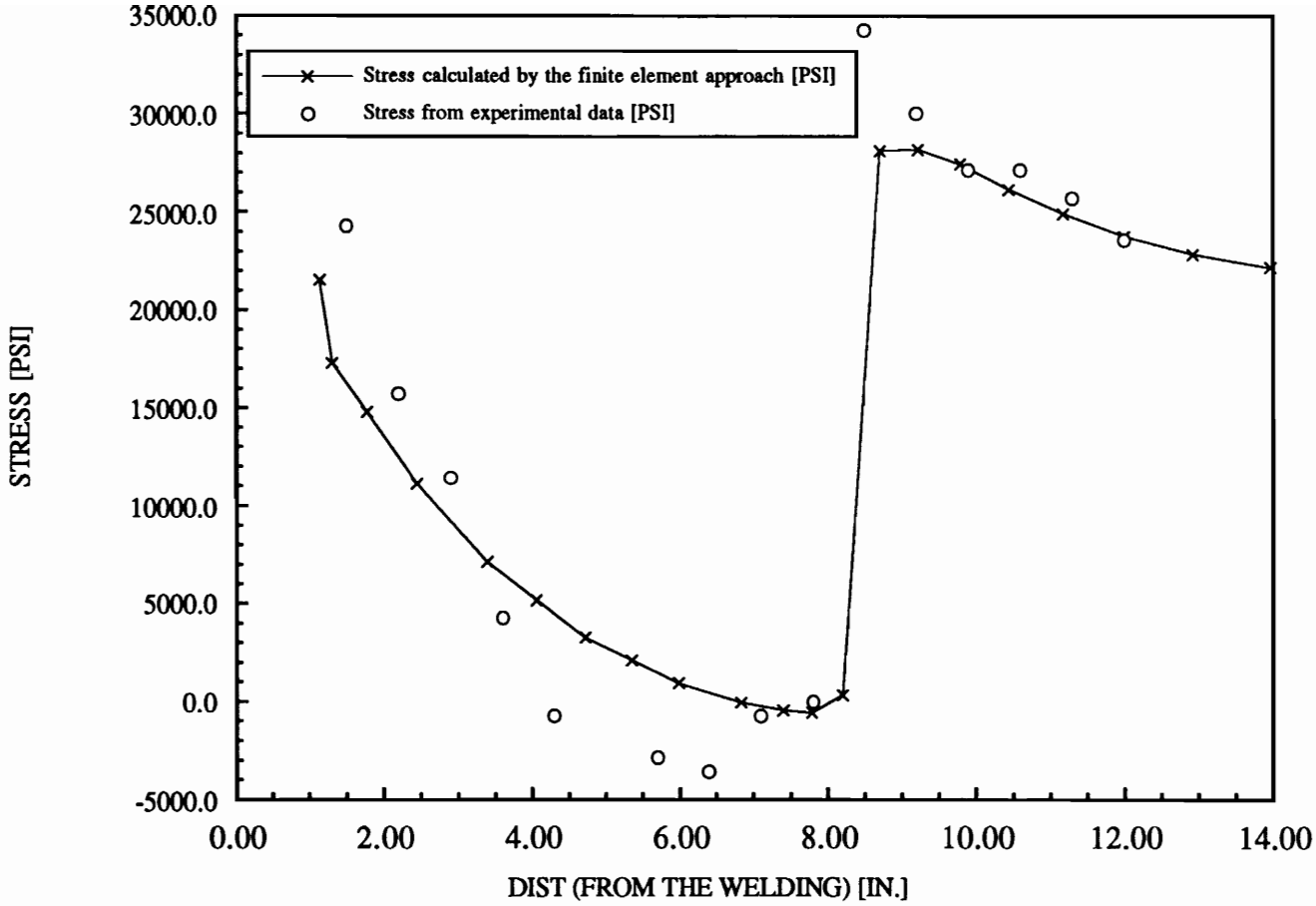

FIG. 4.3.12
MERIDIANAL STRESS AT THE TOP SURFACE OF THE REINFORCEMENT PAD
(3-D QUADRATIC ELEMENT C3D20R)

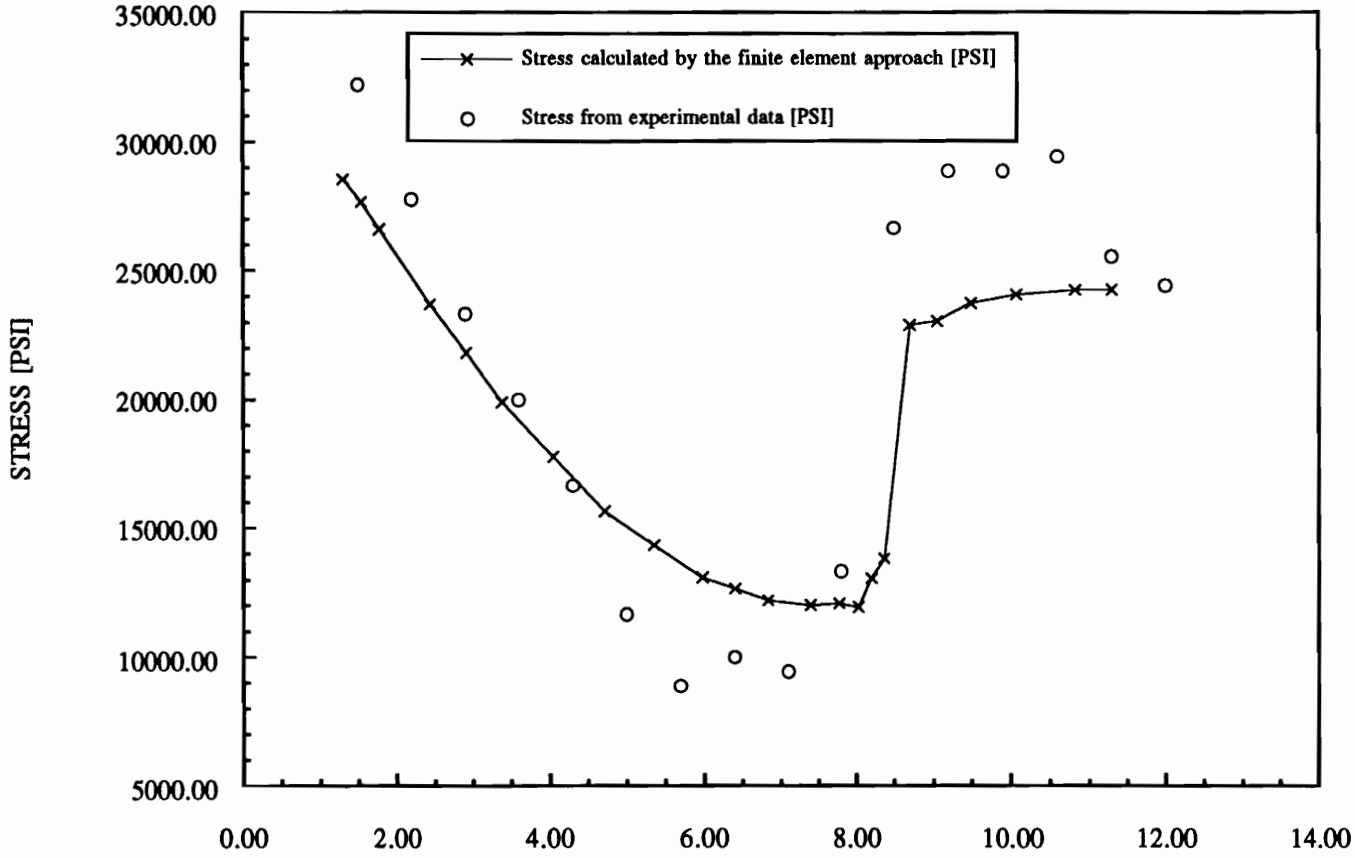

FIG. 4.3.13

CIRCUMFERENTIAL STRESS AT THE TOP SURFACE OF THE REINFORCEMENT PAD (3-D AND 2-D ELEMENT)

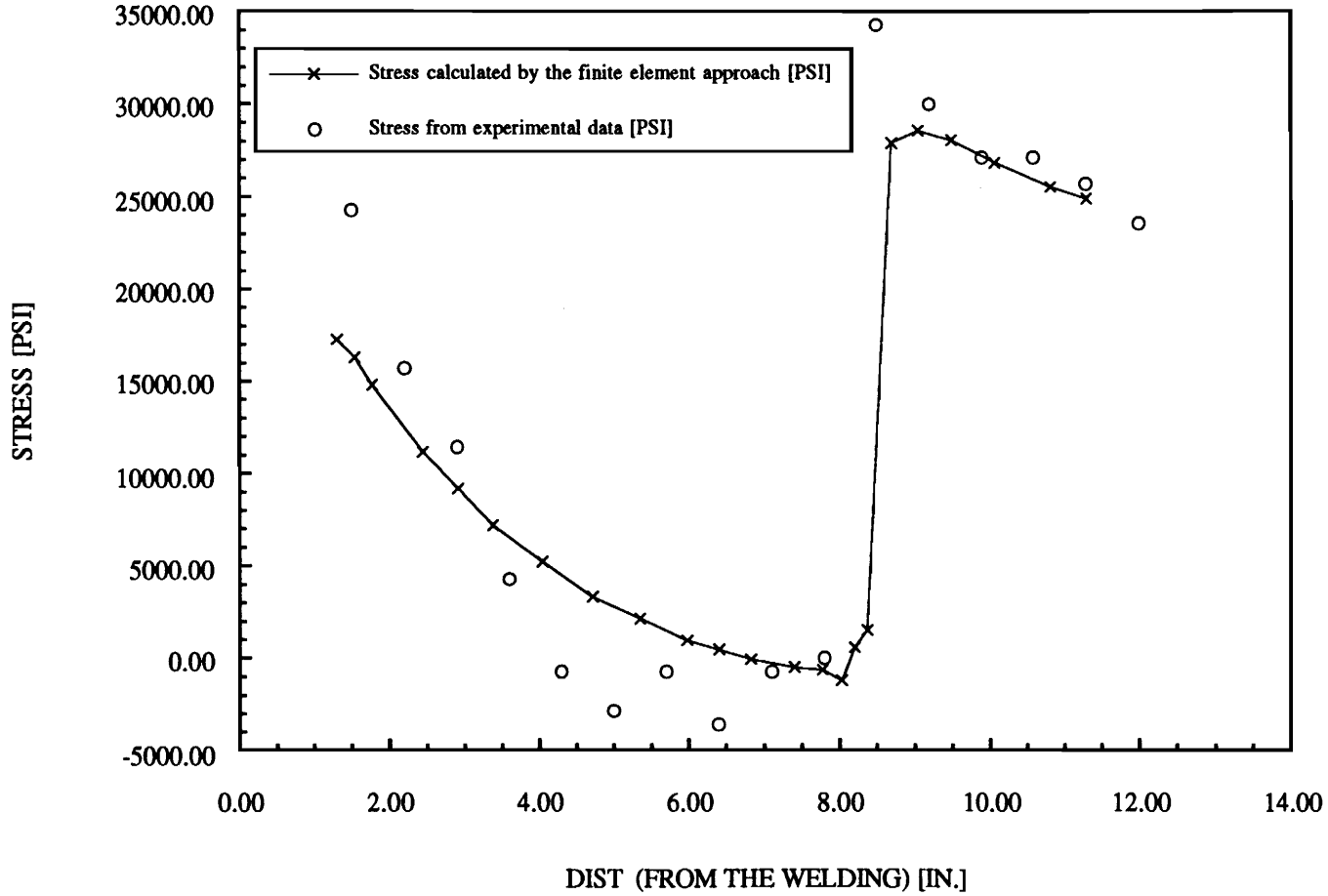

FIG. 4.3.14

MERIDIANAL STRESS AT THE TOP SURFACE OF THE PAD REINFORCEMENT (3-D AND 2-D ELEMENT)

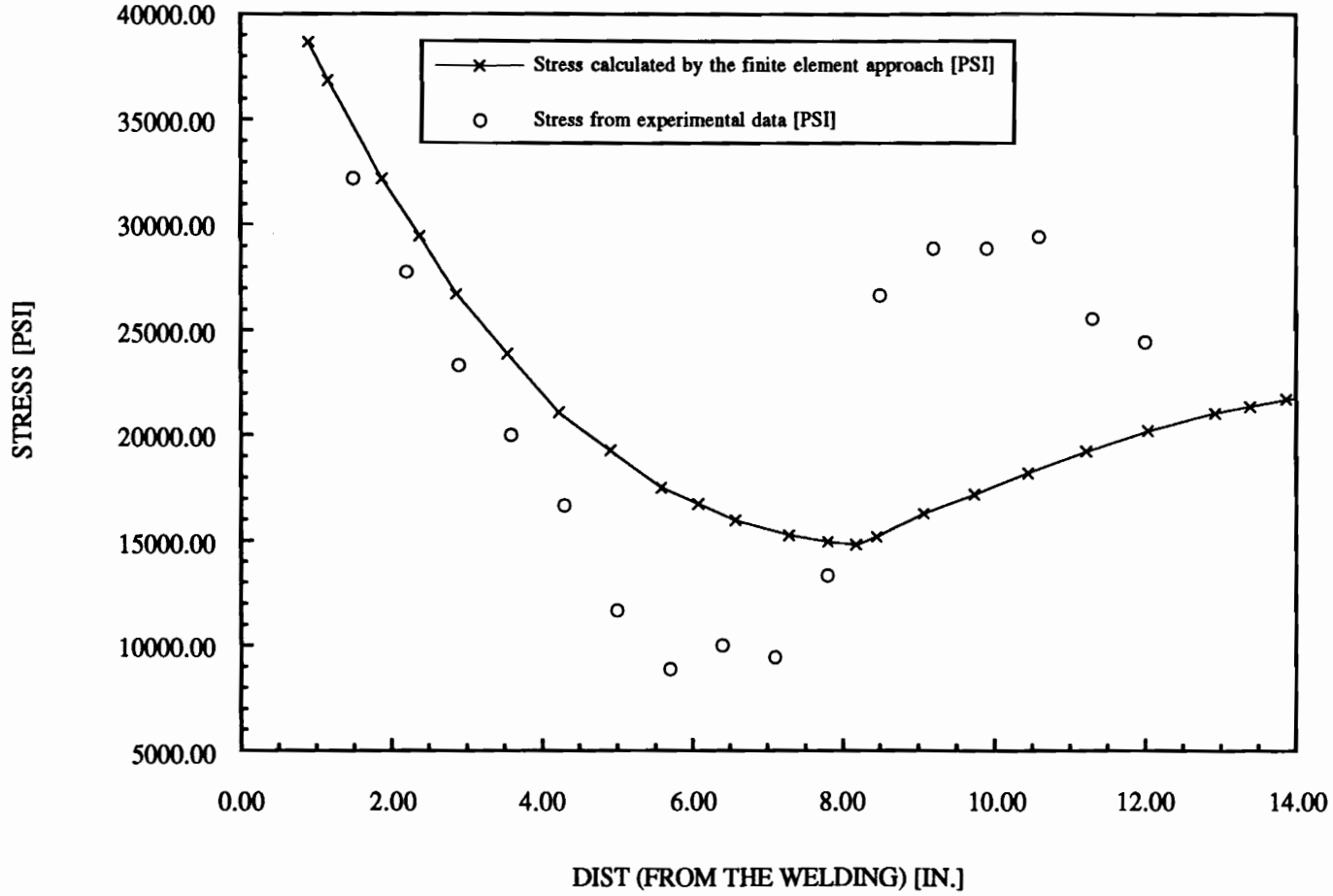

FIG. 4.3.15

CIRCUMFERENTIAL STRESS AT THE TOP SURFACE OF THE REINFORCEMENT PAD (THICK SHELL ELEMENT S8R)

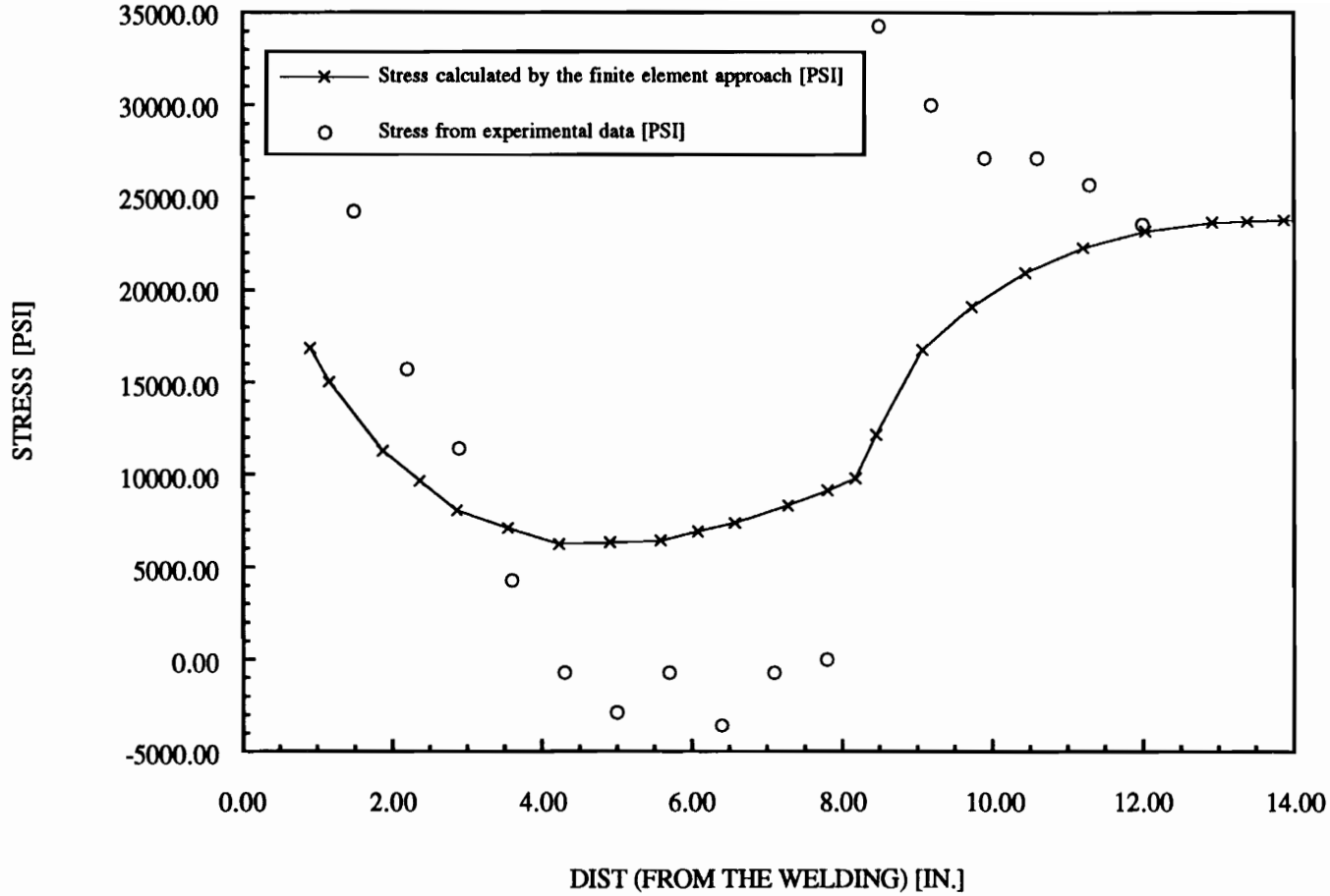

FIG. 4.3.16

MERIDIANAL STRESS AT THE TOP SURFACE OF THE REINFORCEMENT PAD (THICK SHELL ELEMENT S8R)

4.4) INFLUENCE OF THE STRESS DISTRIBUTION AROUND THE SINGULARITY ON THE ACOUSTIC EMISSION TESTING RESULTS

Based on the theory of the linear elastic fracture mechanics (LEFM), the stress intensity factor K which measures the severity of a crack depends upon the applied stress, size and the geometry of the crack [Dowling, 6]. Moreover, according to the orientation of the crack with respect to the stress direction, three modes of stress intensity factor can be defined. However, the mode I, where the stress is normal to the orientation of the crack, is the most common in the practice. As a matter of fact, cracks that begin in mode II or mode III have the tendency to displace in such a way that the mode I will be the final configuration [Dowling, 6]. In brief, the stress distribution over an area can affect tremendously the behavior of a crack. As it was mentioned in chapter 2, the crack displacement constitutes one of the principle sources of acoustic emission. Therefore, it is necessary to look at the stress distribution around the singularity produced by the uniform pressure loading with more detail.

From Fig. 4.4.1, which shows the circumferential stress around a radial nozzle of 16 in. diameter, it can be observed that the highest stress level is presented at the intersection of the nozzle and the vessel; to be specific, it is the red color region with a value of 34.7 ksi. A pattern of 16 colors has been used to represent the stress range. As can be observed, the meridianal stress (Fig. 4.4.2) varies more rapidly in the meridianal direction than the circumferential stress (Fig.4.4.2). However, in both cases, the stress is uniform in the circumferential direction. Therefore, it is possible to demarcate concentric areas of uniform stress. This characteristic of this stress distribution, actually, verifies the axi-symmetric condition of the problem. Since the area near the weld of the reinforcement to the vessel has a very low stress level (Fig. 4.4.1 and 4.4.2), a crack or discontinuity within this area may not be easily detected by the acoustic emission technique. The reason is, as was mentioned in chapter two, the acoustic emission technique requires the displacement of the crack so that acoustic emission from this source can be detected. Actually, a crack oriented in the circumferential direction and found within this area will be almost impossible for the acoustic emission detection because the stress normal to the crack, the meridianal stress, may be negative (Fig. 4.4.2). So far, most of the acoustic emission testing has been performed assuming a constant stress over the thickness, i.e. the flaw location is based on a two dimensional array of sensors over the surface of the vessel [Peacock,

21]. However, it can be observed from both figures 4.4.1 and 4.4.2 that there is a rapid change of stress throughout the thickness, more than 50 % between the maximum and the minimum.

For the case of a support, since the geometric configuration is non-radial, it is not easy to choose some direction of stress to demarcate an area of uniform stress for the purpose of discussion. Therefore, the von Mises stress has been used as the parameter for an initial discussion. Although, there is no evidence to demonstrate a direct relation between the von Mises stress and the behavior of a crack. However, in practice, the von Mises stress has been compared to the yielding strength to determine the integrity of the structure. Actually, for mild steel that constitutes the basic material for pressure vessel construction, it has been shown that the maximum acoustic emission occurs near the yielding point [Dunegan and Green, 8] . As it can be observed in Fig. 4.2.1 or Fig. 4.2.2, the von Mises stress varies from a range of 333 psi to 8000 psi. Moreover, there is a concentric configuration of uniform von Mises stress around the support. Similar to a pad reinforced nozzle, behavior of a discontinuity within this area should be different from the rest of the area of the pressure vessel. In other words, a crack inside the area of low stress (the white colored area in Fig. 4.2.1), would be difficult to detect by the acoustic emission technique.

Another important aspect of the acoustic emission testing by pressurization of the vessel is the loading situation. Most of the time, the pressure vessel under testing is pressurized to a pressure of 10% above the operating pressure. Actually, figures 4.4.3 and 4.4.4 represent the stress distribution of the same 16 inches diameter nozzle from the experimental model with an increase of 10% in pressure. It can be observed that a linear relationship exists between the loading and the stress; i.e., a 10% increase of pressure implies a 10% increase of stress; at least, it is verified for the circumferential stress and the meridianal stress.

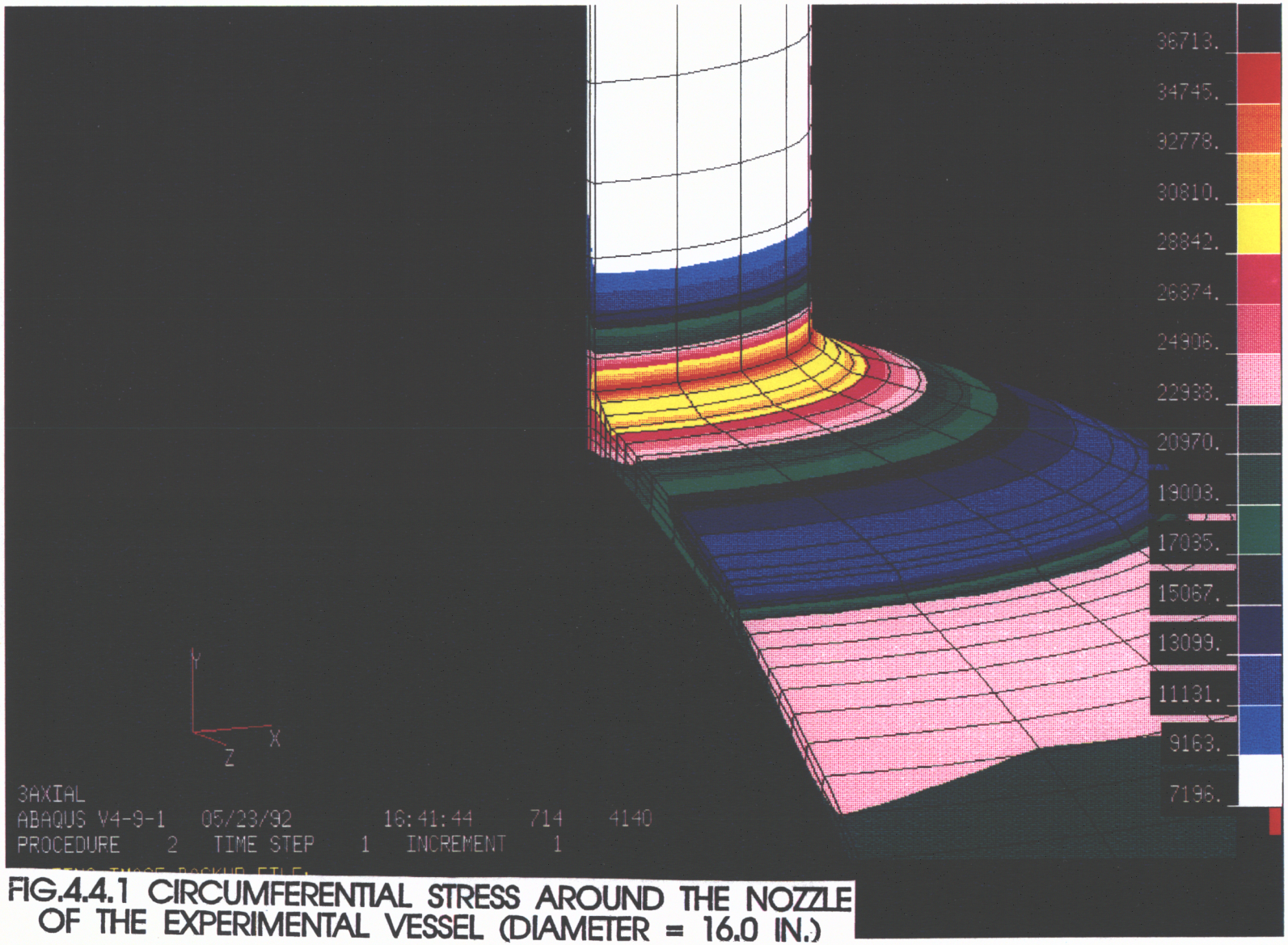

FIG.4.4.1 CIRCUMFERENTIAL STRESS AROUND THE NOZZLE OF THE EXPERIMENTAL VESSEL (DIAMETER = 16.0 IN.)

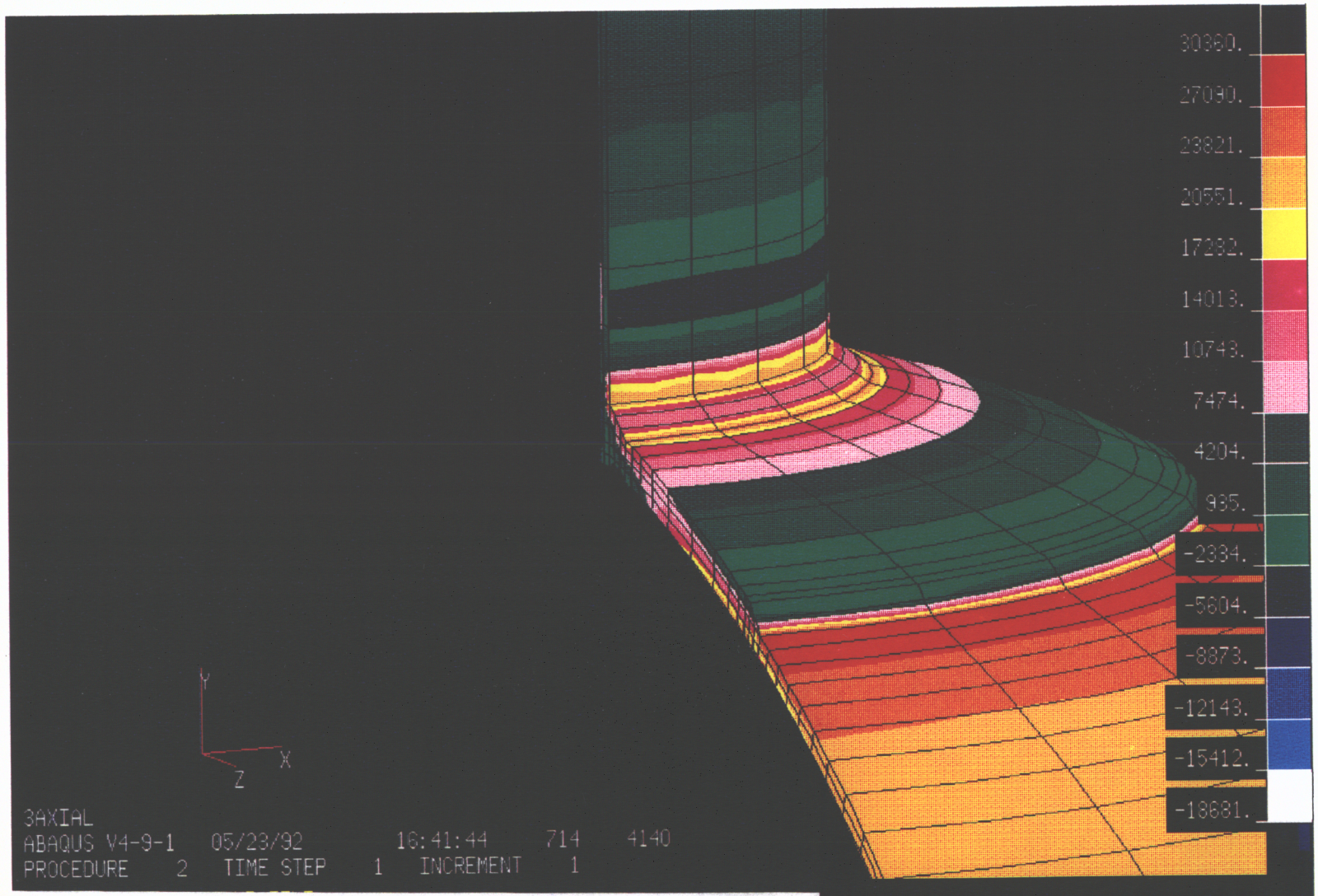

FIG.4.4.2 MERIDIANAL STRESS AROUND THE NOZZLE OF THE EXPERIMENTAL VESSEL (DIAMETER = 16.0 IN.)

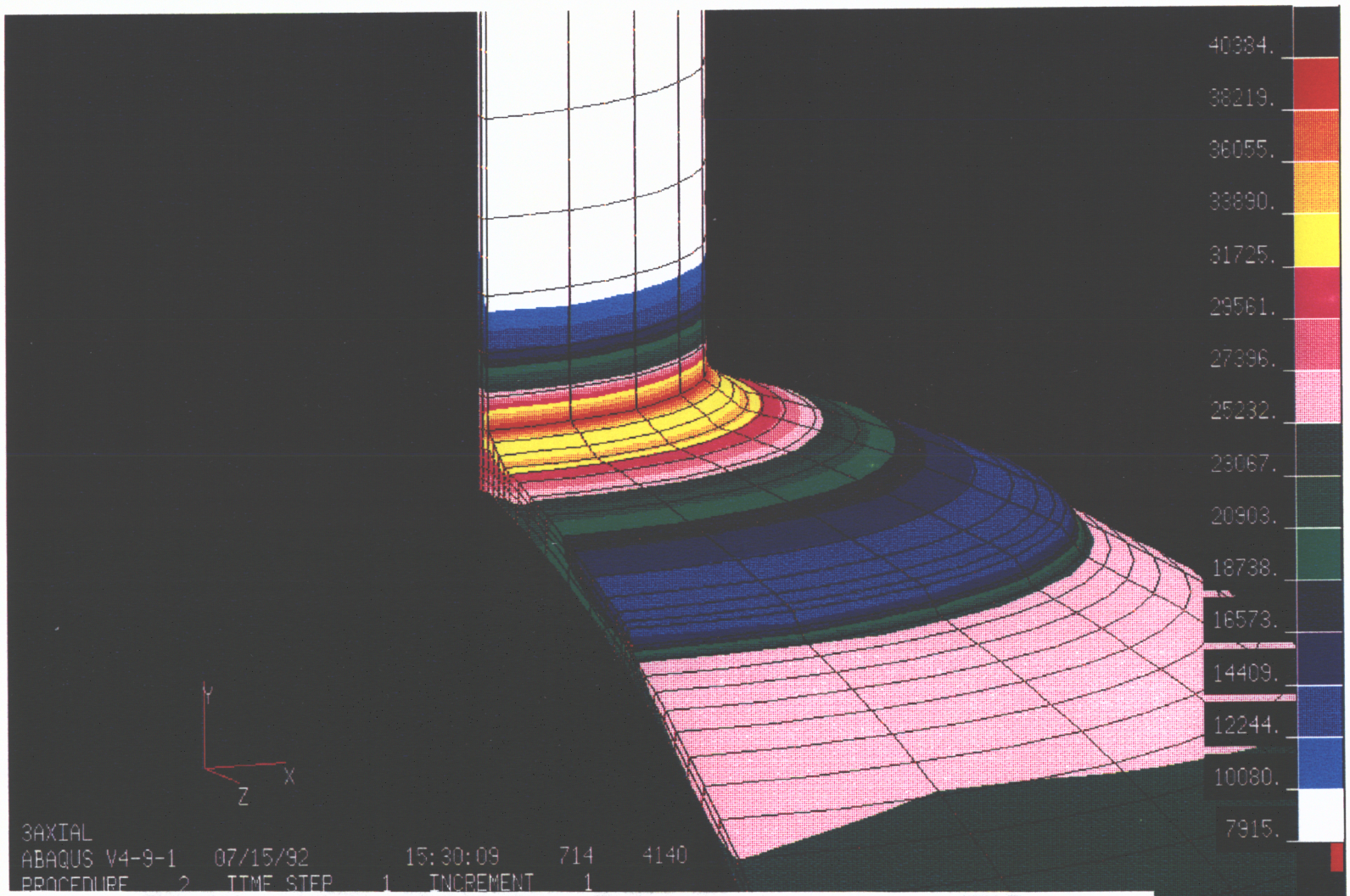

FIG.4.4.3 CIRCUMFERENTIAL STRESS AROUND THE NOZZLE OF THE EXPERIMENTAL VESSEL WITH AN INCREASE OF 10 % IN PRESSURE (DIAMETER = 16.0 IN.)

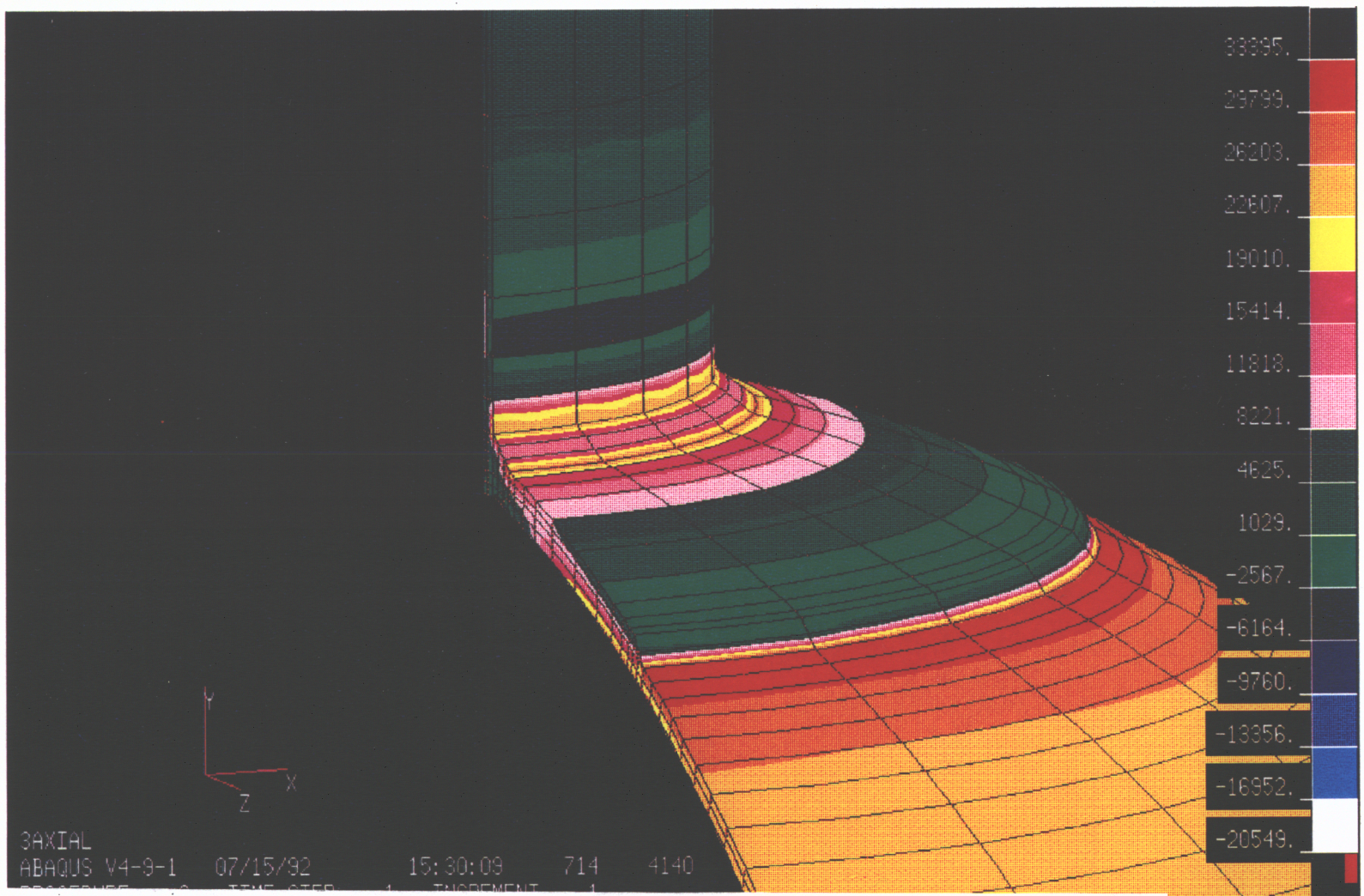

FIG.4.4.4 MERIDIANAL STRESS AROUND THE NOZZLE OF THE EXPERIMENTAL VESSEL WITH AN INCREASE OF 10 % IN PRESSURE (DIAMETER = 16.0 IN.)

5.) CONCLUDING REMARKS

The combined loading of a vapor pressure and a hydrostatic pressure does not produce a significant variation of the stress distribution, compared to uniform internal pressure loading, in a small spherical pressure vessel. However, due to the lack of a general criterion, such as the size of the vessel, to determine the applicability of this affirmation, it is recommended that the calculation based on the membrane analysis should always be performed before stress analysis by means of the finite element approach. Actually, the application of the program in Appendix II does not require too much computational effort. Finally, in cases where the stress variation due to the liquid level is significant, the hydrostatic pressure effect should be included in the finite element model.

The most appropriate elements to perform the stress analysis of a pad reinforced nozzle are the axi-symmetric quadratic element CAX8R and the three dimensional quadratic element C3D20R. The reason is, quadratic elements allow major flexibility in the direction of the thickness which is crucial for an accurate result. Whenever the axi-symmetric condition exists, the axi-symmetric quadratic element should be used, since the required computational time can be reduced enormously. There is no simple rule to determine the size of the element or the mesh refinement that should be used. However, some useful suggestions can be obtained from this study to achieve a more accurate result. Nevertheless, it is worthwhile to mention that the suggestions can be only used to obtained a better approximation to the trends of the stress distribution around the nozzle; thus, a better understanding toward the acoustic emission testing results is possible. For this purpose, the following suggestions apply. Firstly, three or more elements are recommended in the thickness direction of the reinforcement pad and the shell to insure the flexibility. Secondly, the two areas where the weld are presented, the intersection between the nozzle and the vessel and the end of the reinforcement (Fig. 3.5), require a more refined mesh in the meridianal direction, because within these areas a rapid change of stress occurs. Also, a 3-D to 2-D transition scheme is highly recommended to increase the computational efficiency of the finite element model. A distance equivalent to the reinforcement pad length can be used to determine the transition point of the 3-D element to 2-D elements.

The mechanical computer-aided engineering program PATRAN is very convenient in geometric modeling. Moreover, the data representation capacity of PATRAN offers intuitive

insight such as the correctness of the analysis result. The color display of the results, furthermore, allows the simultaneous visualization of various parameters (position and magnitude) so that much more information can be obtained with less time. As a consequence, analysis of the results of the finite element approach can be performed more efficiently.

To summarize, the flow chart 5.1 proposes a general procedure to determine the stress distribution of a pressure vessel to be examined by acoustic emission testing.

As it was mentioned in chapter 4, a nonuniform stress distribution occurs around a singularity in spite of a uniform loading situation. Therefore, a discontinuity within this area is expected to behave differently in comparison to the other areas. To obtain a better interpretation of the acoustic emission testing results, sensors should be placed according to the stress distribution.

The present acoustic emission testing procedure that discriminates the sources in terms of severity based on the level of activity at particular loads is questionable. Since the level of acoustic emission activity is known to be stress dependent, a failure to properly relate the applied load to the stress state throughout the structure clearly might result in improper assessment. This is particularly serious if the assumed level of stress is not of the proper sign, i.e. tension versus compression. In other situations the assumed stress might be lower than the actual stress which might be considered "conservative". However, since the stress level in the vicinity of subcritical cracks might become quite large, the procedure might actually worsen these flaws.

Finally, the infallible nondestructive examination does not exist. Therefore, a reasonable goal must be set concerning the size and the type of discontinuity to be detected. Also, the economic aspect constitutes an important factor in the selection of a specific technique. The acoustic emission technique, that offers an economical way to survey a relatively large structure plus other advantages mentioned in chapter 2, cannot be easily replaced by other nondestructive examination. Thus, more research should be done to obtain a better understanding of the acoustic emission testing results.

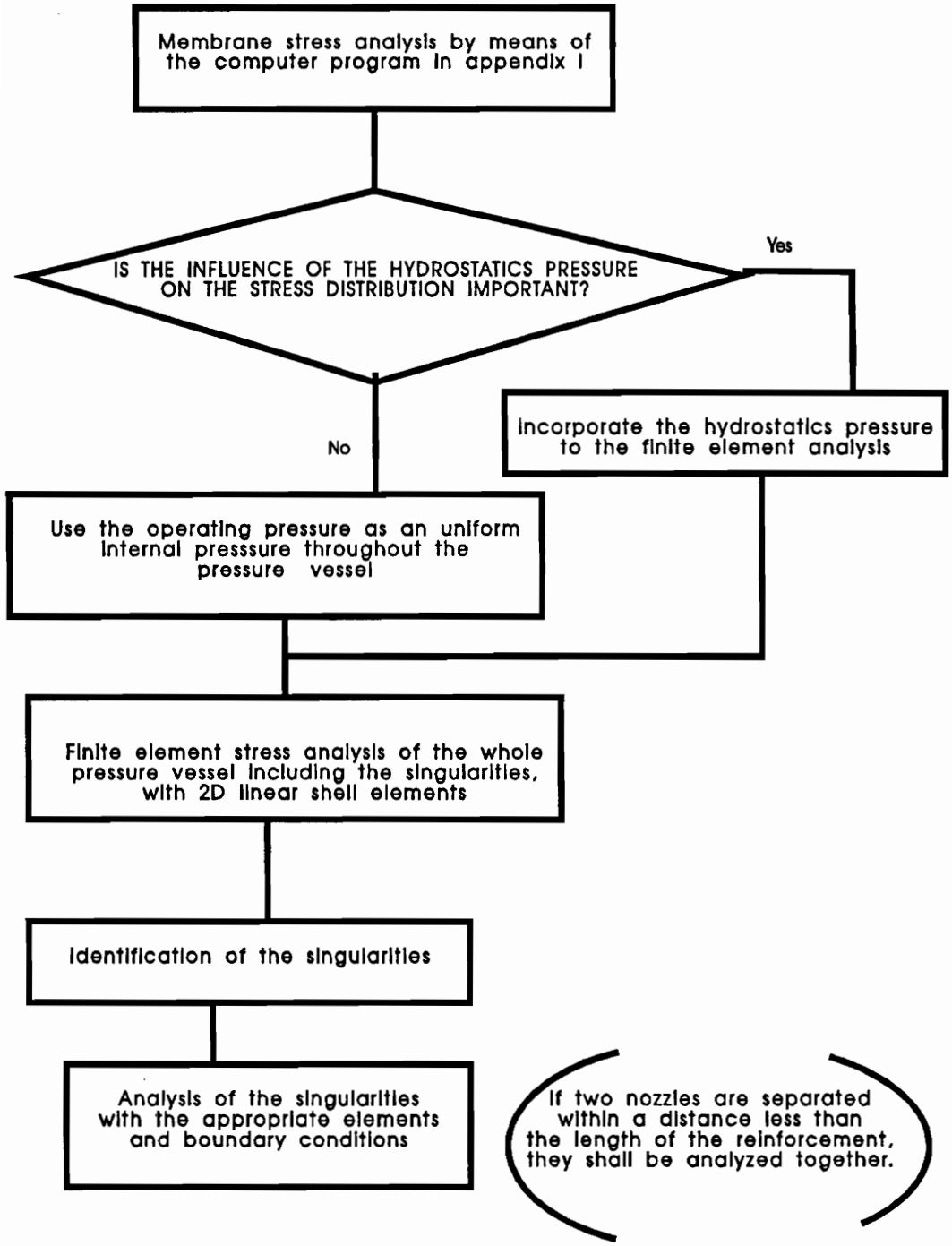

FLOWCHART 5.1
STRESS ANALYSIS PROCEDURE

6.) FUTURE DEVELOPMENT

So far the accuracy of the stress analysis approach has been discussed in relation to the experiment of Gill, Kitching, Kannas & Paine [10] concerning a radial nozzle. Although the supports and the non-radial nozzle are geometrically very similar to a radial nozzle, an experiment of measuring stress distribution around supports and non-radial nozzle can surely offer information to improve the analysis approach.

Concerning the acoustic emission testing, experiments on vessel with notches or induced cracks have been performed [ASTM, 26]. However, sensors are uniformly distributed throughout the vessel without considering the nonuniform stress distribution around the singularities. Therefore, a comparison of the acoustic emission between a vessel with sensors uniformly distributed, and a vessel with sensors conveniently located according to the stress distribution, can definitely demonstrate the influence of the nonuniform stress distribution in the acoustic emission, especially when the notch is located in a stress concentration area.

7) REFERENCES

1.) ABAQUS, Theory Manual, Version 4.8, Hibbit, Karlson & Sorensen, Inc. 1989

2.) ABAQUS, User's Manual, Version 4.8, Hibbit, Karlson & Sorensen, Inc. 1989

3.) Angelsen, S., Conley, M. J. and Williams, D., Ammonia Vessel Integrity Program, a Morden Approach, proceedings of the 1990 AIchE Ammonia Symposium, San Diego, August 1990.

4.) Burgreen, D., Pressure Vessel Analysis, C. P. Press, 1979, pp78-91.

5.) Carnahan, Luther & Wilkers, Applied Numerical Methods, John Wiley & Sons, 1976, pp101-116.

6.) Dowling, N. E., Mechanics of Deformation and Fracture (Lecture Notes), 1989, Chapter 8.

7.) Donell L. H., Beams, Plates and Shells, McGraw-Hill Book Company, 1976.

8.) Dunegan, H. L. and Green, A. T., Acoustic Emission, ASTM STP 505, American Society for Testing and Materials, 1972, pp100.

9.) Gill, S. S., The Stress Analysis of Pressure Vessel and Pressure Vessel Components, Pergamon Press, 1970, pp73-163.

10.) Gill, S. S., Kitching, R. and Paine, R.T., Experiments on Spherical Vessel with Pad-Reinforced Nozzles, Development in Stress Analysis for Pressurized Components, ed. by R. W. Nichols, Applied Science Publishers Ltd. London, 1977, pp67-98.

11.) Gould, P. L., Static Analysis of Shell, Lexington Books, 1977, pp5-7.

12.) Harvey, J. F., Theory and Design of Pressure Vessel, Van Nostrand Reinhold Company Inc.,1985, pp159-192.

13.) Journal of Pressure Vessel Technology, American Society of Mechanical Engineers. 1880-

14.) Kant, T and Dayte, D., Finite Elements Available for the Analysis of Curved Thin Walled Structures, Finite Element Applications to Thin-Walled Structures, ed. By John W. Bull, Elsevier Applied Science (UK),1990, pp1-40.

15.) Kline, R. A., Acoustic Emission Signal Characterization, Acoustic Emission, ed. by James R. Matthews, Gordon and Breach, Science Publishers, Inc.,1983, pp105-138.

16.) Nondestructive Evaluation and Quality Control, ninth edition, American Society for Metals, Metals Handbook, Vol 17, 1989, pp278-294.

17.) Nondestructive Examination, ASME Boiler and Pressure Vessel Code, Section V, American Society of Mechanical Engineers, 1986 with 1989 Addenda.

18.) Nondestructive Testing Handbook, second edition, American Society for Nondestructive Testing, Vol 5, ed. by Ronnie K. Miller and Paul Mclntire, ASNT, 1987.

19.) Onoe, M., Japanese Experience in Laboratory and Practical Application of Acoustic Emission to Welded Structures, Acoustic Emission, ed. by R. W. Nichols, Applied Science Publishers Ltd., London, 1976, pp75-101.

20.) PATRAN Plus User Manual, Release 2.5, PDA Engineering, October 1990.

21.) Peacock, M. J., Acoustic Emission Monitoring of a Large Pressure Vessel during a Pneumatic Re-qualification Test, Journal of Acoustic Emission, Vol. 8, Number 3, Acoustic Emission Group, 1989.

22.) Pressure Vessel, ASME Boiler and Pressure Vessel Code, Section VIII, Division 1, American Society of Mechanical Engineers, 1986 with Addenda 1988.

23.) Primm, A. H. and Stoneking, J.E., Accuracy of the Finite Element Method for Pressure Vessel/Nozzle Design, Design and Analysis of Pressure Vessels and Components, Vol. 175, American Society of Mechanical Engineers, 1989, pp3-10.

24.) Reddy, J. N., An Introduction to the Finite Element Method, McGraw-Hill Book Company, 1984.

25.) Scott, I. G., "Basic Acoustic Emission", Nondestructive Testing Monographs and Tracts, Vol. 6, Gordon and Breach Science Publishers, 1991, pp55-63.

26.) Spanner, J. C., Acoustic Emission - Some Examples of Increasing Industrial Maturity, "Acoustic Emission Monitoring of Pressurized Systems", ASTM STP697, American Society for Testing and Materials, 1979, pp 1-31.

27.) Spartan 3000, User Manual, Physical Acoustics Corporation, New Jersey, 1987.

28.) Timoshenko and Woinowsky, Theory of Plates and Shells, McGraw-Hill Book Company, 1989, p429-433.

29.) T. Oikawa & T. Oka, A New Technique for Approximating the Stress in Pad Reinforced Nozzle Attached to a Spherical Shell, Journal of Pressure Vessel Technology, Vol 109, Number 2, May 1987.

30.) Williams, R. V., Acoustic Emission, Adam Highler Ltd., Bristol, 1980, pp21-26.

31.) Zienkiewicz, O. C., The Finite Element Method, McGraw-Hill Book Company (UK), 1977.

Additional General References:

Mollmann, H., Introduction to the Theory of Thin Shells, John Wiley & Sons, 1981.

Bednar, H. H., Pressure Vessel Design Handbook, Van Nostrand Reinhold Company,1981.

Megyesy, E. F., Pressure Vessel Handbook, Pressure Vessel Handbook Publishing Inc., 1977

Explicit Solution of the Integral: $P = \int_{\emptyset_1}^{\emptyset_2} \gamma\left[R(\cos\emptyset_1 - \cos\emptyset)\right] 2\pi R * \sin\emptyset * R * d\emptyset * \cos\emptyset$

$$P = 2\pi R^3 \gamma \int_{\emptyset_1}^{\emptyset_2} (\cos\emptyset_1 - \cos\emptyset)\, \sin\emptyset\cos\emptyset d\emptyset$$

$$P = 2\pi R^3 \gamma \int_{\emptyset_1}^{\emptyset_2} (\cos\emptyset_1 \sin\emptyset\cos\emptyset - \sin\emptyset\cos^2\emptyset) d\emptyset$$

$$P = 2\pi R^3 \gamma \left(\int_{\emptyset_1}^{\emptyset_2} \frac{\cos\emptyset_1}{2} \sin 2\emptyset d\emptyset - \int_{\emptyset_1}^{\emptyset_2} \sin\emptyset\cos^2\emptyset d\emptyset \right)$$

Since: $\frac{d}{d\emptyset}\left(\frac{\cos^3\emptyset}{3}\right) = \frac{-3\cos^2\emptyset\sin\emptyset d\emptyset}{3} = -\cos^2\emptyset\sin\emptyset d\emptyset$

Therefore:

$$P = 2\pi R^3 \gamma \left\{ \left[\frac{-\cos\emptyset_1}{2} \frac{\cos 2\emptyset}{2} \right]_{\emptyset_1}^{\emptyset_2} + \left[\frac{\cos^3\emptyset}{3} \right]_{\emptyset_1}^{\emptyset_2} \right\}$$

$$P = 2\pi R^3 \gamma \left\{ \frac{-\cos\emptyset_1}{4} \left[\cos 2\emptyset_2 - \cos 2\emptyset_1\right] + \frac{1}{3}\left(\cos^3\emptyset_2 - \cos^3\emptyset_1\right) \right\}$$

$$P = 2\pi R^3 \gamma \left\{ \frac{\cos\emptyset_1}{4} \left[\cos 2\emptyset_1 - \cos 2\emptyset_2\right] + \frac{1}{3}\left(\cos^3\emptyset_2 - \cos^3\emptyset_1\right) \right\}$$

Appendix II

-. Computer Program to Calculate the Stress Distribution of a Spherical Vessel under Hydrostatic Pressure and Vapor Pressure.

```
C     Program to Calculate the Stress Distribution of a Spherical Vessel Due to Hydrostatic and
C     Vapor Pressure
C     Definition of Variables:
C     R = Radio of the Spherical Vessel
C     SD = Distance from the centerline to the Support
C     T = Thickness of the Vessel
C     Z0 = Fluid Level
C     GAMMA = Specific Density (Water = 62.3714 lb/ft**3 @ 60 F)
C     PV = Vapor Pressure
      IMPLICIT DOUBLE PRECISION (A-H,O-Z)
      PARAMETER (N=40)
      DIMENSION Z(N), PHI2(N),SIGMAP(N), SIGMAT(N), P(N), PRESS(N)
C     INITIALIZATION OF THE ARRAYS
      DO 5 I=1,N
         Z(I) = 0.0
         P(I) = 0.0
         PHI2(I) = 0.0
         SIGMAP(I) = 0.0
         SIGMAT(I) = 0.0
         PRESS(I) = 0.0
5     CONTINUE
C     INPUT OF DATAS
      READ(5,*) R, SD, T
      READ(5,*) Z0, GAMMA, PV
C     PRE - CALCULATION
      PHI1 = DACOS(1.0D0 - Z0/R)
      PHI1 = 1.D0-Z0/R
      PI = DACOS(-1.0D0)
      PHI0 = PI - DACOS(SD/R)
      SIGMA = PV* R/(2.*T)
      VOL = 4.*PI*R**3/3. - PI*ZO**2*(R - Z0/3.)
      W = VOL * GAMMA
C     CALCULATION OF STRESS
```

```
      THETA = 0.0
      DO 10 I=1,20
         THETA = THETA + PI/20.D0
         Z(I) = R - R*DCOS(THETA)
         PHI2(I) = THETA
         PRESS(I) = GAMMA * (Z(I) - Z0)
            IF (PHI2(I) .LT. PHI1) THEN
               SIGMAP(I) = 0.0 + SIGMA
               SIGMAT(I) = 0.0 + SIGMA
            ELSE
               P(I) = 2.D0*PI * R**3 * GAMMA *(PPHI1/4.D0 *(DCOS(2*PHI1)
     /                    -DCOS(2.*PHI2(I)))
     /                    +1.D0/3.DO*(DCOS(PHI2(I))**3-PPHI1**3))
                     IF(PHI2(I) .LT. PHI0)  THEN
                        P(I) = P(I)
                     ELSE
                        P(I) = P(I) + W
                     ENDIF
                  SIGMAP(I) = (P(I)/(2.*PI*R*DSIN(PHI2(I))**2))*1.D0/T+ SIGMA
                  SIGMAT(I) = (R*(GAMMA*(R*(PPHI1-DCOS(PHI2(I))))
     /                          -P(I)/(2.* PI * R**2* DSIN(PHI2(I))**2)))*1.D0/T + SIGMA
            ENDIF
10    CONTINUE
C     PRINT OUT OF THE RESULTS
      WRITE(6,100)
      DO 20 I=1,20
         WRITE(6,200) Z(I), SIGMAP(I), SIGMAT(I), PRESS(I)
20    CONTINUE
100   FORMAT(5X,'ELEVATION',10X,'SIGMA-PHI',10X,'SIGMA-THETA',5X,
     /          'HYDROSTATIC PRESSURE',/)
200   FORMAT(5X,E10.3,9X,E10.3,9X,E10.3,5X,E10.3)
      STOP
      END
```

VITA

The author was born in November of 1962 in Hong Kong. He attended the Tang Kang Po technical high school from 1975 to 1977. Then he emigrated to Venezuela where he completed his high school education in "Liceo Gustavo Herrera". In 1982, he began his undergraduate studies in the University Simón Bolívar. He graduated in August 1987 with a title of Bachelor in mechanical engineer from the University Simón Bolívar. From 1987 he has been working in the engineer consulting firm "Inelectra" as a pressure vessel designer, also he has worked in the area of piping design and controller of mechanical construction in situ. In 1989 he was promoted to the position of project engineer. He began his graduate studies in August 1989 in the Engineering Science and Mechanics Department at Virginia Polytechnic Institute and State University. After he completes his Master of Science degree, he will go back to Venezuela and work in the consulting firm "Inelectra". As a professional goal, the author is interested in the application of computer visualization technology for enhancement of the nondestructive examination, especially, in the area of petroleum industry.